Nearshore Sediment Resuspension at Lake Tahoe

By

KRISTIN EASTMAN REARDON

B.S. (New Mexico State University) 1999
M.S. (Universität Stuttgart) 2004

DISSERTATION

Submitted in partial satisfaction of the requirements for the degree of

DOCTOR OF PHILOSOPHY

in

Civil and Environmental Engineering

in the

OFFICE OF GRADUATE STUDIES

of the

UNIVERSITY OF CALIFORNIA

DAVIS

Approved:

_____

S. Geoffrey Schladow, Chair

_____

Fabián A. Bombardelli

_____

David H. Schoellhamer

Committee in Charge

2015

Kristin Eastman Reardon
March 2015
Civil and Environmental Engineering

Nearshore Sediment Resuspension at Lake Tahoe

Abstract

To investigate wind-driven nearshore sediment resuspension at Lake Tahoe, California-Nevada (USA), we combined field observations, computations from field data, and wind-wave modeling. We found that wind-waves resulted in sediment resuspension as corroborated by simultaneous increases in total measured suspended sediment concentration. We developed management charts illustrating relationships between fetch, wind speed, and wave height and between water depth, wave height, and nearshore bottom dynamics (i.e., the potential for mobilization of different sized particles). We evaluated the potential for sediment resuspension with changing lake levels, considering a range of possible future scenarios. For a representative grain size of 150 μm, the wind-driven surface waves influence the sediments to a maximum water depth of about 9 m. However, in situ measurements of suspended sediment concentration and particle size distribution revealed that the concentration of fine particles (<16 μm) was unchanged by wind events; instead, larger particles were resuspended. We investigated the use of acoustic backscatter from acoustic Doppler devices to infer nearshore suspended sediment concentration for those times when direct measurements were not available. We found that there was limited applicability of such techniques due to an unexplained but consistent lag between time series of signal strength and bottom shear stress. In conclusion, while the data verified that wind-driven nearshore sediment resuspension occurs at Lake Tahoe, the resuspended particles were generally larger in size than those that most negatively impact water clarity. This confirms that the nearshore lakebed sediments are generally devoid of fine particles.

Acknowledgements

My committee members, Geoffrey Schladow, Fabián Bombardelli, and David Schoellhamer have invested in my development as a researcher and educator over the past seven years, and I am grateful for their mentorship. I am especially grateful for Fabián's encouragement. The Department of Civil and Environmental Engineering has offered me opportunities to teach, both undergraduate and graduate students, and I have learned that I love sharing science and engineering. I acknowledge the support of my fellow graduate students in the Environmental Dynamics Laboratory and key staff at UC Davis and the Tahoe Environmental Research Center. Also, Francisco Rueda and his students graciously hosted my family in Granada, Spain during a short-term research assignment, where my elder son was born unexpectedly and prematurely. Thank you to each of you. The extended UC Davis community has offered me a rich experience, which I will carry with me.

The Office of Graduate Studies supported me generously with the Eugene Cota-Robles Fellowship. My research was also funded in part by a grant from the US Department of Agriculture Forest Service Pacific Southwest Research Station using funds provided by the Bureau of Land Management through the sale of public lands as authorized by the Southern Nevada Public Land Management Act. Field equipment was provided as part of the Nortek 2008 Student Equipment Grant Award program and on loan from the California Department of Water Resources and the US Geological Survey. The source code for STWAVE in Fortran was provided by researchers at the US Army Corps of Engineers, Coastal and Hydraulics Laboratory.

I wish to thank my sister Chelsea for her support since she arrived at UC Davis as a graduate student herself. She has helped me care for my fledgling family at the same time that she has understood better than anyone else the merit of my successes and disappointments. And

she has always taken my side. For that, I am grateful. I am grateful for the reinforcement I have received from all the women in my family.

I also wish to wholeheartedly acknowledge my husband Kyle for being a supportive and loving partner. We married my first quarter in the PhD program. He didn't know what we were getting into, and yet we have stayed the course. I take great pride in the stories he recounts to our two boys about mommy as a scientist. I hope that they marvel in nature and that as their parents we foster in them the tenacity and resilience necessary to pursue art, science, and engineering.

Finally, as my father has said many times, writing a dissertation is an exercise in perseverance. At some point, this intellectual endeavor became nearly purely a test of my mettle. But as my father has also said many times, among his three daughters, I am the willful one. So here we are, at the end. I did it, Dad!

Table of Contents

List of Tables

List of Figures

Chapter 1. Introduction

1.1 Purpose

The overarching goal of the research presented in this dissertation is to understand wind-driven nearshore sediment resuspension and its implications for water clarity at a deep lake. First, this required a comprehensive field campaign to observe wind-driven nearshore sediment resuspension in summer and winter. Second, this required computations of bottom shear stress. We present a novel approach for quantifying the total bottom shear stress in a lacustrine environment according to its components attributed to wind-waves, mean currents, and random motions, validating it with further computations from field data. Third, this required modification of the wind-wave model STWAVE. We developed what we believe is the first application and validation of a modification of the code STWAVE to simulate wind-wave induced sediment resuspension for a viscous-dominated flow in lakes. Next, this required a function for sediment entrainment rates appropriate for a lacustrine environment. We validated a function that was developed under open channel conditions. Lastly, this required an investigation of the use of acoustic backscatter from acoustic Doppler devices to infer nearshore suspended sediment characteristics for those times when direct measurements were not available. This research was conducted at Lake Tahoe, California-Nevada (USA), an example of a lake that is deep and oligotrophic. Moreover, nearshore sediment resuspension had never before been extensively studied at Lake Tahoe.

The specific aims of the overall study are addressed by answering the following research questions.

1) Is it possible to gain insight into and quantify the contributions to total bottom shear stress coming from wind-waves, currents, and random motions in lakes?

2) Is it feasible to adapt numerical models for wave motion (usually employed to address fully-turbulent flows in lakes from hurricane conditions) to simulate wave fields in lakes under typical flow conditions?
3) Do resuspension formulae of the same type as those applied in shallow lakes and coming from open channel flows well represent the resuspension phenomenon in the nearshore of a deep lake?
4) What are the observed nearshore patterns in summer and winter?
5) To what water depth do wind-driven surface waves influence the sediments?
6) What lake area does this influence extend, and how does it change with changing lake level?
7) What are the implications of wind-driven nearshore sediment resuspension for lake clarity?
8) Does the signal strength from acoustic Doppler devices serve as a reliable surrogate for suspended sediment concentration in water of high transparency?
9) Does the Rousean distribution reflect the daily-averaged vertical profile of suspended sediment we inferred in the nearshore?

1.2 Background

1.2.1 Lake Tahoe Total Maximum Daily Load

Lake Tahoe, the jewel of the Sierra Nevada Mountains on the California-Nevada border, appears startlingly deep and blue. Nevertheless, lake transparency has been declining since the 1960s. In 1980 California declared Lake Tahoe an Outstanding National Resource Water, a designation for exceptional waters requiring special protection. In 1982 Lake Tahoe was designated an impaired water body by the U.S. Environmental Protection Agency. Under the

Federal Clean Water Act, a Total Maximum Daily Load (TMDL) was required to address its impairment. The agreed-upon water quality objective for Lake Tahoe is deep water transparency equal to the average annual Secchi depth measured between 1967 and 1971 (29.7 m). The Lake Tahoe TMDL identifies the external pollutants responsible for the loss of transparency as fine sediment (<16 μm), nitrogen, and phosphorus. The TMDL also identifies the load of each pollutant entering the lake, the contributing sources of these loads, the reductions needed, the reduction opportunities that are available for each source, and the implementation plan to achieve these reductions [*Lake Tahoe Total Maximum Daily Load Technical Report*, 2010].

The Clean Water Act protects the beneficial use of a water body. In the case of Lake Tahoe, this protects the aesthetic enjoyment of its historical deep water and nearshore clarity. However, the Lake Tahoe TMDL only addresses external sources of pollution as they relate to a reduction in mid-lake clarity and assumes that achieving an improvement in mid-lake clarity will necessarily mean an improvement in nearshore water quality as well. Considering only external sources of pollutants, this may be a reasonable assumption as surface discharges entering the lake result in pollutant loading. Considering internal sources of pollution, this assumption may no longer be valid as nearshore processes may impact nearshore water clarity independent of watershed impacts to mid-lake clarity.

Until now, an investigation of the potential for internal sources of fine sediment (e.g., resuspended sediment) has been lacking. Yet at other wind-exposed lakes, sediment resuspension can be a significant source of fine particulates. A recent investigation at the Salton Sea, California (USA) suggested that resuspension-driven, internal nutrient loading was the dominant source of nutrient enrichment [*Schladow et al.,* 2006]. Indeed, a general review of the empirical evidence indicates that the long-term contribution of resuspended matter to the total flux of

particulate matter can be as high as 85 percent [*Evans*, 1994]. This suggests that sediment resuspension could contribute to internal pollutant loading resulting in a reduction in lake transparency. More information is needed regarding the internal sources and impacts of particle and nutrient loads at Lake Tahoe.

1.2.2 Process of wind-driven sediment resuspension

The most common cause of nearshore sediment resuspension is wind. Wind stresses on a lake contribute to the development of surface waves, surface currents, internal seiches, and strong horizontal currents below the water's surface [*Horne and Goldman*, 1994]. All of these in turn contribute to the transfer of momentum and turbulent mixing through the water column [*Fischer et al.*, 1979]. If the transfer of momentum is sufficient to generate bottom shear stress in excess of the critical shear stress, then this results in sediment entrainment into the water column. Sediment may be kept in suspension by diffusion of turbulence from the sediment-water interface as long as the turbulence is great enough to overcome the fall velocity of the particles in suspension [*Raudkivi*, 1998]. In a deep lake, wind-driven sediment resuspension is limited to the nearshore zone.

Quantitative estimates of sediment resuspension may be made a number of different ways. Methods include optical and acoustic instrumentation, instantaneous multiple-point water samplers, sediment traps, sediment cores and grabs, radiotracers, mass balance calculations, modeling approaches, correlation analysis, and laboratory experiments [*Bloesch*, 1994]. Optical and acoustic devices allow for the direct measurement of suspended sediment concentration (SSC), or surrogate for SSC, as a time series at a particular location. This makes possible observations of event-based sediment resuspension, which is the approach best suited to our purpose.

In addition to the mechanism of wind, sediment resuspension may also periodically result from sediment slumping, seismic activity, inflows from streams and storm outfalls, and outflows [*Bloesch*, 1994; *Fischer et al.*, 1979; *Håkanson and Jansson*, 1983].

1.2.3 Implications for water quality

Water quality in lakes may be affected by sediment resuspension in several ways. At Lake Tahoe, the most important issues related to sediment resuspension are optical water quality (clarity) and internal nutrient loading.

Optical water quality

Discussions regarding Lake Tahoe's water quality (e.g., the development of the Lake Tahoe TMDL) most often center on preserving its clear blue waters. Optical water quality, or more precisely, the visual quality of water [*Davies-Colley et al.*, 1993], therefore is of significant interest. While the appearance of the lake as part of a cultural landscape cannot be understated, neither can the ecological aspects of optical water quality. It is of vital importance for photosynthesis as well as the suitability of aquatic habitat for sighted organisms [*Davies-Colley and Smith,* 2001].

Light penetrates a water body and is attenuated by its absorption and scattering [*Kirk*, 2011]. Fine suspended sediment, phytoplankton, and organic detritus reduce light transmission through water by increasing scattering and light absorption, phenomena which result in a water body's increased turbidity. This was recently observed at the Salton Sea [*Schladow et al.*, 2006]. Increased turbidity effectively decreases the vertical extent of the photic zone, which in turn limits the growth of phytoplankton [*Horne and Goldman*, 1994; *Wetzel*, 1983]. Almost all energy that forms the basis of life in freshwater ecosystems comes from the sun and enters the aquatic food web via the primary production of phytoplankton. In addition to altering primary production, changes in the distribution of light can affect the behavioral adaptations of

organisms, such as the diurnal migration of zooplankton in response to sunlight [*Horne and Goldman*, 1994], as well as change the density stratification of the upper water column (by changing the distribution of heat). Therefore, changes in the distribution of light can have profound ecological consequences.

Internal nutrient loading

Phosphorus has been intensely studied in aquatic ecosystems, particularly as it is often the least abundant of the major nutrients for biota, and therefore most commonly limits biological productivity. Phosphorus limitation is due in part to the fact that in its soluble form it readily adsorbs to soil particles and is not available for phytoplankton growth. [See *Horne and Goldman*, 1994; *Wetzel*, 1983.]

Phosphorus most often enters water bodies as a result of erosion and is transported bound to the sediment particles, eventually settling from the water column and entering the lake sediments. Generally in oligotrophic lakes, the net flux of phosphorus on a yearly basis is toward the sediment [*Håkanson and Jansson*, 1983], and therefore the phosphorus content in the lake bed may be several orders of magnitude greater than that of the water [*Wetzel*, 1983]. As sediment is resuspended, however, it introduces particulate-bound phosphorus back into the water column. When conditions are such that soluble phosphates are released from the particles (or pore-water) and increase aqueous phosphorus concentrations, the process is known as internal nutrient loading.

One consequence of internal loading is that even if lake managers achieve drastic reductions in external phosphorus inputs to a lake, productivity may not decline for many years due to the phosphorus in the sediment that will continue to transfer into the water column as the concentration gradient across the sediment-water interface is favorable. The transfer of phosphorus is accelerated if the sediment is disturbed by turbulence and resuspended. Indeed,

Søndergaard et al. [1992] suggests that internal loading as a product of sediment resuspension at Lake Arresø (Denmark) may result in 20 to 30 times greater phosphorus release than from an undisturbed sediment bed. Although Lake Tahoe was previously nitrogen-limited, as is typical of lakes in dry climates [*Horne and Goldman*, 1994], it is now phosphorus-limited [*Goldman*, 1988]. Therefore, controlling phosphorus inputs at Lake Tahoe may be the most reasonable means of slowing cultural eutrophication of both the mid-lake and nearshore. However, if internal loading proves to be great enough, then the desired environmental improvements may not be achieved until the accumulated deposit of phosphorus in the lake bed is exhausted. This study focuses on wind-driven resuspension of particulate matter; characterization of the potential for phosphorus loading is beyond the scope of this work.

1.3 Organization

This dissertation is divided into five chapters. An introduction to the study is presented in this chapter. The second chapter describes wind-driven nearshore sediment resuspension at Lake Tahoe in winter, by means of field investigations, computations from field measurements, and wind-wave modeling. The third chapter explores patterns of wind-driven nearshore sediment resuspension on a seasonal basis, as well as the implications of nearshore sediment resuspension on water clarity. The fourth chapter investigates the use of acoustic backscatter from acoustic Doppler devices to infer suspended sediment characteristics. The final chapter summarizes key findings and presents conclusions and suggestions for future research.

References

Bloesch, J. 1994. A review of methods used to measure sediment resuspension. *Hydrobiologia*. 284:13-18.

Davies-Colley, R. J., W. N. Vant, and D. G. Smith (1993), *Colour and Clarity of Natural Waters: Science and Management of Optical Water Quality*, Ellis Harwood Limited, London, UK.

Davies-Colley, R. J. and Smith, D. G. (2001), Turbidity, suspended sediment, and water clarity: A review. *J. Am. Water Resour. Assoc.*, 37, 1085–1101, doi: 10.1111/j.1752-1688.2001.tb03624.x

Evans, R.D. 1994. Empirical evidence of the importance of sediment resuspension in lakes. *Hydrobiologia*. 284:5-12.

Fischer, H.B., E.J. List, R.C.Y. Koh, J. Imberger, and N.H. Brooks. 1979. *Mixing in Inland and Coastal Waters*. Academic Press. New York.

Goldman, C. R. (1988), Primary productivity, nutrients, and transparency during the early onset of eutrophication in ultra-oligotrophic Lake Tahoe, California-Nevada, *Limnol. Oceanogr.*, 33, 1321-1333.

Håkanson, L. and M. Jansson (1983), *Principles of Lake Sedimentology*, Springer-Verlag, Berlin, Germany.

Horne, A. J. and C. R. Goldman (1994), *Limnology*, 2nd ed., McGraw-Hill, Inc., New York, USA.

Kirk, J. T. O. (2011), *Light and Photosynthesis in Aquatic Ecosystems*, 3rd ed., University Press, Cambridge, UK.

Lake Tahoe Total Maximum Daily Load Technical Report (2010), California Regional Water Quality Control Board, Lahontan Region and Nevada Division of Environmental Protection, June.

Raudkivi, A. J. (1998), *Loose Boundary Hydraulics*, 3rd ed., Pergamon Press, Oxford, UK.

Schladow, S. G., F. J. Rueda, W. E. Fleenor, and E. G. Chung (2006), Predicting the effects of configuration changes on Salton Sea stratification using a three-dimensional hydrodynamic model, Report to CH2M HILL and California Department of Water Resources, TERC Report 06-007.

Søndergaard, M., P. Kristensen, and E. Jeppesen. 1992. Phosphorus release from resuspended sediment in the shallow and wind-exposed Lake Arresø, Denmark. *Hydrobiologia*. 228:91-99.

Wetzel, R. G. (1983), *Limnology*, 2nd ed., Saunders, Philadelphia, USA.

Chapter 2. Wind-driven nearshore sediment resuspension in a deep lake during winter

This chapter is based on work that was published as a regular research article in Water Resources Research, a journal of the American Geophysical Union.

Citation:

Reardon, K. E., F. A. Bombardelli, P. A. Moreno-Casas, F. J. Rueda, and S. G. Schladow (2014), Wind-driven nearshore sediment resuspension in a deep lake during winter, *Water Resour. Res.*, 50, doi:10.1002/2014WR015396.

2.1 Abstract

Ongoing public concern over declining water quality at Lake Tahoe, California-Nevada (USA) led to an investigation of wind-driven nearshore sediment resuspension that combined field measurements and modeling. Field data included: wind speed and direction, vertical profiles of water temperature and currents, nearbed velocity, lakebed sediment characteristics, and suspended sediment concentration and particle size distribution. Bottom shear stress was computed from ADV-measured nearbed velocity data, adapting a turbulent kinetic energy method to lakes, and partitioned according to its contributions attributed to wind-waves, mean currents, and random motions. When the total shear stress exceeded the critical shear stress, the contribution to overall shear stress was about 80 percent from wind-waves and 10 percent each from mean currents and random motions. Therefore, wind-waves were the dominant mechanism resulting in sediment resuspension as corroborated by simultaneous increases in shear stress and total measured sediment concentration. The wind-wave model STWAVE was successfully modified to simulate wind-wave induced sediment resuspension for viscous-dominated flow typical in lakes. Previous lake applications of STWAVE have been limited to special instances of fully-turbulent flow. To address the validity of expressions for sediment resuspension in lakes,

sediment entrainment rates were found to be well represented by a modified 1991 García and Parker formula. Lastly, in situ measurements of suspended sediment concentration and particle size distribution revealed that the predominance of fine particles (by particle count) that most negatively impact clarity was unchanged by wind-related sediment resuspension. Therefore, we cannot assume that wind-driven sediment resuspension contributes to Lake Tahoe's declining nearshore clarity.

Keywords: sediment resuspension; wave-induced shear stress; entrainment formula; STWAVE; Lake Tahoe; nearshore

2.2 Introduction

Many lakes suffer from water quality issues associated with bed sediment-water column interactions. Over time, particles, nutrients, and contaminants accumulate in the lakebed sediment, resulting in a lakebed which is itself an internal source of pollution. Resuspension of lakebed sediment is of particular interest because it alters the quality of the attendant water by three mechanisms [*Wetzel*, 1983]. First, resuspension adds previously-deposited particulates to the water column. This increases turbidity and can change the water temperature distribution [*Schladow et al.,* 2006; *Swift et al.,* 2006]. Increased turbidity in turn reduces the visual quality of water and the vertical extent of the photic zone, which limits phytoplankton growth [*Wetzel*, 1983; *Davies-Colley et al.*, 1993; *Horne and Goldman*, 1994; *Davies-Colley and Smith*, 2001]. Modified water temperature alters lake stratification and affects biological processes and chemical reaction rates [*Horne and Goldman*, 1994]. Second, resuspension releases nutrients and other contaminants attached to resuspended particulates. This may accelerate eutrophication via internal nutrient loading [*Wetzel*, 1983; *Chung et al.*, 2009a] and may also increase the availability of toxic heavy metals in the water column [e.g., *Mian and Yanful*, 2003, 2004;

Massoudieh et al., 2010]. Third, resuspension increases the exchange between pore-water and the overlying water. This may also contribute to lake pollution [*Wetzel*, 1983].

Wind-driven sediment resuspension is the result of the transfer of momentum from the air to the water surface layers in the lake. When large enough surface waves are produced such that the wave momentum reaches the bed sediment-water column interface, this can lead to the entrainment of bed particles into the water column [*Håkanson and Jansson*, 1983]. In a deep lake, wind-driven sediment resuspension is limited to the shallow nearshore zone.

In open channels, the mean current is the primary contributing factor to the generation of bottom shear stress that leads to sediment resuspension. However, it has been shown that surface waves contribute significantly more than currents to sediment resuspension in lake environments, such as the nearshore of the Laurentian Great Lakes [see *Hawley et al.*, 2004] and in shallow lakes and ponds [e.g., *Luettich et al.*, 1990; *Mian and Yanful*, 2004; *Chung et al.,* 2009a]. To predict sediment resuspension, we follow the standard practice by which we assume that it occurs only when the excess shear stress (i.e., the difference between the shear stress and the critical shear stress for incipient motion) is larger than a certain value. Critical shear stress is related to lakebed properties [*Håkanson and Jansson*, 1983] and is therefore variable in space and time. Wind is also highly variable, which further obfuscates the determination of cause-effect relationships.

Most approaches to estimate the action of wave fields in lakes have been based on empirical formulae [e.g., *Hamilton and Mitchell*, 1996] and parametric models [e.g., *Luettich et al.*, 1990; *Hawley et al.*, 2004; *Chung et al.,* 2009a]. More recently, models based on first principles (i.e., conservation laws) have simulated the wave fields in lakes in order to analyze the

effects of hurricanes [e.g., *Bunya et al.*, 2010; *Dietrich et al.*, 2010], which are characteristically fully-turbulent flows similar to the conditions in some marine coastal environments. Lakes, however, are typically low-energy environments, episodically punctuated by high-energy wind events. This means the flow regime close to the lakebed is characteristically viscous-dominated, and until now not well represented in the available models.

Widely-used formulae to predict sediment entrainment rates as a function of water flow and sediment characteristics for open channels are available in the literature [e.g., *Sutherland*, 1967; *Van Rijn*, 1984; *García and Parker*, 1991, 1993]. Typically, these formulae are limited to equilibrium conditions for a representative, non-cohesive particle and a uniform distribution of shear stress in space, which is, of course, in sharp contrast to what we observe in natural systems. *Chung et al.* [2009a] investigated sediment resuspension at a shallow lake (Salton Sea, California, USA) and found that sediment entrainment into suspension was nevertheless predicted by an extension of the formula proposed by *García and Parker* [1993]. *Chung et al.* [2009b] found that this extended formula coupled with a hydrodynamic and water quality lake model well represented water quality characteristics. Furthermore, *Lou et al.* [2000] integrated the formula proposed by *García and Parker* [1993] into a suspended sediment transport model that included sediment resuspension at Lake Michigan (USA) and found reasonable agreement between simulated and measured results.

Although the nearshore water quality of Lake Tahoe, a subalpine lake located on the California-Nevada border (Figure 2-1), has degraded over time [*Taylor et al.*, 2004], an understanding of the role of wind-driven sediment resuspension has been lacking. The lake's large size permits the development of sizable wind-driven waves and currents and offers an opportunity to link wind exposure, lakebed sediment characteristics, and nearshore sediment

resuspension. In addition to providing the first dataset on sediment resuspension at Lake Tahoe, this study aims to answer the following research questions:

1) Is it possible to gain insight into and quantify the contributions to total bottom shear stress coming from wind-waves, currents, and random motions in lakes?
2) Is it feasible to adapt numerical models for wave motion (usually employed to address fully-turbulent flows in lakes from hurricane conditions) to simulate wave fields in lakes under typical flow conditions?
3) Do resuspension formulae of the same type as those applied in shallow lakes and coming from open channel flows well represent the resuspension phenomenon in the nearshore of a deep lake?
4) And finally, does nearshore sediment resuspension contribute to declining nearshore clarity at Lake Tahoe?

2.3 Methods

To answer our research questions, we collected field measurements of hydrodynamic and sediment variables, directly computed estimates of shear stress using field data, and carried out numerical modeling.

2.3.1 Field measurements

Lake Tahoe is an example of an oligotrophic lake as characterized by low nutrient concentrations, high dissolved oxygen concentrations, and transparent waters to relatively great depths. The lake is deep (maximum depth 505 m; average depth 313 m) and has a volume of 156 km^3 with a total shoreline of about 116 km. The watershed area is only 800 km^2 compared to

the lake's total surface area of 500 km^2. Owing to the large lake volume and small watershed, the average hydraulic residence time is extremely long at about 700 years [*Goldman*, 1988].

The nearshore study site was located at the south end of Lake Tahoe about 1000 m offshore on a shallow, broad shelf that slopes gently (about 0.3 percent) before dropping abruptly. There are similar shelf structures on the west and north shores of Lake Tahoe (accounting for approximately 25 percent of the total lake perimeter), but much of the lake has very steep sides (approximately 75 percent). Due to its shallow water depth and previously observed periods of elevated turbidity [*Taylor et al.*, 2004], the study site was thought to be favorable for observing wind-driven nearshore sediment resuspension.

Lake measurements were taken at a water depth of 4.5 to 5 m from 13 November 2008 to 14 January 2009; a complete dataset was collected from 11 to 19 December 2008. We measured wind speed and direction 5 m above lake level at long-term meteorological stations maintained by the University of California, Davis, Tahoe Environmental Research Center, on the piers at Timbercove near the City of South Lake Tahoe and the US Coast Guard (USCG) station at Tahoe City (Figure 2-1). We measured vertical profiles of nearshore water temperature with a thermistor chain made up of eight Onset Stow Away TidbiT temperature loggers. We measured vertical profiles of water currents with a Nortek acoustic Doppler current profiler and directional wave gauge (AWAC). The AWAC was bottom-mounted and provided profiles of current magnitude and direction in three dimensions in 0.50 m vertical bins. The frame and blanking distance precluded velocity measurements in the first 0.60 m above the lakebed. The Acoustic Surface Tracking (AST) feature of the AWAC malfunctioned and therefore data on surface wave properties were somewhat limited. We measured nearbed velocities with two acoustic Doppler velocimeters (ADV), a Nortek Vector and a Sontek ADVOcean Probe. Both were mounted on a

sawhorse frame located about 200 m shoreward from the AWAC (Figure 2-1). We measured suspended sediment concentration and particle size distribution with a Laser In Situ Scattering and Transmissometry 100X type B instrument (LISST-100X) from Sequoia Scientific, Inc. The LISST-100X was deployed alongside the sawhorse frame on two aluminum risers and sampled at the same height as the sampling volume of the Vector (0.2 m above lakebed). The two instruments were about 2 m apart. We characterized lakebed sediment from two grab samples taken from the study site on 22 July 2008. Generally, the sediment was well-sorted, non-cohesive, and with no apparent bedforms. Samples were analyzed using an LS 13 320 MW particle size analyzer from Beckman Coulter, Inc. We also reviewed a recent study by *Herold et al.* [2007] describing the nearshore lakebed sediment at Lake Tahoe. Details regarding the field measurements are listed in Table 2-1 and include the parameter(s) measured, instrument, location(s), sensor height(s) or orientation, period, sampling rate/interval, sampling duration, and burst interval, as applicable.

For the nearbed velocity measurements, the flow perturbation from the sawhorse-frame legs did not extend to the sampling volumes. *Sumer and Fredsøe* [1997] compiled experimental results and characterized the effect of a cylinder on the flow as a function of cylinder Reynolds number. In our case, with observed nearbed velocities ranging from 0.02 to 0.2 m s^{-1} and a cylinder diameter equal to about 0.05 m, the cylinder Reynolds number was between 10^3 and 10^4. This corresponded to a perturbation with a spatial extent of up to six times the cylinder diameter [*Sumer and Fredsøe*, 1997]. The ADV sampling volumes were at a distance of more than 13 times the cylinder diameter from the sawhorse-frame legs. Additionally, sampling heights were confirmed by a diver at the start and end of the deployment period and did not change.

For the suspended sediment concentration and particle size distribution measurements, the LISST-100X uses laser diffraction to obtain the suspended sediment particle size distribution in 32 logarithmically-spaced size classes of median diameter from 1.25 to 250 μm and reports concentration in volume units of $\mu L\ L^{-1}$. The raw data were processed and converted according to *Andrews et al.* [2011]. The Lake Tahoe Basin is dominated by granitic soils [*California Geological Survey*, 2005] so we assumed suspended sediment density equal to 2650 kg m^{-3} in order to report mass concentration ($\mu g\ L^{-1}$). To report particle counts, we assumed discrete, spherical particles with a representative diameter equal to the median-sized particle of each logarithmically-spaced size class and uniform density. The presence of organic material and the formation of flocs were verified to be negligible.

For the lakebed sediment characterization from two grab samples, the Beckman Coulter particle size analyzer used laser diffraction to measure the particle size distribution in 34 user-defined logarithmically-spaced size classes of median diameter from 0.04 to 2000 μm and reports concentrations in volume units of $\mu L\ L^{-1}$. To report mass concentration ($\mu g\ L^{-1}$), we assumed lakebed sediment density also equal to 2650 kg m^{-3}.

2.3.2 Computations from field measurements

Direct estimates of bottom shear stress

We directly estimated bottom shear stress from ADV-measured velocity data collected from the Sontek ADVOcean Probe adapting a variant of the turbulent kinetic energy (TKE) method as described by *Kim et al.* [2000]. (The Sontek ADVOcean Probe resulted in better quality data [i.e., had better quality checks] than the Nortek Vector.) The method of *Kim et al.* [2000] relies on linear relationships between turbulent kinetic energy and total shear stress. Yet currently there is no widely-accepted method to discriminate contributions to the shear stress

coming from waves, currents, and random motions. Therefore, we developed the method described in this section and provide validation of our results in Section 2.4.3.

We defined the velocity vector, denoted in bold, $\boldsymbol{u} = (u, v, w)$ in a Cartesian coordinate system (x, y, z) in which x is aligned east-west, y is aligned north-south, and z is aligned vertically. The total bottom shear stress is given by

$$|\tau| = C_1 \, \rho \, E, \tag{2-1}$$

where C_1 is a proportionality constant equal to 0.21 [*Kim et al.*, 2000]; ρ is the density of water, taken at Lake Tahoe as, approximately, 1000 kg m^{-3}; and E is a given measure of the TKE. The TKE is defined by $E = 0.5\ (\overline{u'^2} + \overline{v'^2} + \overline{w'^2})$, where prime indicates fluctuations, and the overbar refers to averaging over time. *Kim et al.* [2000] also argued that another plausible expression for the bottom shear stress is

$$|\tau| = C_2 \, \rho \, \overline{w'^2}, \tag{2-2}$$

where C_2 is a proportionality constant equal to 0.9. Considering only the vertical velocity fluctuations is a reasonable variation of the TKE method since instrument noise errors associated with the vertical velocity component are much smaller than for the horizontal components [*Kim et al.*, 2000, p. 403]. In this study, we followed Equation (2-2) for the computation of bottom shear stress. With a burst interval of 1 h, we directly estimated the total bottom shear stress from the velocity measurements collected in each burst of 3 min at 10 Hz (see Table 2-1). (By comparing power spectral density plots corresponding to different burst lengths, we determined that 3-min bursts adequately described the flow components [see Appendix A].)

In order to partition the contributions to total bottom shear stress from wind-waves, mean currents, and random motions, we filtered the signals of each directional component of velocity

for each burst in three steps using a second-order Butterworth filter. To the best of our knowledge, guidance from the literature to address this complicated issue was otherwise lacking. Initially, we applied a bandpass filter that passed all frequencies between 0.03 and 2 Hz. This corresponded to wave periods between 0.5 and 30 sec, commonly referred to as the wind-wave band (see *NortekUSA*, www.nortekusa.com). Then we applied a lowpass filter that passed all frequencies below 0.03 Hz. This corresponded to wave periods longer than 30 sec, which we attributed to mean currents. Lastly, we applied a highpass filter that passed all frequencies above 2 Hz. This corresponded to wave periods shorter than 0.5 sec, which we attributed to random motions. After separating velocity into three contributing parts such that,

$$\boldsymbol{u}_{total} = \boldsymbol{u}_{wind-waves} + \boldsymbol{u}_{mean\ currents} + \boldsymbol{u}_{random\ motions}, \quad (2\text{-}3)$$

we directly estimated the bottom shear stress due to wind-waves, mean currents, and random motions using Equation (2-2). In this way we partitioned the total bottom shear stress according to its provenance using the high-frequency nearbed velocity signal. Such partitioning requires validation with field data since the non-linear nature of any measure of energy of near-bottom motions involving, for instance, products between the components of waves and currents may affect the results. Thus, partitioning of this type is justified only if these products are small compared to the square of other components. We justify such partitioning below.

Figure 2-2a shows the east-west (u) component of the velocity vector, filtered to obtain all contributions from a 3-min sampling burst with the ADVOcean Probe on 13 December 2008 at 7 a.m. This example, which corresponds to an instance of relatively high wind intensity, shows the velocity signal measured with the ADVOcean Probe to have three distinct parts of the form indicated by Equation (2-3). The velocity signal resulting from the wind-wave contribution oscillated about null from a minimum of -0.23 m s^{-1} to a maximum of 0.17 m s^{-1}. The velocity

signal resulting from the mean current contribution was on average 0.13 m s^{-1} and maintained a positive value indicating that in spite of the considerable oscillatory motion of the waves, net flow was positive (eastward) during the 3-min sampling burst.

In order to show that the designed methodology to separate different contributions to flow was physically sound, we present in Figure 2-2b the plot of the power spectral density of the total velocity signal shown in Figure 2-2a. We observed the most energetic peak in the power spectral density at 0.33 Hz (Figure 2-2b), which corresponded to the wind-wave contribution (wave period equal to 3 sec). That peak was captured by the imposed wind-wave band and is clearly distinguishable relative to other individual contributions to flow (i.e., currents and random motions) and dominant when compared to the non-linear interactions among currents and waves. This indicates that the separation was appropriate. We also reviewed power spectral density plots for bursts throughout the study period. During windy periods, we observed clear peaks in power spectral density of about 0.3 to 0.35 Hz. For low-wind periods, no such peaks existed (not shown). Our observations suggested that no further adaptations to our methodology were warranted (see Section 3.5.3).

We anticipated that values of shear stress coming from the wind-wave component would agree well with values computed from linear wave theory (LWT; see Section 2.4.3). To address the sensitivity of the results of bottom shear stress attributed to wind-waves, we varied the precise limits of the filter band. We found that the results changed very modestly, which reinforced that our imposed filter band indeed captured the bulk of the influence of the wind-waves to bottom shear stress (see Appendix B).

Estimate of critical shear stress

For practical purposes, the Shields diagram [*Shields*, 1936] for threshold of sediment particle motion in unidirectional, steady, uniform flow has been found adequate to characterize incipient conditions under oscillatory flows [see *Raudkivi*, 1998, p. 342]. Experimental data for wave-induced entrainment have agreed reasonably well with the Shields diagram [*Komar and Miller*, 1974; *Madsen and Grant*, 1975]. We assessed the critical bottom shear stress as

$$\tau_{critical} = \tau_c^* \rho_s R g D, \quad (2\text{-}4)$$

where τ_c^* is the non-dimensional critical Shields parameter, ρ_s is the sediment density, R is the submerged specific gravity, g is the acceleration due to gravity, and D is the representative sediment grain size [from *Parker*, 2004]. The non-dimensional critical Shields parameter [from *Parker et al.*, 2003] was calculated as $\tau_c^* = 0.5\left[0.22Re_p^{-0.6} + 0.06 \times 10^{\left(-7.7Re_p^{-0.6}\right)}\right]$, where Re_p is the explicit particle Reynolds number of the form $Re_p = \sqrt{gRD^3}/\nu$, and ν is the kinematic viscosity of water, taken equal to 10^{-6} m^2 s^{-1}. The submerged specific gravity is defined as $R = (\rho_s - \rho)/\rho$.

2.3.3 Simulations of sediment resuspension

Modification to the wind-wave model STWAVE

To numerically estimate the wave-induced bottom shear stress, we implemented the full-plane version of the US Army Corps of Engineers (USACE) wind-wave model STWAVE [*Massey et al.*, 2011] to which we introduced a key change as detailed in this section. STWAVE is a finite difference, steady-state, spectral wave model that solves the wave action balance equation, including wave generation and transformation by refraction and shoaling, wave breaking, generation by wind-input, wave-wave interaction, and white capping [*Smith*, 2007;

Holthuijsen, 2007; *Massey et al.*, 2011]. In earlier versions of STWAVE, the model could be used in the so-called half-plane only, which was suitable for coastal applications and required boundary conditions for the waves [*Smith et al.*, 2001]. Now a full-plane version is available [*Massey et al.*, 2011], which encompasses the entire closed domain without the need for such boundary conditions and is therefore especially suitable for lakes [*Smith and Zundel*, 2006].

Additionally, in earlier versions of STWAVE, the sink term in the spectral energy density due to bed friction was absent [*Smith et al.*, 2001]. To account for bottom friction, STWAVE now relies on Manning's equation [*Massey et al.*, 2011], which is applicable to fully-turbulent flow regimes [*Gioia and Bombardelli*, 2002; *Bombardelli and García*, 2003]. Lake applications of STWAVE have so far been limited to hurricane conditions which result in fully-turbulent flow regimes [e.g., *Bunya et al.*, 2010; *Dietrich et al.*, 2010; see also http://chl.erdc.usace.army.mil/chl.aspx?p=s&a=software;9]. In order to reflect typical lake conditions with flow regimes that are viscous-dominated, it was necessary to correct the bottom-friction formulation. We were able to produce such an update because we were kindly provided the source code of STWAVE in Fortran by researchers at the USACE. Considering the criterion in the friction factor diagram by *Kamphuis* [1975], it was easily concluded from the field data that the lake flow near the bed was viscous-dominated as the wave Reynolds number was always smaller than 10^4.

The bottom shear stress due to waves was computed using the modified STWAVE, according to the formulation

$$|\tau_{waves}| = 0.5\,\rho\,C_f\,u_{b,rms}^2, \tag{2-5}$$

where τ_{waves} denotes the magnitude of the bottom shear stress due to waves, C_f represents the bottom-friction coefficient, and $u_{b,rms}$ is the magnitude of the root-mean-square orbital velocity at the lake bottom. This orbital velocity is calculated in STWAVE as

$u_{rms}^2 = \int_0^{\infty} \int_0^{2\pi} \frac{\sigma^2}{\sinh^2 k H} \; S(f, \; \beta) \; d\beta \; df$, where σ is equal to 2 π times the wave frequency, f, calculated as the reciprocal of the wave period, *k* represents the wave number, H denotes the water depth, and the wave direction is given by β [*Holthuijsen*, 2007]. The spectrum as a function of the frequency and the wave direction is given by *S*.

We updated the code to estimate bottom friction for viscous-dominated flow [see *Kamphuis*, 1975] with the expression $C_f = 2/\sqrt{Re_w}$, where Re_w denotes the wave Reynolds number, $Re_w = u_{b,rms} \, A_w/\nu$. The amplitude of particle motion, $A_w = u_{b,rms}/\omega$; the wave angular frequency, $\omega = 2\pi/T_p$; and the wave period is T_p. Changes to STWAVE were introduced to the subroutine `friction`, while the rest of the code remained unchanged. It is worth mentioning here that wave heights and periods change with this modification and, thus, results with the original and modified STWAVE code are intrinsically different.

In order to validate the development, we compared model results including the above viscous-dominated regime with observations of waves measured at the Salton Sea [*Chung et al.*, 2009a; *Chung et al.*, 2009b]. Good agreement was found between field measurements and results from the modified STWAVE (Appendix 2-A, Figure 2-A1). Additionally, we considered results from the Sverdrup-Munk-Bretschneider (SMB) model for shallow water waves [*Coastal Engineering Research Center (CERC),* 1984] and found good agreement. (See Appendix 2-A for comparisons of field data and results from the modified STWAVE model; SMB model results are not shown here.) This model validation suggested that the modified STWAVE was an

appropriate tool to calculate the effect of wind-waves on the development of bottom shear stress leading to sediment resuspension in shallow areas. See also Appendix C for background and further comparisons of STWAVE.

Modeling of the wave field and bottom shear stress

To implement the modified STWAVE for Lake Tahoe, we utilized 50 m square grid cells covering the entire lake in which we specified bathymetry data. The bathymetric data was prepared by merging US Geological Survey multi-beam sonar and USACE SHOALS bathymetry data sets, both with a grid spacing of 10 m (unpublished data, 2009). We used the wind record at Timbercove station (see Table 2-1) and assumed a spatially constant (though temporally variable) wind field. Because STWAVE is a steady-state model, we conducted simulations every 2 h, updating the model input wind speed and direction from the wind record. Based on review of the meteorological data, we were able to determine that the duration of strong wind events was usually greater than 2 h; hence, we can reliably capture their changes and follow the wind-wave behavior taking a snapshot of the wave field by numerical simulation every 2 h. We output model results at the grid cell where the instruments were located.

Modeling entrainment of sediment in suspension

We modeled entrainment of uniform, non-cohesive lakebed sediment into suspension according to the entrainment formula given by *García and Parker* [1991]. For this formulation, the dimensionless coefficient for sediment entrainment into suspension, $E_S = c_{ae}$, defined as the ratio between the vertical flux of sediment close to the bed and the terminal fall velocity, v_S [*García and Parker*, 1991, 1993; *Bombardelli and García*, 1999; *Parker*, 2004; *Chung et al.*, 2009a] is given, for quasi-equilibrium or mild-disequilibrium conditions, as

$$E_s = AZ_u{}^5/\left(1 + (A/0.3)Z_u{}^5\right), \quad (2\text{-}6)$$

where A is a constant and Z_u is a similarity variable for uniform sediment. The constant $A = 1.3 \times 10^{-7}$ and the similarity variable for uniform sediment is $Z_u = (\tilde{u}_*/v_s)\alpha Re_p{}^n$, where $\tilde{u}_*$ is the skin shear (friction) velocity, α is a fitting parameter that we introduced in this study, and n is the power in similarity variable for uniform sediment. Because we observed no bedforms at the study site, the skin shear velocity, $\tilde{u}_* = u_*$, where u_* is the shear velocity. The total bottom shear stress and shear velocity are related as $|\tau_{total}| = \rho u_*^2$. The sediment fall velocity was computed according to the formula by *Dietrich* [1982] for natural particles such that $v_s = \exp(-b_1 + b_2\ln(Re_p) - b_3\left(\ln(Re_p)\right)^2 - b_4\left(\ln(Re_p)\right)^3 + b_5\left(\ln(Re_p)\right)^4)\sqrt{gRD}$, where $b_1 = 2.891394$, $b_2 = 0.95296$, $b_3 = 0.056835$, $b_4 = 0.002892$, $b_5 = 0.000245$ [see *Bombardelli and Moreno*, 2012, p. 233]. The value of α was obtained by best fit. *García and Parker* [1991] determined that $n \sim 0.6$ was best and that these formulations were limited to conditions where $0.70 < \tilde{u}_*/v_s < 7.5$ and $3.50 < Re_p < 37.00$. We used this formulation with the time series of total bottom shear stress to calculate the dimensionless sediment entrainment rate, E_s, for those instances when the total bottom shear stress exceeded the critical shear stress; we then compared to the nearbed sediment concentration, c_{ae}, measured directly with the LISST-100X. In doing so, we assumed a condition of quasi-equilibrium [see *Chung et al.*, 2009a, Appendix C].

2.4 Results and discussion

2.4.1 Observed nearshore patterns during winter

Nearshore water temperatures decreased steadily from about 10.5 °C to about 7 °C during the study period, and generally the water column was not subject to thermal stratification

(Figure 2-3). The temperature difference between bottom and top thermistors was typically less than 1°C and never greater than 3 °C; these temperature differences were usually sustained for about 2 to 3 h and no more than 6 h (Figure 2-3), confirming that our time step of 2 h for the application of the modified STWAVE was adequate. Based on these results we assumed that the thermal structure did not impact the transfer of momentum in the water column. See Appendix D for mid-lake temperature profiles during the winter study period.

For times of low-wind intensity, we generally observed wind speeds of about 2 to 3 m s^{-1} and opposite wind directions (180° out of phase) at the Timbercove and USCG stations (Figure 2-4). For periods of strong wind, we observed wind speeds greater than 6 m s^{-1} and alignment (or near-alignment) of the wind direction at Timbercove and USCG stations. There was only one instance of elevated wind speed and misalignment of the wind direction between the meteorological stations during the study period (see Figure 2-4 at day 334).

From 11 to 19 December (days 346-354), the period for which LISST-100X data were available, we twice observed simultaneous peaks in wind speed, nearbed velocity, total bottom shear stress, and suspended sediment concentration, suggesting wind-driven nearshore sediment resuspension (Figure 2-5).

For the most severe storms, elevated winds of nearly 14 m s^{-1} and exceeding 15 m s^{-1} were southwesterly (about 200° clockwise from north) and sustained in a quasi-constant direction for nearly 4 days from 12 to 15 December (days 347-350) and for 1 day on 19 December (day 354), respectively (see Figures 2-5a and 2-5b). The effective fetch for southwesterly winds at the study site was about 1 km. Typical velocities measured with the ADVs were about 0.03 m s^{-1} but reached more than 0.15 m s^{-1} and 0.20 m s^{-1} on 13 and 19 December (days 348 and 354), respectively (Figure 2-5c). Typical nearshore suspended sediment

concentrations were 2 to 2.5 μL L^{-1} (Figure 2-5e). During the first storm event on 13 December (day 348), however, the suspended sediment concentration reached 4 μL L^{-1}. During the second storm event on 19 December (day 354), it was nearly 3 μL L^{-1}. Compared with results at shallow lakes which demonstrate sediment responses that can vary by orders of magnitude [e.g., *Luettich et al.*, 1990; *Chung et al.*, 2009a], we observed at Lake Tahoe much more subtle sediment responses. We attributed this to the relative limitation of available fine material in the nearshore.

From the AWAC-measured current profiles, we saw typical velocities at the study site of about 0.09 m s^{-1} near the surface and generally decreasing with increasing water depth to about 0.05 m s^{-1} in the bottom-most bin. Measured nearbed velocities were about 0.03 m s^{-1}. For the periods of peak wind speed (commencing on days 348 and 354), the direction of water movement (Figures 2-6c to 2-6f) shifted to solidly align with the wave direction (Figure 2-6b) and the sustained wind direction (Figure 2-6a). This offers a clear cause-effect explanation of water motion in the nearshore of the lake.

2.4.2 Sediment properties

According to the Wentworth scale for sediment classification [*Wentworth*, 1922], the lakebed sediment at the study site is about 92 percent sand, 7 percent silt, and <1 percent clay (Figure 2-7). Additionally, the grab samples collected at the study site were consistent with a substrate map developed to assess fish habitat suitability [*Herold et al.*, 2007, Figure 5], which showed that sand dominated in the south shore of Lake Tahoe. After considering the particle size distributions from the grab samples, we assumed a representative grain size of 150 μm (0.15 mm), corresponding approximately to d_{10} (Figure 2-7). Furthermore, 150 μm (0.15 mm) corresponded to the peak in suspended sediment concentration by mass concentration during sediment resuspension events (Figure 2-13a). Using Equation (2-4), the critical shear stress for

incipient motion, $\tau_{critical}$, was therefore 0.081 Pa. Considering the finest material, 1 to 1.5 percent of the total particles by mass concentration were particles ≤10 μm (0.01 mm) and about 2 to 3 percent of the total were particles ≤20 μm (0.02 mm). Compared to shallow lakes, the nearshore of Lake Tahoe has coarse bed material. The study site generally lacks cohesive agents. At the Salton Sea, for example, the sediment has been characterized by a representative grain size of 25 μm [*Chung et al.*, 2009a], and at Lake Balaton (Hungary), the sediment has been characterized as predominantly clay and fine silt [*Luettich et al.*, 1990, Figure 2]. Even at Lake Constance (Europe), a deep lake, the nearshore sediment was characterized by a representative grain size of 60 μm [*Hofmann et al.*, 2011].

2.4.3 Bottom shear stress computation from field measurements and validation

In Figure 2-8 we present a comparison of bottom shear stress generated by wind-waves and currents, computed from the filtered velocity signals. As expected from other studies in shallow waters, the bottom shear stress due to wind-waves was much greater than that due to currents [see *Luettich et al.*, 1990; *Mian and Yanful*, 2004; *Chung et al.*, 2009a]. Also, in order to validate our proposed decomposition of the velocity field, we developed computations of bottom shear stress due to wind-waves using linear wave theory and assuming reasonable wave heights of 0.4, 0.5, and 0.6 m and wave periods of 2.4, 2.6, and 3 sec (since we did not accurately measure wave data with the AWAC). Table 2-2 shows those comparisons, indicating a satisfactory agreement, which improves with increasing wave heights.

The shear stress due to wind-waves exceeded the critical shear on 13 December (day 348) and 19 December (day 354). From Figure 2-5 we know that this resulted in an increase in the suspended sediment concentration so we argue that we have identified by experimental observation two instances of wind-wave induced sediment resuspension.

In Figure 2-9 we quantify the relative contribution of each component of bottom shear stress evaluated via Equation (2-2); we show that with increasing total bottom shear stress, the relative contribution of the each component becomes distinct. When the total bottom shear stress exceeded the critical shear stress, the contribution of the wind-wave component to total bottom shear stress was more than 80 percent. The contributions of the mean current and random motion components were less than 10 percent each. For large values of total bottom shear stress, we observed that it was attributed to wind-waves. When the currents were weak and there was very low wind, then the relative contributions of mean currents and random motions were sometimes greater than 10 percent each, but nevertheless the total bottom shear stress remained very small (i.e., much less than the critical shear stress). Overall, wind-waves contributed most meaningfully to the development of bottom shear stress.

2.4.4 Comparison of measured and modeled bottom shear stress

Measured and modeled bottom shear stress due to wind-waves

Figure 2-10 shows measured wind speed and direction from the Timbercove station as well as simulated significant wave height, wave period, and bottom shear stress resulting from wind-waves at the study site from 13 November to 21 December (days 318-355). Simulated sediment resuspension with the modified STWAVE occurred most often as a result of a northerly wind (see days 319, 334, and 339) of a magnitude of about 10 m s^{-1} or greater. Alternatively, when we simulated a comparably elevated wind speed from the southwest (about 200° clockwise from north), as we observed on 19 December (day 354), the modeled bottom shear stress due to wind-waves did not exceed the critical shear stress. Figure 2-10e shows that simulated wind-wave induced sediment resuspension events occurred five times at the study site during the complete study period.

A comparison of measured and modeled bottom shear stress due to wind-waves is shown in Figure 2-11. Generally, the agreement in bottom shear stress was in the presence of northerly winds. We generally found good agreement between measured and simulated results, particularly considering that the method of *Kim et al.* [2000] was developed for flows different than lake flows.

Modeled rate of sediment entrainment into suspension

With a sediment size of 150 μm (0.15 mm), the value of the explicit Reynolds particle number, Re_p, is 7.39, and the value we found in this work for the fitting parameter α is 0.75. For those times when the total bottom shear stress was in excess of the critical shear stress, the measured suspended sediment concentrations and $\tilde{u}_*/v_s$ were within the limits of Equation (2-6). Figure 2-12 shows good agreement between simulated and measured rates of sediment entrainment into suspension.

2.5 Implications of sediment resuspension on lake clarity

Swift et al. [2006] showed that particles with the greatest potential to negatively impact lake clarity were inorganic and smaller than 10 μm (0.01 mm). Fine inorganic particles strongly scatter light (as opposed to organic particles that strongly absorb light), resulting in decreased lake transparency [*Davies-Colley et al.*, 1993; *Kirk*, 2011]. Due to their small size, their overall mass concentration remains small, whereas the total number of particles is large, relative to larger particle size classes.

During storm periods, the particle size distributions of suspended particles by mass concentration had a dominance of particles of about 150 μm (0.15 mm) (Figure 2-13a), whereas during low-wind periods, the peak was less pronounced and shifted slightly, so there was a

dominance of particles of about 100 μm (0.10 mm) (Figure 2-13c). These larger particles, however, would tend to settle from the water column relatively quickly and therefore have a limited impact on water clarity. While the introduction of wind-wave energy could lead to the formation of flocs resulting in a shift in the dominant particle size class, this is unlikely at the study site due to its utter lack of cohesive material. Alternatively, under both storm and low-wind conditions, the characteristic distributions of suspended particles by particle count demonstrated a clear dominance of much smaller particles at about 4 μm (0.004 mm) (median-sized particles 3.76 and 4.43 μm)(Figure 2-13b and 2-13d). This suggests that irrespective of wind conditions, the predominance of fine particles that negatively impact nearshore lake clarity remained unchanged.

2.6 Discussion and conclusions

The combination of field observations, computations using field data, and modeling presented in this paper provided the first data set for nearshore sediment resuspension at Lake Tahoe during winter. In spite of relatively coarse lakebed sediment but owing to the shallow water depth and periodic strong and sustained winds, we have identified by experimental observation instances of wind-wave induced sediment resuspension in the nearshore of a deep lake. For those instances when the total bottom shear stress exceeded the critical shear stress resulting in sediment resuspension, wind-waves were the driving mechanism for sediment resuspension as the contribution to overall bottom shear stress from wind-waves was about 80 percent and from mean currents and random motions was equally about 10 percent each. The southern part of Lake Tahoe (at a water depth of about 5 m) exposed to typical winter weather may reasonably expect periodic sediment entrainment from the sediment-water interface to the water column of particle sizes on the order of 100 μm (0.10 mm). We were able to directly

quantify the total bottom shear stress and its components induced by wind-waves, mean currents, and random motions by successfully extending to a lake environment the method of *Kim et al.* [2000] (developed for flows different than lake flows).

We simulated bed shear stress with the use of a modified version of STWAVE, in which we changed the formulation of the loss of energy density due to friction. This extended the model's applicability to a viscous-dominated flow regime. The simulated bottom shear stress from the modified STWAVE was in good agreement with the measured bottom shear stress attributed to wind-waves, particularly when wind direction favored a larger fetch, and suggested that the modified STWAVE is a reliable tool to assess sediment resuspension in a lake. We believe this was the first application of the wind-wave model STWAVE to simulate wind-wave induced bottom shear stress for viscous-dominated flow typical in lakes and complements a body of research in coastal marine environments using advanced wind-wave models to address a varied set of problems. Also, we observed agreement between simulated and measured rates of sediment entrainment into suspension according to a slightly modified formula of *García and Parker* [1991].

In situ measurements of suspended sediment concentration and particle size distribution collected with the LISST-100X revealed that the predominance of fine particles (by particle count) was unchanged by storm-related sediment resuspension. Therefore, the evidence to date does not suggest that nearshore sediment resuspension contributes to increased suspended sediment concentration of the size class (≤10 μm) that most negatively impacts lake clarity. Nevertheless, sediment resuspension resulted in a marked increase of suspended sediment concentration by mass concentration of particles on the order of 100 μm (0.1 mm), particles too

large to persist in the water column. Therefore, we cannot assume that nearshore sediment resuspension contributes to declining nearshore clarity at Lake Tahoe.

2.7 Appendix 2-A: Validation of the modification of the STWAVE code

A subset of field measurements that included surface wave characteristics collected at the Salton Sea from 4 August to 29 November 2005 and published by *Chung et al.* [2009a; 2009b] were used to validate numerical modeling results obtained from the modified full-plane version of STWAVE. The field measurements of significant wave height and period were obtained using the AWAC. Figure 2-A1 shows good agreement between measured and modified STWAVE-simulated wave heights and periods.

Acknowledgements

This research was supported by the University of California, Davis and a grant from the US Department of Agriculture Forest Service Pacific Southwest Research Station using funds provided by the Bureau of Land Management through the sale of public lands as authorized by the Southern Nevada Public Land Management Act. The lead author was supported for two years by the Eugene Cota-Robles Fellowship from the Office of Graduate Studies, University of California, Davis. The AWAC was provided on loan from the California Department of Water Resources. The Vector was provided as a Nortek 2008 Student Equipment Grant Award. The ADVOcean Probe was provided on loan from the US Geological Survey. Jane McKee Smith at the US Army Corps of Engineers provided the source code of STWAVE in Fortran, for which we are grateful. We also wish to acknowledge Brant Allen, Steve Andrews, Laura Doyle, Alex Forrest, Daret Kehlet, Bill Sluis, Todd Steissberg, and Feng Yu for their invaluable help. We equally acknowledge David Schoellhamer and anonymous reviewers for improving this manuscript.

Notation

α fitting parameter, dimensionless.

β wave direction, degrees.

ρ water density, kg m^{-3}.

ρ_s sediment density, kg m^{-3}.

τ bottom shear stress, Pa.

τ_c^* critical Shields parameter, dimensionless.

$\tau_{critical}$ critical bottom shear stress, Pa.

τ_{curr} bottom shear stress due to currents, Pa.

τ_{waves} bottom shear stress due to wind-waves, Pa.

ν kinematic viscosity of water, m^2 s^{-1}.

ω wave angular frequency, rad s^{-1}.

a distance above bed that near-equilibrium nearbed suspended sediment concentration is measured, m.

A constant in the García and Parker formula, dimensionless.

A_w amplitude of particle motion just above the boundary layer, m.

$b_{i,i=1-5}$ constants in the Dietrich formula, dimensionless.

c_{ae} near-equilibrium suspended sediment concentration, µL L^{-1} or kg m^{-3}.

C_f bottom-friction coefficient, dimensionless.

C_1 proportionality constant in the expression of bottom shear stress, dimensionless.

C_2 proportionality constant in the expression of bottom shear stress, dimensionless.

D representative grain size (diameter), m.

d_{10} diameter for which 10 percent of the sediment mass is smaller, m.

E measure of turbulent kinetic energy, $m^2\ s^{-2}$.

E_S sediment entrainment coefficient, dimensionless.

f wave frequency, Hz.

g acceleration due to gravity, $m\ s^{-2}$.

H water depth, m.

H_w significant wave height, m.

k wave number, $rad\ m^{-1}$.

n power in similarity variable for uniform sediment, dimensionless.

R submerged specific gravity, dimensionless.

Re_p explicit particle Reynolds number, dimensionless.

Re_w wave Reynolds number, dimensionless.

S spectra, $W\ Hz^{-1}$.

T_p wave period, s.

$\boldsymbol{u}$ water velocity vector, $m\ s^{-1}$.

$\overline{\boldsymbol{u}}$ mean component of the velocity vector, $m\ s^{-1}$.

$\boldsymbol{u}'$ fluctuating component of the velocity vector, $m\ s^{-1}$.

$\boldsymbol{u}_{mean\ currents}$ water velocity signal attributed to mean currents, $m\ s^{-1}$.

$\boldsymbol{u}_{random\ motions}$ water velocity signal attributed to random motions, $m\ s^{-1}$.

$\boldsymbol{u}_{total}$ total water velocity signal, $m\ s^{-1}$.

$\boldsymbol{u}_{wind-waves}$ water velocity signal attributed to wind-waves, $m\ s^{-1}$.

u component of water velocity aligned with x in the Cartesian coordinate system, m s^{-1}.

u_* shear velocity, m s^{-1}.

$\tilde{u}_*$ skin shear velocity, m s^{-1}.

$u_{b,rms}$ magnitude of bottom root-mean-square orbital velocity, m s^{-1}.

v component of water velocity aligned with y in the Cartesian coordinate system, m s^{-1}.

v_S sediment fall velocity, m s^{-1}.

w component of water velocity aligned with z in the Cartesian coordinate system, m s^{-1}.

x Cartesian coordinate system aligned in the east-west direction.

y Cartesian coordinate system aligned in the north-south direction.

z Cartesian coordinate system aligned vertically.

Z_u similarity variable for uniform sediment for García and Parker formula, dimensionless.

References

Andrews, S., D. Nover, S. G. Schladow, and J. E. Reuter (2011), Limitations of laser diffraction for measuring fine particles in oligotrophic systems: Pitfalls and potential solutions, *Water Resour. Res.*, *47*, W05523, doi: 10.1029/2010WR009837.

Bombardelli, F. A., and M. H. García (1999), Numerical simulation of wind-induced resuspension of bed sediments in shallow lakes, Proc. 1999 Int. Water Resources Engineering Conf., ASCE, Seattle, WA, USA.

Bombardelli, F.A., and M.H. García (2003), Hydraulic design of large diameter pipes, *J. Hydraul. Eng.*, *129(11)*, 839-846.

Bombardelli, F. A., and P. A. Moreno (2012), Exchange at the bed sediments-water column interface, in *Fluid Mechanics of Environmental Interfaces*, 2nd ed., edited by Gualtieri C., and D.T. Mihailovic, Taylor & Francis, London.

Bunya, S., J. C. Dietrich, J. J. Westerink, B. A. Ebersole, J. M. Smith, J. H. Atkinson, R. Jensen, D. T. Resio, R. A. Luettich, C. Dawson, V. J. Cardone, A. T. Cox, M. D. Powell, H. J. Westerink, and H. J. Roberts (2010), A high-resolution coupled riverine flow, tide, wind, wind wave, and storm surge model for southern Louisiana and Mississippi. Part I: Model development and validation, *Mon. Weather Rev.*, *138(2)*, 345-377, doi: 10.1175/2009MWR2906.

California Geological Survey. *Geologic Map of the Lake Tahoe Basin, California and Nevada* [map], 1:100,000. Regional Geologic Map Series, Map No. 4. California Department of Conservation, 2005.

Chung, E. G., F. A. Bombardelli, and S. G. Schladow (2009a), Sediment resuspension in a shallow lake, *Water Resour. Res.*, *45*, W05422, doi: 10.1029/2007WR006585.

Chung, E. G., F. A. Bombardelli, and S. G. Schladow (2009b), Modeling linkages between sediment resuspension and water quality in a shallow, eutrophic, wind-exposed lake. *Ecol. Modell., 220(9-10)*, 1251-1265, doi: 10.1016/j.ecolmodel.2009.01.038

Coastal Engineering Research Center (CERC) (1984), Shore protection manual, U.S. Army Corps of Eng., Washington, D.C.

Davies-Colley, R. J., W. N. Vant, and D. G. Smith (1993), *Colour and Clarity of Natural Waters: Science and Management of Optical Water Quality*, Ellis Harwood Limited, London, UK.

Davies-Colley, R. J. and Smith, D. G. (2001), Turbidity, suspended sediment, and water clarity: A review. *J. Am. Water Resour. Assoc.*, *37*, 1085–1101, doi: 10.1111/j.1752-1688.2001.tb03624.x

Dietrich, J. C., S. Bunya, J. J. Westerink, B. A. Ebersole, J. M. Smith, J. H. Atkinson, R. Jensen, D. T. Resio, R. A. Luettich, C. Dawson, V. J. Cardone, A. T. Cox, M. D. Powell, H. J. Westerink, and H. J. Roberts (2010), A high-resolution coupled riverine flow, tide, wind,

wind wave, and storm surge model for southern Louisiana and Mississippi. Part II: Synoptic description and analysis of hurricanes Katrina and Rita, *Mon. Weather Rev.*, *138(2)*, 378-401, doi: 10.1175/2009MWR2907.1.

Dietrich, W. E. (1982), Settling velocities of natural particles, *Water Resour. Res.*, *18(6)*, 1615-1626.

García, M. H., and G. Parker (1991), Entrainment of bed sediment into suspension, *J. Hydraul. Eng.*, *117*, 414-435, doi: 10.1061/(ASCE)0733-9429(1991)117:4(414).

García, M. H., and G. Parker (1993), Experiments on the entrainment of sediment into suspension by a dense bottom current, *J. Geophys. Res.*, *98*, 4793-4807, doi: 10.1029/92JC02404.

Gioia, G., and F.A. Bombardelli (2002), Scaling and similarity in rough channel flows, *Phys. Rev. Letters*, *88(1)*, 014501.

Goldman, C. R. (1988), Primary productivity, nutrients, and transparency during the early onset of eutrophication in ultra-oligotrophic Lake Tahoe, California-Nevada, *Limnol. Oceanogr.*, *33*, 1321-1333.

Håkanson, L. and M. Jansson (1983), *Principles of Lake Sedimentology*, Springer-Verlag, Berlin, Germany.

Hamilton, D. P., and S. F. Mitchell (1996), An empirical model for sediment resuspension in shallow lakes, *Hydrobiologia*, *317*, 209-220, doi: 10.1007/BF00036471.

Hawley, N., B. M. Lesht, and D. J. Schwab (2004), A comparison of observed and modeled surface waves in southern Lake Michigan and the implications for models of sediment resuspension, *J. Geophys. Res.*, *109*, C10S03, doi: 10.1029/2002JC001592.

Herold, M., J. Metz, and J. S. Romsos (2007), Inferring littoral substrates, fish habitats, and fish dynamics of Lake Tahoe using IKONOS data, *Can. J. Remote Sensing*, *33(5)*, 445-456.

Hofmann, H., A. Lorke, and F. Peeters (2011), Wind and ship wave-induced resuspension in the littoral zone of a large lake, *Water Resour. Res.*, *47*, W09505, doi: 10.1029/2010WR010012.

Holthuijsen, L.H. (2007), *Waves in Ocean and Coastal Waters*, University Press, Cambridge, UK.

Horne, A. J. and C. R. Goldman (1994), *Limnology*, 2nd ed., McGraw-Hill, Inc., New York, USA.

Kamphuis, J. W. (1975), Friction factor under oscillatory waves, *J. Waterw. Harbors Coastal Eng. Div., 101*, 135-144.

Kim, S. C., C. T. Friedrichs, J. P. Y. Maa, and L. D. Wright (2000), Estimating bottom stress in tidal boundary layer from acoustic Doppler velocimeter data, *J. Hydraul. Eng.*, *126(6)*, 399-406, doi: 10.1061/(asce)0733-9429(2000)126:6(399).

Kirk, J. T. O. (2011), *Light and Photosynthesis in Aquatic Ecosystems*, 3rd ed., University Press, Cambridge, UK.

Komar, P.D., and M. C. Miller (1974), The initiation of oscillatory ripple marks and the development of plane-bed at high stresses under waves, *Jour. Sed. Petrology, 45(3)*, 697-703.

Lou, J., D. J. Schwab, D. Beletsky, and N. Hawley (2000), A model of sediment resuspension and transport dynamics in southern Lake Michigan, *J. Geophys. Res.*, *105*, C3, 6591-6610.

Luettich, R. A., D. R. F. Harleman, and L. Somlyody (1990), Dynamic behavior of suspended sediment concentrations in a shallow lake perturbed by episodic wind events, *Limnol. Oceanogr.*, *35(5)*, 1050-1067.

Madsen, O.S., and W. D. Grant (1975), Threshold of sediment movement under oscillatory waves, *Jour. Sed. Petrology, 45(1)*, 360-361.

Massey, T. C., M. E. Anderson, J. M. Smith, J. Gomez, and R. Jones (2011), STWAVE: Steady-state spectral wave model user's manual for STWAVE, Version 6.0, ERDC/CHL SR-11-1. Vicksburg, MS, U.S. Army Engineer Research and Development Center, Vicksburg, MS.

Massoudieh, A., F. A. Bombardelli, and T. R. Ginn (2010), A biogeochemical model of contaminant fate and transport in river waters and sediments, *J. Contam. Hydrol.*, 112, 103-117, doi: 10.1016/j.jconhyd.2009.11.001.

Mian, M. H., and E. K. Yanful (2003), Tailings erosion and resuspension in two mine tailings ponds due to wind waves, *Adv. Environ. Res.*, *7*, 745-765, doi: 10.1016/S1093-0191(02)00027-8.

Mian, M. H., and E. K. Yanful (2004), Analysis of wind-driven resuspension of metal mine sludge in a tailings pond, *J. Environ. Eng. Sci.*, *3*, 119-135, doi: 10.1139/s03-076.

Parker, G. (2004), *1D sediment transport morphodynamics with applications to rivers and turbidity currents*, e-book, Natl. Cent. For Earth Surf. Dyn., Minneapolis, Minn. (Available at http://cee.uiuc.edu/people/parkerg/)

Parker, G., C. M. Toro-Escobar, M. A. Ramey, and S. Beck (2003), The effect of floodwater extraction on the morphology of mountain streams, *J. Hydraul. Eng.*, *129*, 885-895, doi: 10.1061/(ASCE)0733-9429(2003)129:11(885).

Raudkivi, A. J. (1998), *Loose Boundary Hydraulics*, 3rd ed., Pergamon Press, Oxford, UK.

Schladow, S. G., F. J. Rueda, W. E. Fleenor, and E. G. Chung (2006), Predicting the effects of configuration changes on Salton Sea stratification using a three-dimensional hydrodynamic model, Report to CH2M HILL and California Department of Water Resources, TERC Report 06-007.

Shields, I. A., 1936, *Anwendung der ahnlichkeitmechanik und der turbulenzforschung auf die gescheibebewegung,* Mitt. Preuss Ver.-Anst., 26, Berlin, Germany.

Smith, J. M. (2007), Full-plane STWAVE: II. Model overview, ERDC TN-SWWRP-07-5. Vicksburg, MS, U.S. Army Engineer Research and Development Center, Vicksburg, MS, https://swwrp.usace.army.mil/.

Smith, J. M., A. R. Sherlock, and D. T. Resio (2001), STWAVE: Steady-state spectral wave model user's manual for STWAVE, Version 3.0, ERDC/CHL SR-01-1. Vicksburg, MS, U.S. Army Engineer Research and Development Center, Vicksburg, MS.

Smith, J.M., and A. Zundel (2006), STWAVE-FP in SMS: Graphical interface. Coastal and Hydraulics Engineering Technical Note CHETN I-69, U.S. Army Engineer Research and Development Center, Vicksburg, MS, http://chl.erdc.usace.army.mil/

Sumer, B. M., and J. Fredsøe (1997), *Hydrodynamics around Cylindrical Structures*, from *Advanced Series on Ocean Engineering, 12,* World Scientific Publishing, London, U.K.

Sutherland, A. J. (1967), Proposed mechanism for sediment entrainment by turbulent flows, *J. Geophys. Res.*, *72(24),* 6183-6194.

Swift, T. J., J. Perez-Losada, S. G. Schladow, J. E. Reuter, A. D. Jassby, and C. R. Goldman (2006), Water clarity modeling in Lake Tahoe: Linking suspended matter characteristics to Secchi depth, *Aquat. Sci.*, *68(1),* 1-15, doi: 10.1007/s00027-005-0798-x.

Taylor, K., R. Susfalk, M. Shanafield, and S. G. Schladow (2004), Near-shore clarity at Lake Tahoe: Status and causes of reduction, Report to Lahontan Water Board (CA), Nevada Division of State Lands, and Tahoe Regional Planning Agency.

Van Rijn, L. C. (1984), Sediment transport: 2. Suspended-load transport, *J. Hydraul. Eng.*, 110, 1613-1641, doi: 10.1061/(ASCE)0733-9429(1984)110:11(1613).

Wentworth, C. K. (1922), A scale of grade and class terms for clastic sediments, *J. Geology*, *30(5)*, 377-392.

Wetzel, R. G. (1983), *Limnology*, 2nd ed., Saunders, Philadelphia, USA.

Table 2-1. Field measurements

Parameter(s) measured	Instrument	Location(s)	Sensor height(s) or orientation	Period	Sampling rate/interval	Sampling duration	Burst interval
Wind speed and direction	Met One Windset 3-cup anemometers	Timbercove[a] USCG[b]	5 m above water level	ongoing	10 min	NA	NA
Vertical profiles of water temperature	Onset Stow Away TidbiT temperature loggers	N 38°56.57' W120°1.18'	0.2, 0.5, 1.0, 1.5, 2.0, 2.5, 3.0, and 3.5 m above lakebed	13 Nov 2008-14 Jan 2009	5 min	NA	NA
Vertical profiles of water currents and surface wave properties	Nortek AWAC	N 38°56.57' W120°1.18'	Bottom-mounted	13 Nov 2008-14 Jan 2009	10 min (currents) 1 h (waves)	NA	NA
Nearbed velocity	Sontek ADVOcean Probe	N 38°56.46' W120°1.17'	0.20 m above lakebed	13 Nov-21 Dec 2008	10 Hz	3 min	1 h
Nearbed velocity	Nortek Vector	N 38°56.46' W120°1.17'	0.10 m above lakebed	13 Nov-19 Dec 2008	64 Hz	2 min	2 h
Suspended sediment concentration and particle size distribution	LISST-100X	N 38°56.46' W120°1.17'	0.20 m above lakebed	11 Dec 2008-14 Jan 2009	1 Hz	2 min	2 h
Lakebed sediment characteristics	Grab samples (2)	N 38°56.46' W120°1.17'	NA	22 July 2008	NA	NA	NA

[a]The Timbercove meteorological station is located at the end of a long pier 270 m offshore and about 4.5 km from the study site at N 38° 56.99' latitude and W 119° 58.07' longitude.

[b]The USCG meteorological station is located 75 m offshore and about 30 km from the study site at N 39° 10.84'latitude and W 120° 07.16'longitude.

NA=not applicable

Table 2-2. Comparison of shear stress attributed to waves (τ_{waves}) coming from Linear Wave Theory (LWT) and Modified STWAVE, considering three scenarios of wave height and period and for a water depth of 5 m (the water depth at the study site).

Parameter	Scenario 1	Scenario 2	Scenario 3
Wave height (m)	0.4	0.5	0.6
Wave period (sec)	2.4	2.6	3
τ_{waves} – LWT (Pa)	0.051	0.095	0.187
τ_{waves} – Modified STWAVE (Pa)	0.075	0.100	0.175

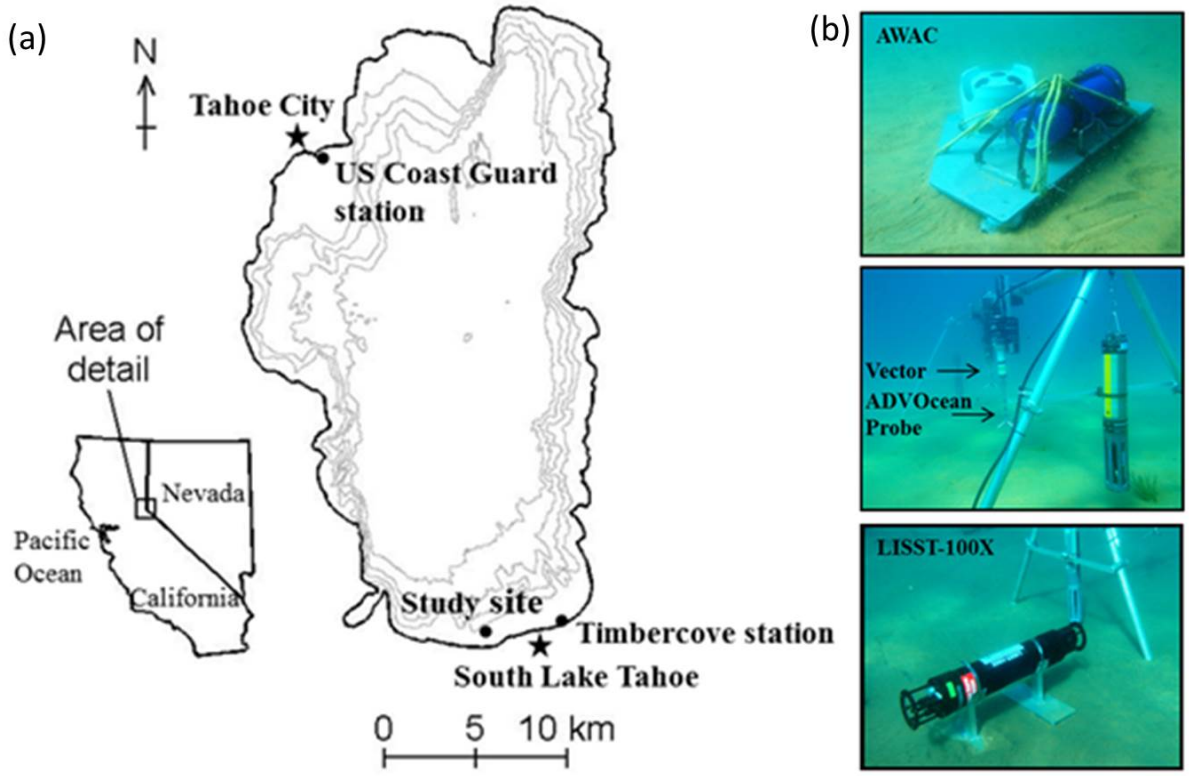

Figure 2-1. (a) Lake Tahoe bathymetry and orientation. Meteorological data were collected at the Timbercove and US Coast Guard stations. Lake measurements were made at the location indicated as the study site. Contours are shown at 100 m intervals. Lake Tahoe is located at approximately 39°N latitude and 120°W longitude. (b) In situ lake measurements were collected with instruments as shown.

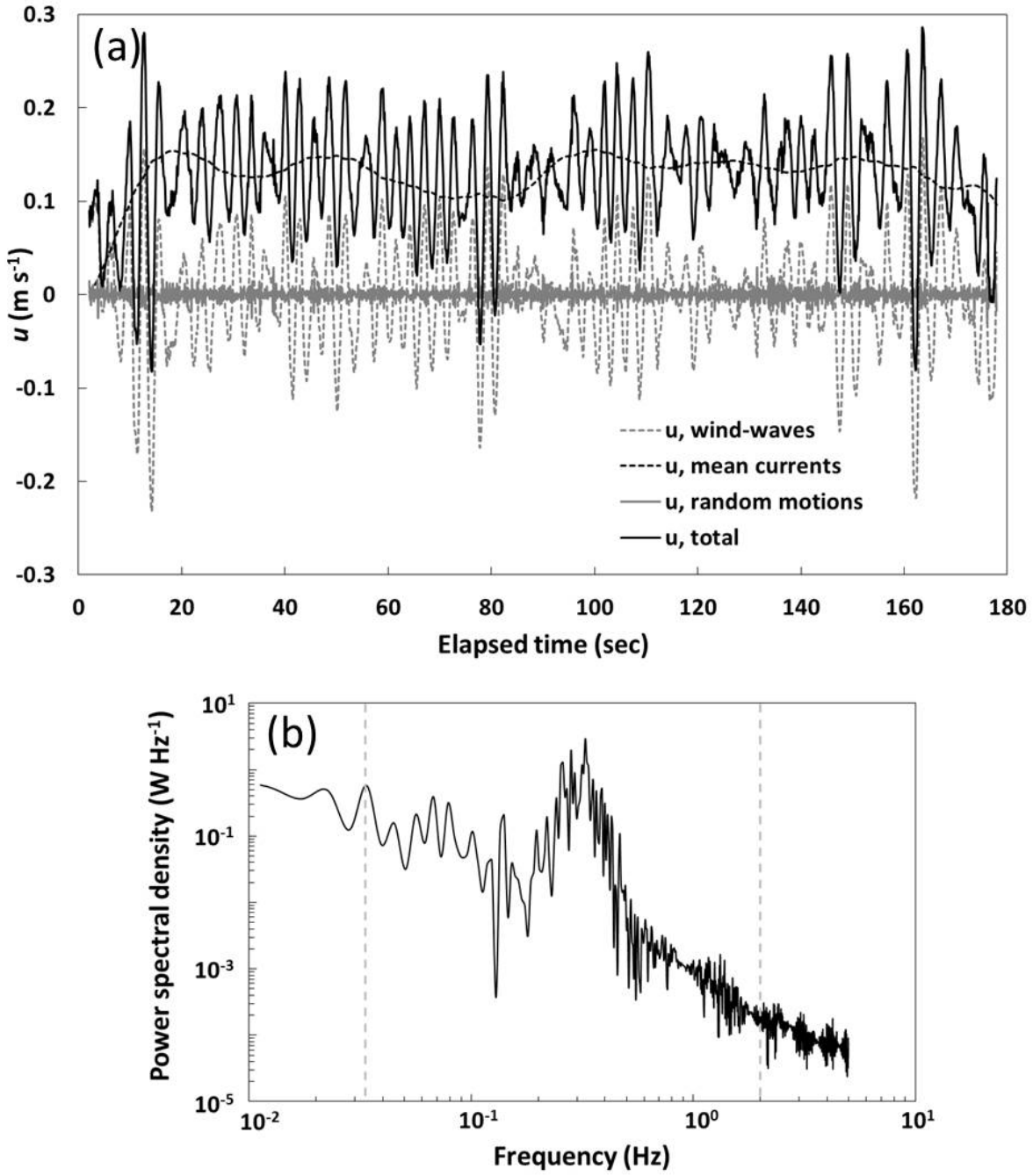

Figure 2-2. (a) East-west (*u*) component of the velocity vector measured during one 3-min sampling burst with the ADVOcean Probe on 13 December 2008 at 7 a.m. Data collected for each directional component of each burst were filtered to partition the velocity contribution from wind-waves, mean currents, and random motions. (b) Power spectral density. The peak of the power spectral density is at 0.33 Hz (corresponding to a wave period equal to 3 sec). The vertical dashed lines demarcate the so-called wind-wave band from 0.033 to 2 Hz (corresponding to wave periods between 0.5 and 30 sec).

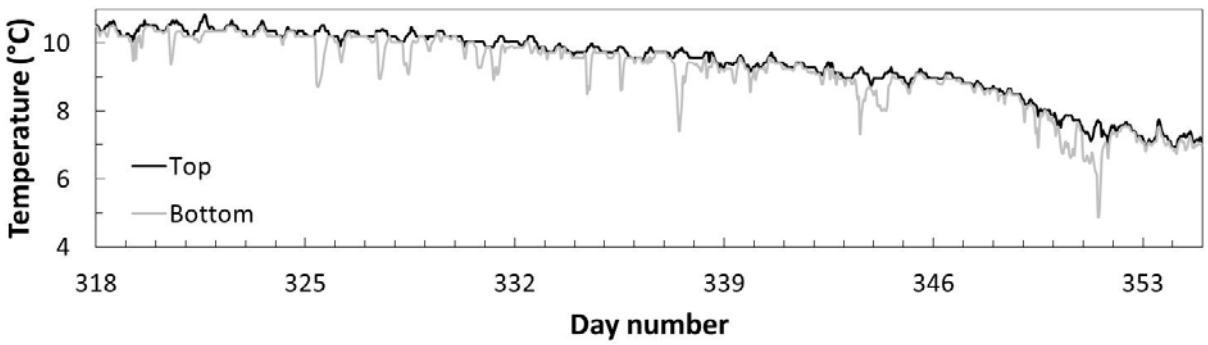

Figure 2-3. Water temperature observed from 13 November through 19 December 2008 at the study site for top and bottom thermistors. The temperature at the top thermistor remains nearly equal to or greater than that of the bottom thermistor, implying thermodynamic neutrality or stability.

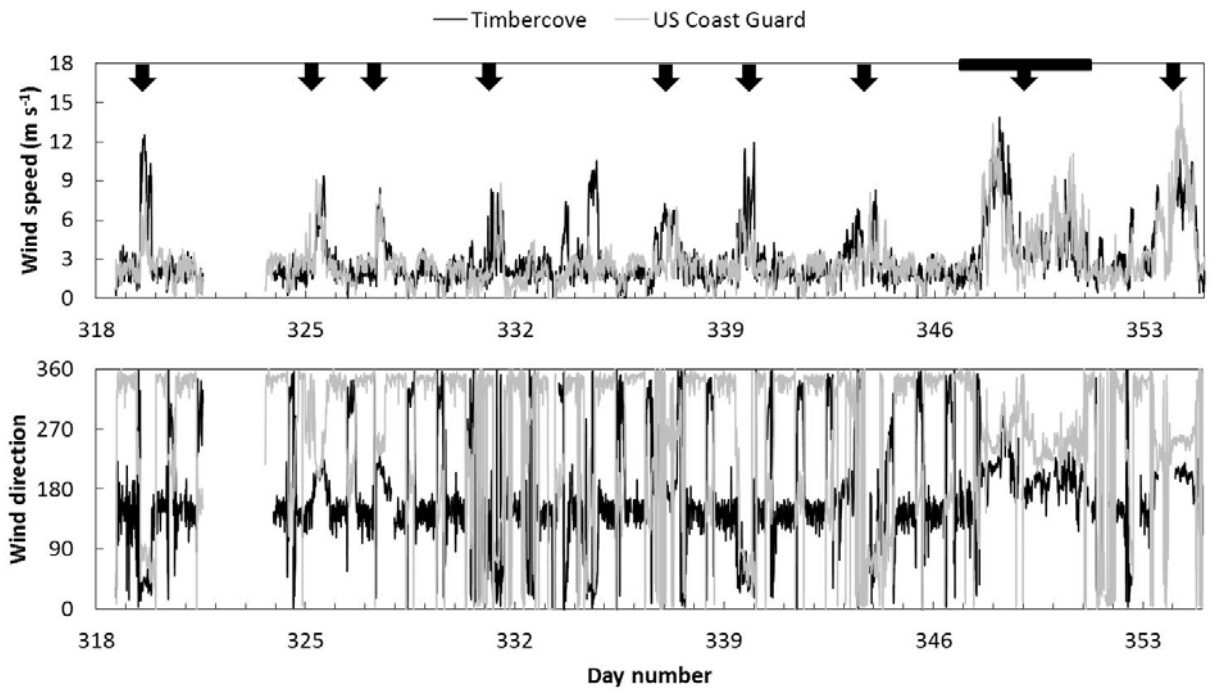

Figure 2-4. Meteorological data from 13 November through 19 December 2008 at the Timbercove and US Coast Guard stations. Arrows (and overbar at days 347 to 351) indicate instances of elevated wind speed and alignment (or near-alignment) of the wind direction at both stations. Wind direction is denoted as degrees clockwise from north.

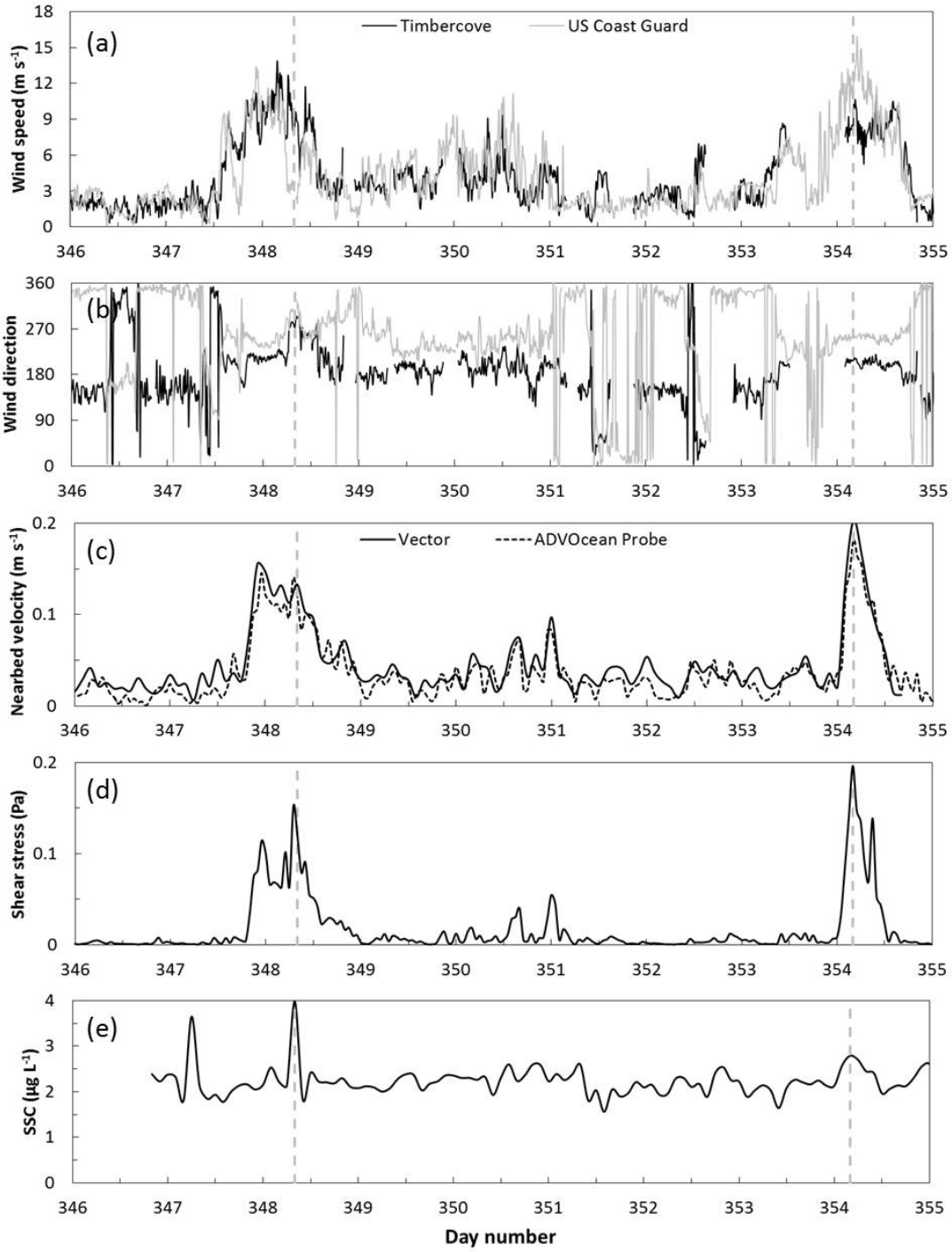

Figure 2-5. Comparison of observed variables from 11 through 19 December 2008: (a) wind speed and (b) wind direction (degrees clockwise from north) measured at Timbercove and USCG stations, (c) burst-averaged nearbed velocity resolved in the horizontal plane at 0.20 m (Vector) and 0.10 m (ADVOcean Probe) from the bottom, and (d) total bottom shear stress computed according to Equation (2-2) from data collected by the ADVOcean Probe, and (e) nearbed suspended sediment concentration (SSC). Dashed vertical lines indicate the simultaneous occurrence of peaks in several variables.

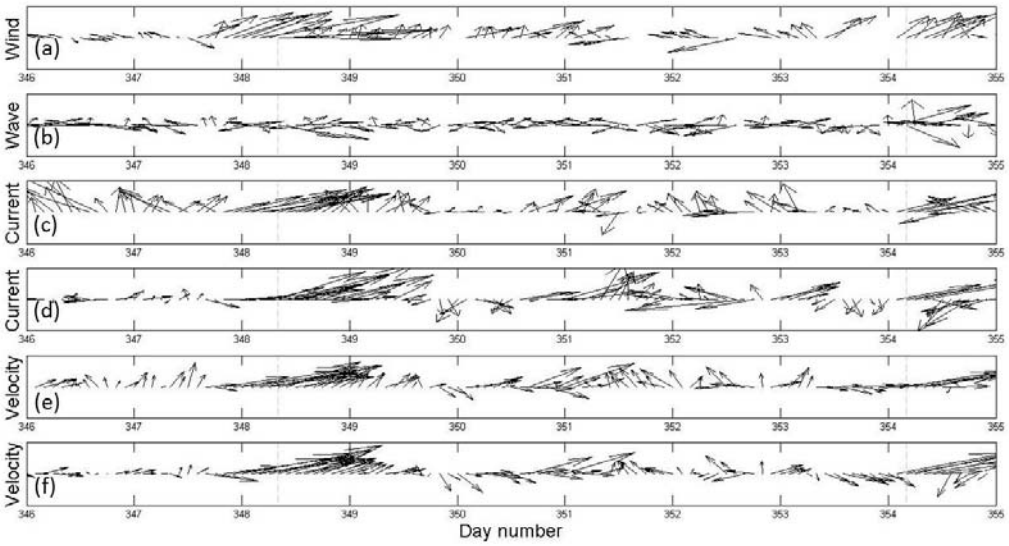

Figure 2-6. Vector plot of measured variables from 11 to 19 December 2008: (a) wind measured at Timbercove station, (b) significant wave height, (c) hourly-averaged currents near the water surface, (d) hourly-averaged currents at the bottom-most AWAC bin, (e) burst-averaged nearbed velocity at 0.20 m from bottom, and (f) burst-averaged nearbed velocity at 0.10 m from bottom. Dashed vertical lines indicate concurrence of wind-driven sediment resuspension.

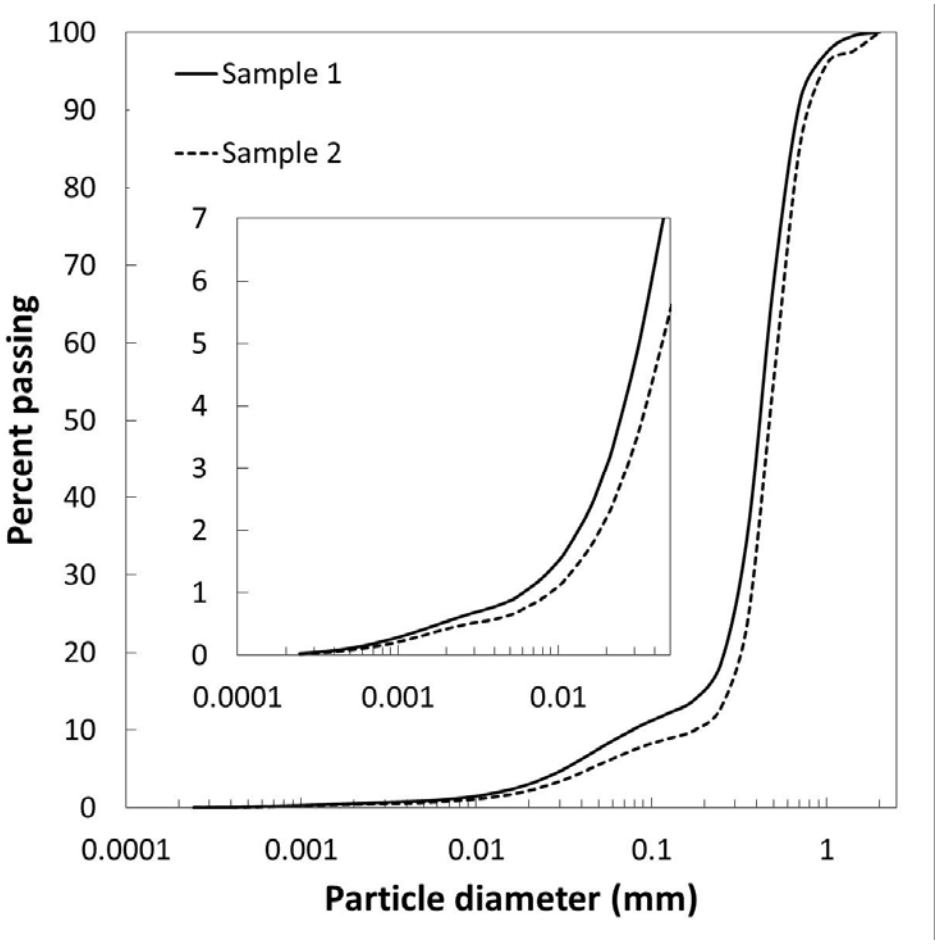

Figure 2-7. Particle size distribution of lakebed sediment at the study site. (inset) Detailed view of the distribution of particles on the order of 10 µm (0.01 mm).

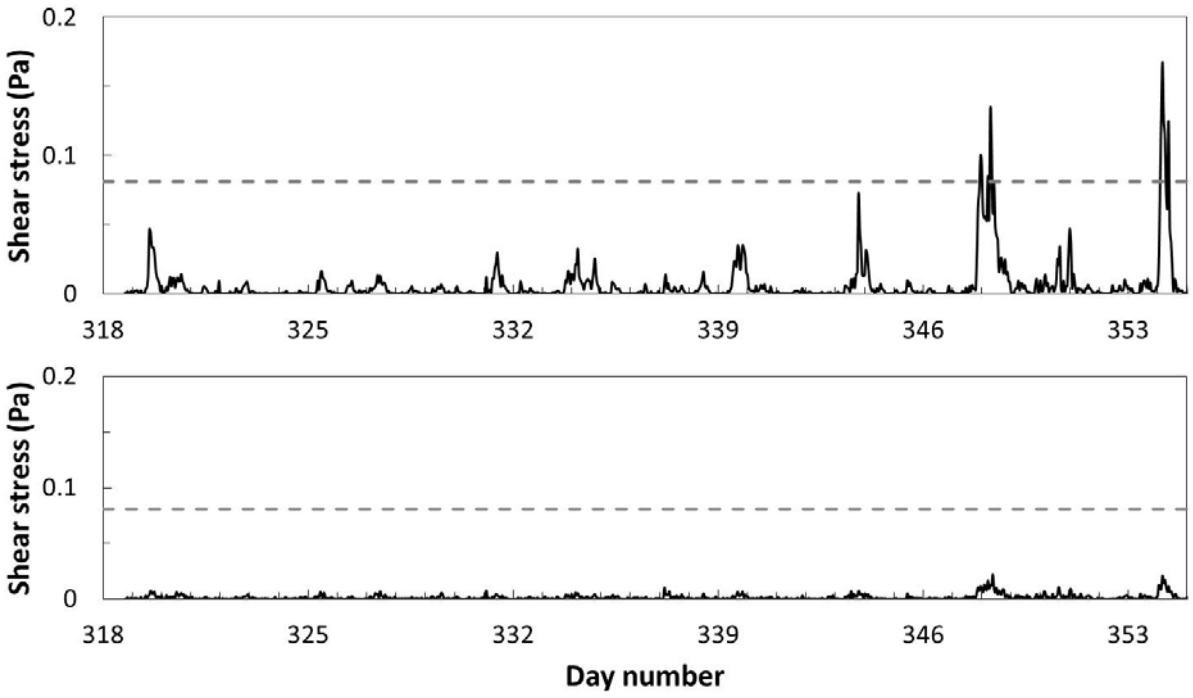

Figure 2-8. Comparison of bottom shear stress generated by (top) wind-waves and (bottom) currents, computed according to Equation (2-2) from data collected by the ADVOcean Probe. The dashed line at 0.081 Pa indicates the critical shear stress for incipient motion for a representative particle size of 150 μm.

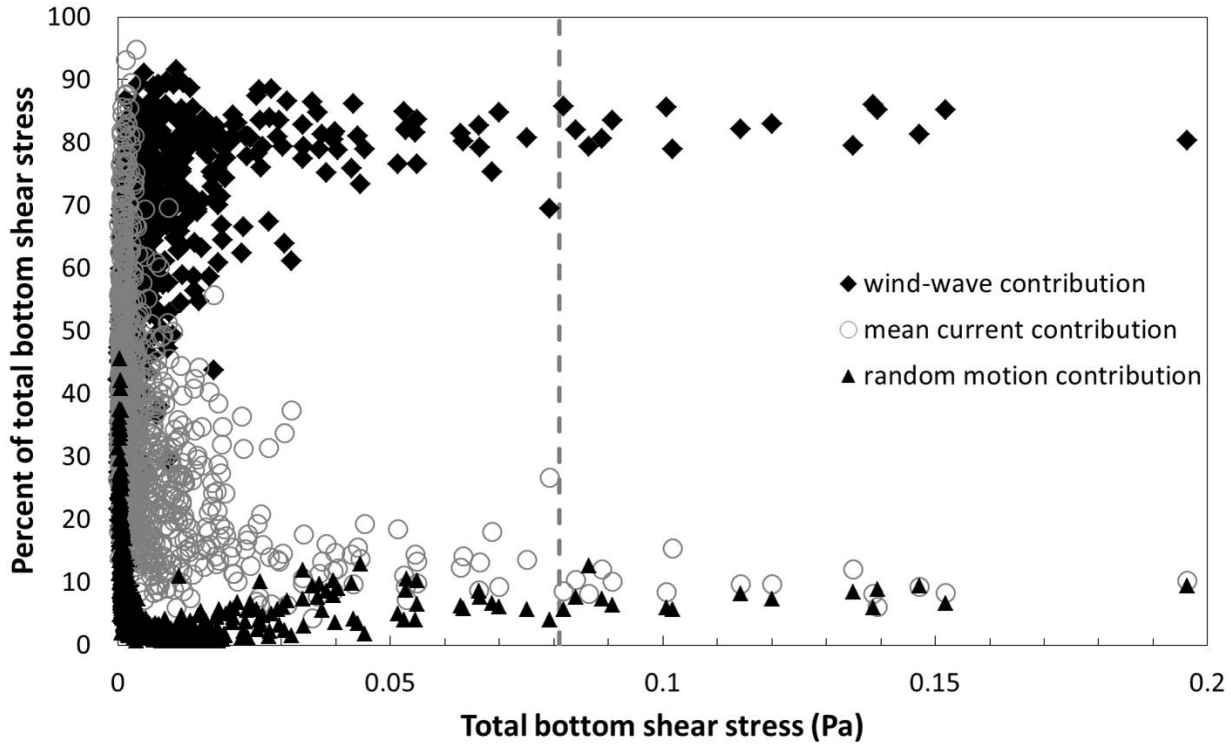

Figure 2-9. Contributions in percent of wind-waves, mean currents, and random motions to total bottom shear stress, computed according to Equation (2-2) from data collected by the ADVOcean Probe, as a function of total bottom shear stress. The dashed line at 0.081 Pa indicates the critical shear stress for incipient motion for a representative particle size of 150 μm.

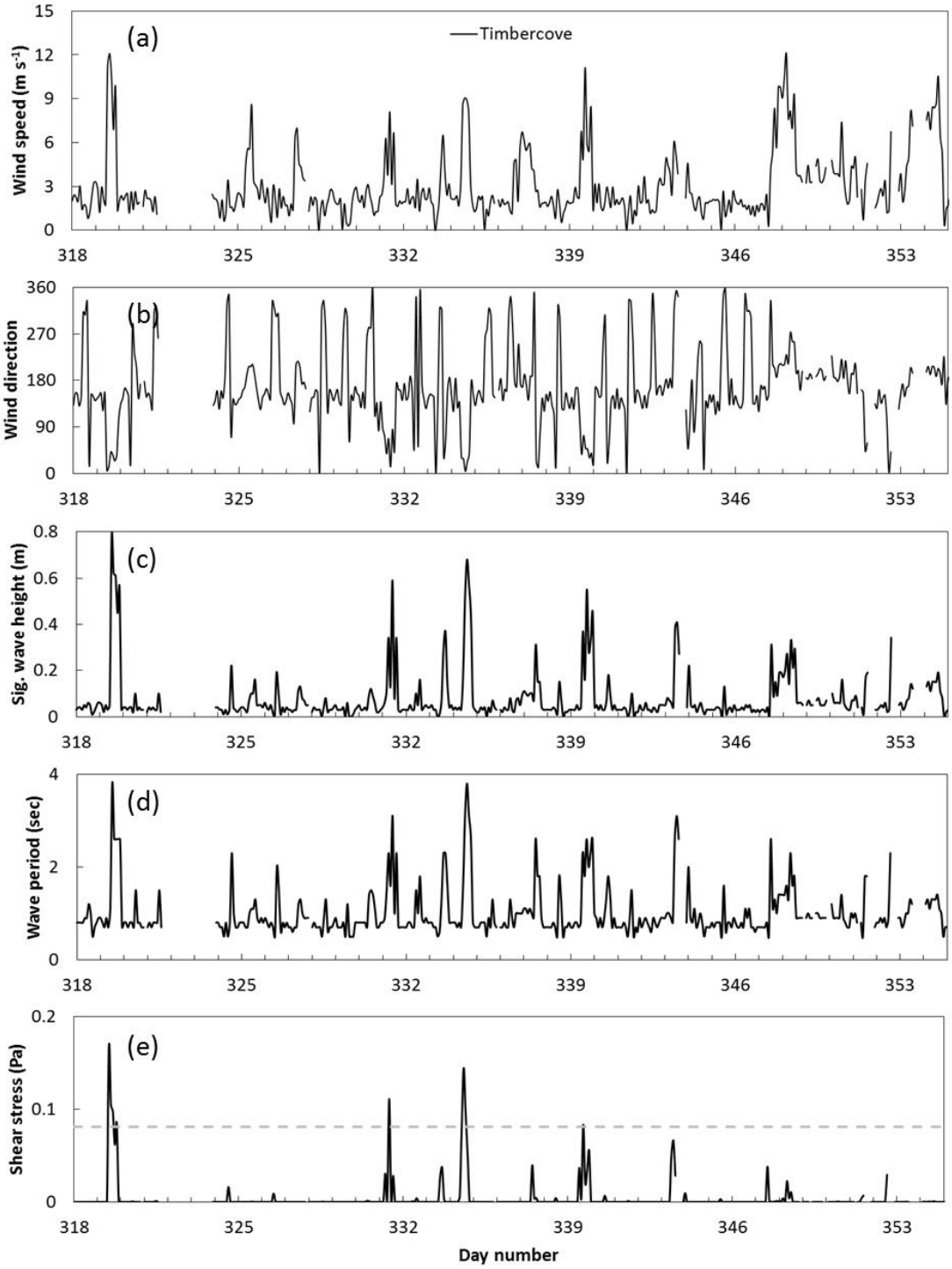

Figure 2-10. Input variables of (a) wind speed and (b) wind direction (measured degrees clockwise from north) and results simulated with the modified STWAVE of (c) significant wave height, (d) wave period, and (e) bottom shear stress due to wind-waves. The horizontal dashed line at 0.081 Pa indicates the critical shear stress for incipient motion for a representative particle size of 150 μm.

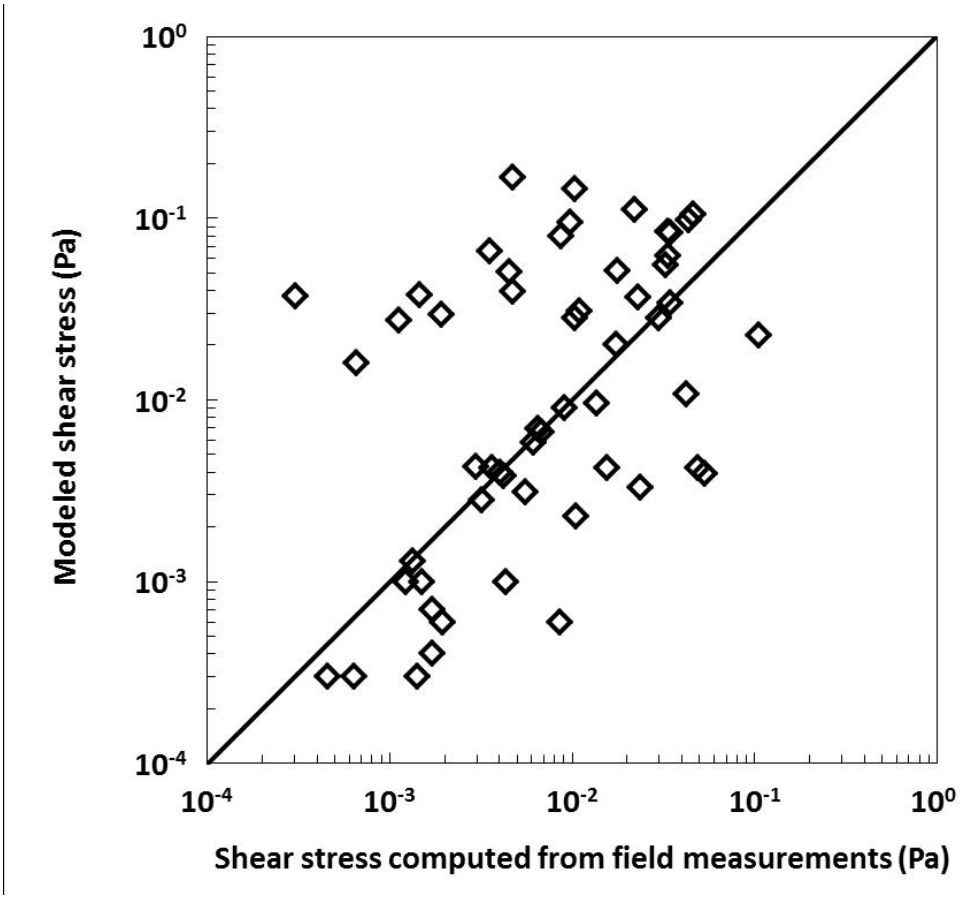

Figure 2-11. Comparison of bottom shear stress directly estimated from field data and modeled with the modified STWAVE, both attributed to wind-waves. For all wind directions except southerly (from 135 to 225 degrees clockwise from north); thus excluding the times when the wind was of shortest fetch and would not be reasonably represented by the model.

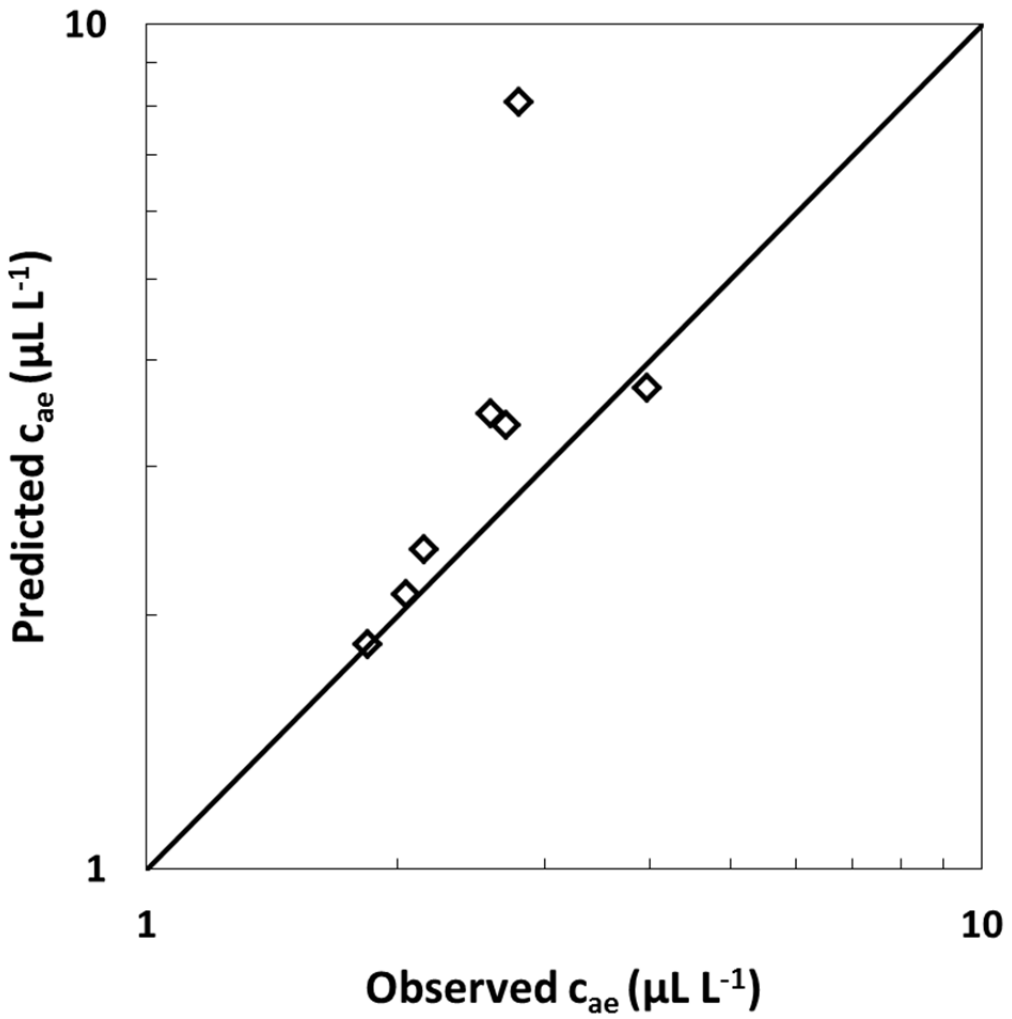

Figure 2-12. Comparison of predicted and observed values of equilibrium nearbed concentration using Equation (2-6) for those instances when the bottom shear stress exceeds the critical shear stress for incipient motion for a particle size of 150 µm.

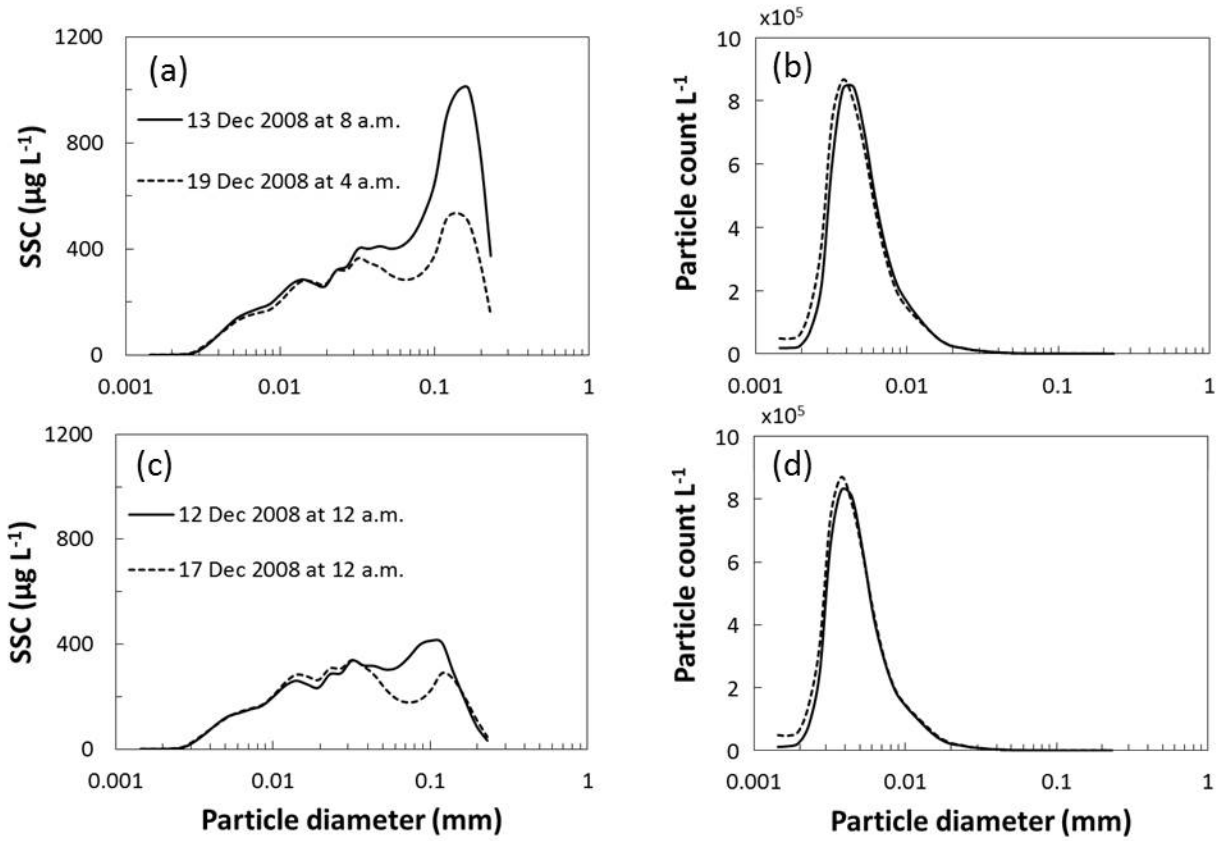

Figure 2-13. Characteristic particle size distributions of suspended particles by mass concentration at the study site during (a) storm periods (13 December 2008 at 8 a.m. and 19 December 2008 at 4 a.m.) and (c) low-wind periods (12 December 2008 at 12 a.m. and 17 December 2008 at 12 a.m.). Characteristic distributions of suspended particles by particle count at the study site during (b) storm periods (same dates as (a)) and (d) low-wind periods (same dates as (c)).

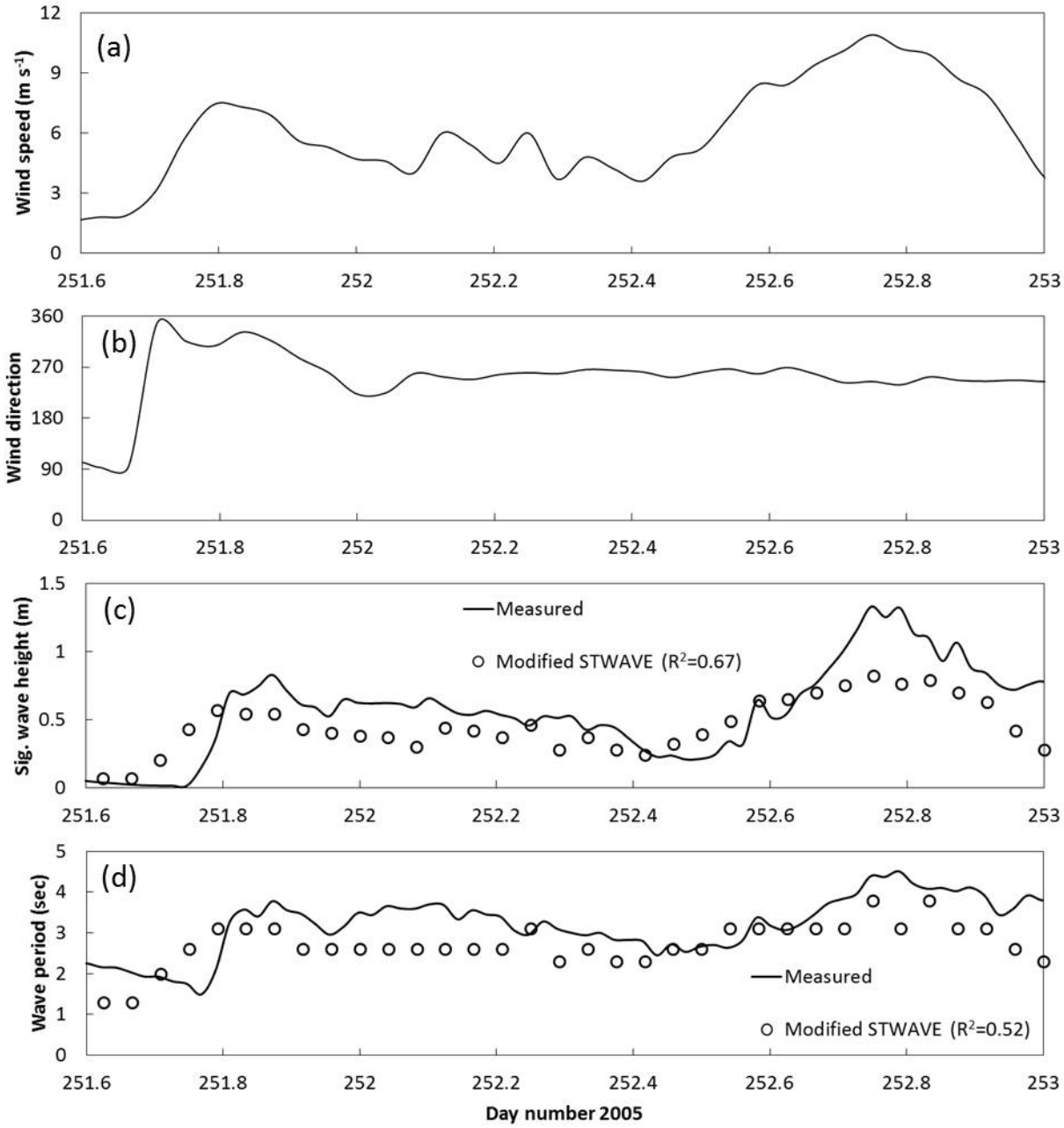

Figure 2-A1. Input variables of (a) wind speed and (b) wind direction (measured degrees clockwise from north) and comparison of measured and the modified STWAVE-simulated results of (c) significant wave height and (d) wave period.

Chapter 3. Seasonal differences in nearshore sediment resuspension at Lake Tahoe

This chapter is based on work that has been prepared for potential publication as a regular article in Lake and Reservoir Management, the journal for the North American Lake Management Society. The authors are: Kristin E. Reardon (UC Davis), Patricio A. Moreno-Casas (Universidad de los Andes), Fabián A. Bombardelli (UC Davis), and S. Geoffrey Schladow (UC Davis).

3.1 Abstract

Motivated by declining water clarity at Lake Tahoe, California-Nevada (USA), this investigation synthesized field observations and modeling with the purpose of informing decision-makers facing management challenges at wind-exposed lakes. We present the first field observations of nearshore sediment resuspension in summer and winter at Lake Tahoe and offer key findings. Also, using the previously modified and validated wind-wave model STWAVE we develop management charts that illustrate relationships between fetch, wind intensity, and wave height and between water depth, wave height, and nearshore bottom dynamics (i.e., the potential for mobilization of different sized particles). For a representative grain size of 150 μm, the wind-driven surface waves were found to influence the sediments to a maximum water depth of about 9 m. We evaluated the potential for nearshore sediment resuspension with changing lake levels, considering a range of possible future scenarios. (Changes in wind intensity and direction were not considered, because wind conditions are projected to change only moderately.) Wind-waves resulted in periodic nearshore sediment resuspension in summer and winter. However, the particle size distribution of the resuspended material revealed that the concentration of fine particles was unchanged by wind events; instead, larger particles were resuspended. Therefore,

we conclude that wind-driven nearshore sediment resuspension does not result in an increase in particle loading of the size class that has been identified to most negatively impact water clarity. The potential for internal loading of nutrients impacting water clarity, by both resuspension and hypolimnetic anoxia, has yet to be assessed.

Key words: clarity, Lake Tahoe, nearshore sediment resuspension, STWAVE, wind-waves

3.2 Introduction

Interactions at the sediment-water interface can critically affect water quality in natural systems. Particulates and nutrients enter a water body from diverse external sources or they are reintroduced from within the system itself, such as when previously-deposited sediment is resuspended from the sediment bed. The general concept of sediment resuspension is predicated on the comparison of a destabilizing parameter (e.g., bottom shear stress) and a sediment parameter (often taken as critical shear stress for a representative grain size). We assume sediment resuspension occurs when the destabilizing parameter exceeds the sediment parameter, as is standard practice. Wind-driven sediment resuspension occurs when the water depth is shallow enough to transfer sufficient momentum of the wind-waves from the water surface to the sediment-water interface [*Håkanson and Jansson*, 1983]. Therefore, in an otherwise deep lake, only the shallow nearshore zone is susceptible to wind-driven sediment resuspension. This is in contrast to a shallow lake, where wind-driven sediment resuspension may occur over the entire areal extent of the lake [see *Luettich et al.,* 1990; *Chung et al.,* 2009].

Lake Tahoe is a deep, sub-alpine lake that appears startlingly blue. Nevertheless, lake transparency has declined since long-term monitoring began in the 1960s. In 1982 Lake Tahoe was designated an impaired water body by the US Environmental Protection Agency. Under the Federal Clean Water Act, a Total Maximum Daily Load (TMDL) was required to address its

impairment. The agreed-upon water quality objective for Lake Tahoe is deep water transparency equal to the average annual Secchi depth measured between 1967 and 1971 (29.7 m). The Lake Tahoe TMDL identifies the pollutants responsible for the loss of transparency as fine sediment (<16 μm), nitrogen, and phosphorus. The TMDL also identifies the load of each pollutant entering the lake, the contributing sources of these loads, the reductions needed, the reduction opportunities that are available for each source, and the implementation plan to achieve these reductions [*Lake Tahoe Total Maximum Daily Load Technical Report*, 2010]. Until now, a comprehensive investigation of the potential for internal sources of fine sediment (e.g., resuspended sediment) has been lacking. Yet at other wind-exposed lakes, sediment resuspension can be a significant source of fine sediment [*Evans*, 1994; *Bloesch*, 1995; *Chung et al.*, 2009].

In the previous chapter (also *Reardon et al.* [2014]), we investigated wind-driven nearshore sediment resuspension at Lake Tahoe in winter and found that wind-waves resulted in sediment resuspension as corroborated by simultaneous increases in shear stress and total measured sediment concentration. As previous lake applications of the wind-wave model STWAVE had been limited to special instances of fully-turbulent flow, we modified and validated STWAVE to simulate wind-wave induced sediment resuspension for viscous-dominated flow typical in lakes. Additionally, we considered in situ measurements of suspended sediment concentration and particle size distribution for several instances of low-wind and high-wind periods; the data suggested that the predominance of fine particles that most negatively impact clarity was unchanged by wind-related sediment resuspension.

Here we consider the complete time series of suspended sediment concentration and particle size distribution at Lake Tahoe, and focus on the seasonal differences. To investigate seasonal differences of wind-driven nearshore sediment resuspension, we combined

comprehensive field observations, computations of bottom shear stress from field data, and wind-wave modeling with the aim of answering the following questions:

1.) What are the observed nearshore patterns in summer and winter?

2.) To what water depth do wind-driven surface waves influence the sediments?

3.) What lake area does this influence extend, and how does it change with changing lake level?

4.) What are the implications of wind-driven nearshore sediment resuspension for lake clarity?

3.3 Study site

Lake Tahoe is located in the western United States on the California-Nevada border in the mountains of the Sierra Nevada (Figure 3-1). It is an example of a deep, oligotrophic lake as characterized by low nutrient concentrations, high dissolved oxygen concentrations, and exceptionally transparent water to great depths. Lake Tahoe is large within a small watershed, and therefore has an extremely long hydraulic residence time. Table 3-1 lists pertinent lake information. Ongoing public concern over the onset of cultural eutrophication as described in *Goldman* [1988] has focused research attention on preserving and protecting the lake's famed clarity. At the same time, we have continued to develop an understanding and predictive tools which are useful for other lakes.

The nearshore study site was located at the south end of Lake Tahoe about 1000 m offshore on a shelf that was shallow, broad, and gently-sloping (~0.3 percent; Figure 3-1). We conducted measurements at a water depth of 5 m. We also collected meteorological data from the long-term meteorological station maintained by the University of California, Davis, Tahoe Environmental Research Center on the pier at Timbercove near the City of South Lake Tahoe.

Timbercove station was located about 4.5 km from the study site; this was the closest long-term meteorological station to the study site. Due to its shallow water depth and regular wind exposure, the study site was thought to be favorable for observing wind-driven nearshore sediment resuspension. Additionally, it had been previously identified as an area of impaired water quality, particularly in summer-time [*Alexander and Wigart*, 2013; *Taylor et al.*, 2004].

3.4 Methods

We collected field measurements of hydrodynamic and sediment variables in summer and winter, directly estimated bottom shear stress from field data, and employed a recently modified wind-wave model.

3.4.1 Field observations and computations from field data

Lake measurements were taken in summer from 22 July to 3 September 2008 and in winter from 13 November 2008 to 14 January 2009. We measured wind speed and direction, vertical profiles of water temperature, nearbed velocity, lakebed sediment characteristics, and suspended sediment concentration and particle size distribution, as described in the previous chapter. Instrument deployments in summer and winter were the same (and at the same location) with two exceptions. Lakebed sediment characteristics were determined from grab samples collected solely in summer (22 July 2008) and are described in the previous chapter. We assumed that lakebed sediments characteristics did not change from summer to winter; this was reasonable considering our visual estimation of the study site. Measurements of suspended sediment concentration and particle size distribution were collected solely in winter (11 December 2008 to 14 January 2009) and are also described in the previous chapter. A summary of the field campaigns is presented in Table 3-2 and includes the parameter(s)

measured, instrument, location(s), sensor height(s) or orientation, period, sampling interval, sampling duration, and burst interval, as applicable.

In addition to measurements collected during the two study periods, we analyzed 10 years of wind data collected at Timbercove station from 1 June 2003 to 31 July 2013 with the purpose of characterizing the seasonal wind exposure at the study site. Summer is herein defined from June through September and winter from December through March. Details regarding the meteorological station are provided in the previous chapter and summarized in Table 3-2.

We directly estimated bottom shear stress from ADV-measured velocity data collected from the Sontek ADVOcean Probe according to the method developed in the previous chapter. Bottom shear stress was partitioned into three components attributed to wind-waves, mean currents, and random motions. We demonstrated that wind-waves (the wind-wave band was defined by periods from 0.5 to 30 sec) contributed most consistently to the development of bottom shear stress.

To compute the value of critical shear stress, we used the formulation from *Parker* [2004] that incorporates the non-dimensional critical Shields parameter. The Shields diagram [*Shields*, 1936] for threshold of sediment particle motion in unidirectional, steady, uniform flow has been found adequate to characterize incipient conditions under oscillatory flows [*Raudkivi*, 1998; p. 342]. Therefore, this is a reasonable approach considering the wind-exposed nearshore of many lakes.

3.4.2 Predictive tools developed from wind-wave modeling

To estimate the wave-induced bottom shear stress, we implemented a modified form of the full-plane version of the US Army Corps of Engineers wind-wave model STWAVE.

STWAVE is a finite difference, steady-state, spectral wave model that solves the wave action balance equation, including wave generation and transformation by refraction and shoaling, wave breaking, generation by wind-input, wave-wave interaction, and white capping. We modified the bottom-friction formulation to reflect typical lake conditions with flow regimes that were viscous-dominated. Previously, lake applications of STWAVE had been limited to special instances of fully-turbulent flow [e.g., *Bunya et al.*, 2010; *Dietrich et al.*, 2010]. In order to validate the development, we compared model results and field observations and found good agreement [*Reardon et al.*, 2014]. This model validation suggested that the modified STWAVE was an appropriate tool to calculate the effect of wind-waves on the development of bottom shear stress leading to sediment resuspension in shallow areas.

The modified STWAVE was used to consider a range of wind conditions and the resulting bottom sediment dynamics. We based our analysis on the work of *Norrman* [1964], who presented relationships between wave height, wind conditions, effective fetch, and sediment response at one particular lake [*Håkanson and Jansson*, 1983; Figure 6.21]. As these figures were based on observations at Lake Vättern (Sweden) alone, there is difficulty in applying them generally to all lakes. Using the modified STWAVE, we have developed similar figures based on Lake Tahoe and suggest that other lakes could be considered likewise.

In particular, we reproduced wind events ranging from 3 to 21 m s^{-1} coming from different directions. A total of seven wind velocities (3, 6, 9, 12, 15, 18, and 21 m s^{-1}) and five wind directions (0°, 30°, 45°, 60°, and 90°, measured clockwise from north) were selected to represent a range of realistic wind events at Lake Tahoe. A total of 35 simulations were implemented in the modified STWAVE with a 50 m square grid cell resolution. Considering the study site in the southern part of Lake Tahoe, the longest fetch (~30 km) results from a northerly

wind (i.e., a wind direction equal to 0°). The shortest fetch is achieved when the wind blows from east to west (i.e., a wind direction of 90°); this is when the wind blows offshore very near the study site (~1 km). Significant wave heights, peak wave periods, bottom orbital velocities, and bottom shear stresses were calculated for each cell, based on wave motions alone, i.e., neglecting the presence of mean currents and turbulent motions. The results of modeled bottom shear stress were used to calculate the corresponding maximum particle diameter that could be resuspended from the lakebed considering the formulation of critical shear stress. Once the potential resuspension of the maximum particle diameter was obtained for each incremental bottom shear stress, a multivariate regression was used to develop predictive equations relating wind, water depth, and nearshore bottom dynamics (i.e., the potential for mobilization of different sized particles).

To understand the areal extent of wind-driven nearshore sediment resuspension at Lake Tahoe and how it changes with changing lake water level, we ran the modified STWAVE model with water surface elevations between 2 m below the natural rim (1895 m) and the maximum legal limit (1899 m) in increments of 0.5 m (the natural rim of the lake is 1897 m; all referenced to NAVD 88), and for wind speed and direction that generated the maximum shear stress. Thus, we define an area of maximum potential wind-driven sediment resuspension. Lake water level is influenced by stream inflow, groundwater inflow, direct precipitation, evaporation, outflow, and overflow, as applicable, and is therefore affected by climate change. *Sahoo et al.* [2012; Figure 13] projected lake water levels at Lake Tahoe over the next century, which may increase or decrease within the range we have identified for our model runs. Future climate conditions that are drier than normal will likely result in a water surface elevation below the natural rim;

conversely, future climate conditions that are wetter than normal will likely result in water surface elevations above the natural rim, up to the maximum legal limit.

We do not consider future scenarios in which the wind intensity changes. In general, researchers predict a decrease in wind intensity as average global temperatures increase [*Ren*, 2010]. Focusing on the Tahoe Basin in particular, *Dettinger* [2012] spatially downscaled meteorology output from the coupled ocean-atmosphere general circulation model (CM2.1) of the National Oceanic and Atmospheric Administration's Geophysical Fluid Dynamics Laboratory in response to two greenhouse-gas emissions scenarios (A2 and B1). Under both scenarios, *Dettinger* [2012] projected relatively small changes in wind speeds. In the Tahoe Basin, wind speeds were projected to decrease 4 to 5 percent over the next century relative to historical averages [*Dettinger*, 2012; Figure 9]. Therefore, our consideration of wind intensity represents our understanding of the greatest potential for wind energy input into the lake.

3.5 Results

3.5.1 Wind exposure

Considering the Timbercove wind record from 1 June 2003 to 31 July 2013, we observed predominantly southerly winds (SW, S, SE); they represented 60 percent of the winds over the 10 year period (not shown) and between 60 and 70 percent of the winds measured in summer and winter (Figure 3-2). Northerly winds (NW, N, NE) represented between 22 and 31 percent of the wind record measured in summer and winter (Figure 3-2). For summer, the mean wind speed ranged from 2.1 to 5.9 m s^{-1}, and was most frequently from the southeast direction (Figure 3-2a). Similarly for the study period, the mean wind speed ranged from 2.0 to 5.7 m s^{-1}, and was most frequently southeasterly as observed in daily mid-afternoon peaks (Figure 3-2b; see Figure 3-4a).

The average maximum wind speeds were 12.3 and 8.0 m s^{-1} for the entire summer record and the summer study period, respectively. Large values of wind speed (13.4 m s^{-1} for the entire summer record; 11.3 m s^{-1} for the summer study period) were of southwesterly direction (Figure 3-2a and 3-2b). For winter, the mean wind speed ranged from 2.1 to 6.1 m s^{-1}, and the largest mean wind speed was associated with northeasterly winds, then second-largest, southwesterly winds (Figure 3-2c). The average maximum wind speeds were 14.7 and 10.5 m s^{-1} for the entire winter record and the winter study period, respectively (Figure 3-2c and 3-2d). The greatest value of wind speed over the entire winter record was from the northeast (18.1 m s^{-1}; Figure 3-2c); the greatest value of wind speed over the winter study period was from the southwest (13.9 m s^{-1}; Figure 3-2d). Although the maximum wind speed observed during the study periods of 2008 and 2009 were less than those over the 10 year record, the mean wind speed is comparable.

3.5.2 Observed nearshore patterns in summer and winter

There were different patterns of physical phenomena in summer and in winter. For summer, we observed a reliable diurnal pattern of nearshore water warming and cooling with a daily difference of about 2 °C (Figure 3-3a). In winter, the diurnal pattern was more subtle and, in general, the temperature of bottom and top thermistors tracked closely (Figure 3-3b). Summer-time nearshore water temperatures varied from 16.6 to 21.0 °C, but beginning and ending at 19.8 and 20.0 °C, respectively. We saw a greater temperature difference between bottom and top thermistors in summer (about 3 °C on average; Figure 3-3a) than in winter (about 1 °C on average; Figure 3-3b). These temperature differences, however, were usually sustained for about 2 to 4 h and no more than 6 h. Generally, the onset of wind events ended the thermal stratification of the water column within several hours.. Based on these results, we assumed that the thermal structure did not greatly impact the transfer of momentum in the water column.

During the summer study period, we observed a pattern of daily, elevated, mid-afternoon wind speeds greater than 6 m s^{-1} that were of south-southeasterly direction. Wind speeds of 9 m s^{-1} or greater were observed several times; these were of south-southwesterly direction (see Figures 3-4a and 3-4b; days 209, 216, 221, 231-232, and 238-239). For the winter study period, we observed low wind speeds punctuated by high-energy wind events; there were no regular daily patterns of wind observed in winter (Figure 3-5a and 3-5b).

During the summer study period, we observed nearbed current speed measured with the Vector and ADVOcean Probe on average of about 0.03 m s^{-1}. Peaks in nearbed current speed were less than 0.10 m s^{-1} (Figure 3-4c and 3-4d); this is in contrast to winter conditions with nearbed current speed peaks of 0.15 to 0.20 m s^{-1} (Figure 3-5c and 3-5d).

For the summer study period, we observed a pattern of daily, elevated, mid-afternoon bottom shear stress; we observed two instances where the bottom shear stress exceeded the critical shear stress, indicated in Figure 3-4e at 8 August 2008 (day 221) and 18 August 2008 (day 231). For the winter study period, we observed bottom shear stress that demonstrated no regular daily patterns; like for the wind record, there were very low measures interrupted by abrupt increases (Figure 3-5e). We observed three instances where the bottom shear stress exceeded the critical shear stress, indicated in Figure 3-5e at 8 December 2008 (day 343), 13 December 2008 (day 348), and 19 August 2008 (day 354).

Spectra from different bursts collected at Lake Tahoe during high wind events throughout the summer and winter yield similar results and have similar form (Figure 3-6). We see that the peak of the power spectral density ranges from 0.28 to 0.37 Hz (corresponding to wave periods between 2.7 and 3.2 sec). For the two summer-time bursts corresponding to the instances when

bottom shear stress exceeded the critical shear stress, we observed the most energetic peak in the power spectral density plots at 0.28 and 0.37 Hz (Figure 3-6a), which corresponded to the wind-wave contribution from wave periods equal to 3.6 and 2.7 sec, respectively. For windy periods in winter, more pronounced peaks in power spectral density of about 0.3 to 0.35 Hz were observed (Figure 3-6b). See also Figure 2-2 with a peak of the power spectral density equal to 0.33 Hz (corresponding to a wave period of 3.0 sec). Therefore, the wind-wave band we have imposed reasonably reflects the nature of the wind-wave contribution to flow and bottom shear stress.

3.5.3 Sediment characteristics

Herold et al. [2007; Figure 5] showed that sand dominated in the entire south shore of Lake Tahoe; *Reardon et al.* [2014] showed that sand dominated at the study site. We assumed a representative grain size of 150 μm, corresponding approximately to d_{10} from the particle size distributions from two grab samples (Figure 2-7). Furthermore, 150 μm corresponded to the peak in suspended sediment concentration by mass concentration during sediment resuspension events (Figure 2-13a). According to the formulation from *Parker* [2004], the critical shear stress for incipient motion for a particle size of 150 μm was 0.081 Pa.

3.5.4 Bottom shear stress and sediment resuspension

We present the mean and maximum bottom shear stress separated by wind direction for the study periods in summer and winter. For summer, the mean bottom shear stress over the study period ranged from 0.001 to 0.007 Pa. The maximum bottom shear stress was 0.093 Pa and associated with wind of southwesterly direction; this was the only wind direction for which the bottom shear stress exceeded the critical shear stress (Figure 3-7a). Generally, values of bottom shear stress were greater in winter than summer. This was attributed to greater wind intensity observed in winter. For winter, the mean bottom shear stress ranged from 0.003 to 0.036 Pa. The

maximum bottom shear stress was 0.182 Pa and associated with wind of southwesterly direction; bottom shear stress also exceeded the critical shear for southerly (0.119 Pa) and westerly (0.106 Pa) wind directions (Figure 3-7b). The wind directions associated with maximum bottom shear stress were the same wind directions as for the maximum observed wind speeds.

During winter we collected in situ measurements of suspended sediment concentration (SSC) with a LISST-100X. We observed that suspended sediment concentration did not change with increasing total bottom shear stress for particles of median diameter 2.5 to 16 μm (Figure 3-8a). The Lake Tahoe TMDL attributes the loss of deep water transparency, in part, to fine sediment (<16 μm). Furthermore, *Swift et al.* [2006] showed that particles with the greatest potential to negatively impact lake clarity were inorganic and <10 μm. Fine inorganic particles strongly scatter light, which results in decreased lake transparency [*Davies-Colley et al.,* 2001; *Kirk*, 2011]. However, we observed a modest increase in suspended sediment concentration for several instances when the bottom shear stress exceeded the critical shear stress for particles of median diameter 100 to 250 μm (Figure 3-8b).

3.5.5 Predictive tools developed from wind-wave modeling

Wind-driven nearshore sediment resuspension results in the entrainment of bed particles into the water column and those resuspended particles are subject to horizontal transport by local currents. Figure 3-9 illustrates how wave height and water depth influence the potential for resuspension. Increasing wave heights result in increased bottom shear stress, leading to greater potential for resuspension. Conversely, increasing water depth results in decreased bottom shear stress, leading to the diminished potential for resuspension. For example, Figure 3-9 shows that if a particle of 10 μm were at a water depth of 5 m, a wave height of 0.37 m could initiate

entrainment into suspension. Considering our representative grain size of 150 μm, the maximum water depth to which wind-driven surface waves influence the sediments is about 9 m.

Figure 3-10 shows the combination of wind speed and direction, fetch, and particle resuspension for three different water depths. No matter the water depth, the largest resuspension potential occurs at the largest fetch. Fetch and wind direction are linked in Figure 3-10 (relative to the study site). At the study site, the largest fetch occurs as a result of a northerly wind (i.e., a wind direction equal to 0° clockwise from north). The no resuspension area (gray area) shown in Figure 3-8 enlarges with increasing water depth, emphasizing that deeper water experiences weaker bottom shear stresses at the same wave height.

Due to the complex bathymetry of the nearshore of Lake Tahoe, and particularly due to its steep sides, the relationship between lake water level and potential areal extent of wind-driven nearshore sediment resuspension is not linear. Figure 3-11 shows the areal extent of wind-driven nearshore sediment resuspension at Lake Tahoe's south nearshore zone and how it changes with changing lake water level. For a lake water level equal to the natural rim (1897 m), the potential area affected is 8.3 km^2 (Figure 3-11b). For a lake water level equal to the maximum legal limit (1899 m), the potential area affected is 7.2 km^2 (Figure 3-11c). Finally, for a lake water level equal to 2 m below the natural rim (1895 m), the potential area affected is 4.7 km^2 (Figure 3-11a). Figure 3-11d shows that as the lake water level drops below the natural rim, the potential areal extent of wind-driven nearshore sediment resuspension decreases. This is because with dropping lake water level, the areal extent of the shallow nearshore shelf at Lake Tahoe decreases (i.e., the nearshore zone is no longer submerged to the same extent). As the lake water level increases from the natural rim to the maximum legal limit, the potential areal extent of wind-driven nearshore sediment resuspension also decreases (Figure 3-11d).

3.6 Summary and conclusions

We offer the following key findings considering our nearshore observations in summer and winter. In summer, we observed regular increases in wind speed each afternoon. The time series is characterized by a strong diurnal pattern with wind intensity peaking each day at mid-afternoon. By contrast, in winter, we observed low-wind periods punctuated by high-energy storm events. Both low-wind and high-wind periods were sustained for days at a time with no regular pattern. Most often, the instances of greatest bottom shear stress and the concomitant wind-driven sediment resuspension at the study site, both in summer and winter, resulted from strong and sustained southwesterly winds. This was not the direction of maximum fetch, but it was the direction from which the strongest winds occurred. Observed wind-waves had periods of about 3 sec, in both summer and winter.

Considering the nature of the wind-waves, we observed that the peak in the power spectral density plots corresponded to a wave period of 3 sec (Figure 3-6). In summer, the form of the power spectral density plot is less pronounced than that of those for winter. In winter, we see strong peaks of similar form for each burst. We attribute this to the fact that in winter the wind intensity was greater and therefore revealed in the high-frequency nearbed velocity signal when presented in the frequency domain.

We considered the wind conditions that derive the maximum bottom shear stress and found that wind-driven surface waves resulted in potential sediment resuspension up to a water depth of 9 m. This influence extended to a lake area of 8.3 km^2 for a lake water level equal to the natural rim and decreased both as the lake water level increased to the maximum legal limit (7.2 km^2) and decreased to 2 m below the natural rim (4.7 km^2; Figure 3-11).

We determined that wind-waves do not have a major impact on the lakebed sediment at the study site (i.e., the south end of Lake Tahoe about 1000 m offshore at a water depth of 5 m). With increasing bottom shear stress attributed to wind-waves, the suspended sediment concentration of particles of median diameter 2.5 to 16 μm did not change (Figure 3-8a). For particles of median diameter 100 to 250 μm, we see a modest increase (same order of magnitude) in suspended sediment concentration for several instances when the bottom shear stress exceeded the critical shear stress (Figure 3-8b). In general, the lakebed sediment at the nearshore of Lake Tahoe is coarse and granular and we suspect that the relative lack of fine material available for resuspension is a result of the armoring of the lakebed sediment.

An important consideration is how these research findings can be translated to management strategies. Because these results suggest that wind-driven nearshore sediment resuspension does not produce an increase in particle loading of the size class that has been identified to most negatively impact water clarity, these findings do not counter the Lake Tahoe TMDL conclusions concerning the source of fine particle loads. However, the resuspension of coarser material has the potential to increase the internal loading of phosphorus and other contaminants from the sediments. The chemical impact of sediment resuspension was beyond the scope of this study, but it is an aspect that requires further examination.

Acknowledgments

This research was supported by the University of California, Davis and a grant from the US Department of Agriculture Forest Service Pacific Southwest Research Station using funds provided by the Bureau of Land Management through the sale of public lands as authorized by the Southern Nevada Public Land Management Act. The lead author was supported for two years by the Eugene Cota-Robles Fellowship from the Office of Graduate Studies, University of California, Davis. The AWAC was provided on loan from the California Department of Water Resources. The Vector was provided as a Nortek 2008 Student Equipment Grant Award. The ADVOcean Probe was provided on loan from the US Geological Survey. The Western Regional Climate Center, Desert Research Institute provided the meteorological data which was collected at the Timbercove station by the Tahoe Environmental Research Center (TERC). We also wish to acknowledge key students and staff from the Environmental Dynamics Laboratory and TERC, both of the University of California, Davis. In particular, we thank Erik Maroney for cleaning 10 years of meteorological data.

References

Alexander, M. T. and R. C. Wigart (2013) Effect of motorized watercraft on summer nearshore turbidity at Lake Tahoe, California-Nevada. *Lake Reserv Manage*. *29*, 4:256a-256b, doi: 10.1080/10422381.2013.866013.

Bloesch, J. (1994) A review of methods used to measure sediment resuspension. *Hydrobiologia*. 284:13-18.

Bunya, S., J. C. Dietrich, J. J. Westerink, B. A. Ebersole, J. M. Smith, J. H. Atkinson, R. Jensen, D. T. Resio, R. A. Luettich, C. Dawson, V. J. Cardone, A. T. Cox, M. D. Powell, H. J. Westerink, and H. J. Roberts (2010), A high-resolution coupled riverine flow, tide, wind, wind wave, and storm surge model for southern Louisiana and Mississippi. Part I: Model development and validation, *Mon. Weather Rev.*, *138(2)*, 345-377, doi: 10.1175/2009MWR2906.

Chung, E. G., F. A. Bombardelli, and S. G. Schladow (2009), Sediment resuspension in a shallow lake, *Water Resour. Res.*, *45*, W05422, doi: 10.1029/2007WR006585.

Davies-Colley, R. J. and Smith, D. G. (2001), Turbidity, suspended sediment, and water clarity: A review. *J. Am. Water Resour. Assoc.*, *37*, 1085–1101, doi: 10.1111/j.1752-1688.2001.tb03624.x

Dettinger, M. D. (2012), Projections and downscaling of 21st century temperatures, precipitation, radiative fluxes and winds for the Southwestern US, with focus on Lake Tahoe. *Climatic Change*, doi: 10.1007/s10584-012-0501-x

Dietrich, J. C., S. Bunya, J. J. Westerink, B. A. Ebersole, J. M. Smith, J. H. Atkinson, R. Jensen, D. T. Resio, R. A. Luettich, C. Dawson, V. J. Cardone, A. T. Cox, M. D. Powell, H. J. Westerink, and H. J. Roberts (2010), A high-resolution coupled riverine flow, tide, wind, wind wave, and storm surge model for southern Louisiana and Mississippi. Part II: Synoptic description and analysis of hurricanes Katrina and Rita, *Mon. Weather Rev.*, *138(2)*, 378-401, doi: 10.1175/2009MWR2907.1.

Evans, R.D. (1994) Empirical evidence of the importance of sediment resuspension in lakes. *Hydrobiologia*. 284:5-12.

Goldman, C. R. (1988), Primary productivity, nutrients, and transparency during the early onset of eutrophication in ultra-oligotrophic Lake Tahoe, California-Nevada, *Limnol. Oceanogr.*, *33*, 1321-1333.

Håkanson, L. and M. Jansson (1983), *Principles of Lake Sedimentology*, Springer-Verlag, Berlin, Germany.

Kirk, J. T. O. (2011), *Light and Photosynthesis in Aquatic Ecosystems*, 3rd ed., University Press, Cambridge, UK.

Lake Tahoe Total Maximum Daily Load Technical Report (2010), California Regional Water Quality Control Board, Lahontan Region and Nevada Division of Environmental Protection, June.

Luettich, R. A., D. R. F. Harleman, and L. Somlyody (1990), Dynamic behavior of suspended sediment concentrations in a shallow lake perturbed by episodic wind events, *Limnol. Oceanogr.*, *35(5)*, 1050-1067.

Massey, T. C., M. E. Anderson, J. M. Smith, J. Gomez, and R. Jones (2011), STWAVE: Steady-state spectral wave model user's manual for STWAVE, Version 6.0, ERDC/CHL SR-11-1. Vicksburg, MS, U.S. Army Engineer Research and Development Center, Vicksburg, MS.

Norrman, J. O. (1964), Lake Vättern: Investigations on shore and bottom morphology, *Geogr. Ann., 46*, 1-238.

Parker, G. (2004), *1D sediment transport morphodynamics with applications to rivers and turbidity currents*, e-book, Natl. Cent. For Earth Surf. Dyn., Minneapolis, Minn. (Available at http://cee.uiuc.edu/people/parkerg/)

Raudkivi, A. J. (1998), *Loose Boundary Hydraulics*, 3rd ed., Pergamon Press, Oxford, UK.

Reardon, K. E., F. A. Bombardelli, P. A. Moreno-Casas, F. J. Rueda, and S. G. Schladow (2014), Wind-driven nearshore sediment resuspension in a deep lake during winter, *Water Resour. Res., 50,* doi:10.1002/2014WR015396.

Ren, D. (2010) Effects of global warming on wind energy availability, *J. Renewable Sustainable Energy*, *2*, 052301, doi: 10.1063/1.3486072.

Sahoo, G. B., S. G. Schladow, J. E. Reuter, R. Coats, M. Dettinger, J. Riverson, B. Wolfe, and M. Costa-Cabral (2012), The response of Lake Tahoe to climate change, *Climatic Change*, doi: 10.1007/s10584-012-0600-8.

Shields, I. A., 1936, *Anwendung der ahnlichkeitmechanik und der turbulenzforschung auf die gescheibebewegung,* Mitt. Preuss Ver.-Anst., 26, Berlin, Germany.

Swift, T. J., J. Perez-Losada, S. G. Schladow, J. E. Reuter, A. D. Jassby, and C. R. Goldman (2006), Water clarity modeling in Lake Tahoe: Linking suspended matter characteristics to Secchi depth, *Aquat. Sci.*, *68(1),* 1-15, doi: 10.1007/s00027-005-0798-x.

Taylor, K., R. Susfalk, M. Shanafield, and S. G. Schladow (2004), Near-shore clarity at Lake Tahoe: Status and causes of reduction, Report to Lahontan Water Board (CA), Nevada Division of State Lands, and Tahoe Regional Planning Agency.

Table 3-1. Summary information about Lake Tahoe

Maximum depth	505 m
Average depth	313 m
Lake surface area	500 km^2
Watershed area	800 km^2
Lake volume	156 km^3
Shoreline	116 km
Mean hydraulic residence time	700 years
Elevation of natural rim[a]	1897 m
Elevation of maximum legal limit[a, b]	1899 m
Annual average Secchi depth (target)[c]	29.7 m
Annual average Secchi depth (2013)[d]	21.4 m

[a]Referenced to NAVD 88
[b]Fixed according to the Truckee River Operating Agreement (https://troa.net/)
[c]Lake Tahoe Total Maximum Daily Load Technical Report 2010
[d]Tahoe: State of the Lake Report 2014
All other information from *Goldman* [1988]

Table 3-2. Field measurements in summer and winter

Parameter(s) measured	Instrument	Sampling period[a]		Sampling interval	Sampling duration	Burst interval
		Summer	Winter			
Wind speed and direction	Met One Windset 3-cup anemometer	ongoing	ongoing	10 min	NA	NA
Vertical profiles of water temperature[b]	Onset Stow Away TidbiT temperature loggers	23 Jul – 3 Sep	13 Nov – 14 Jan	5 min	NA	NA
Nearbed velocity[c]	Sontek ADVOcean Probe	23 Jul – 29 Aug	13 Nov – 21 Dec	10 Hz	3 min	1 h
Nearbed velocity[d]	Nortek Vector	23 Jul – 27 Aug	13 Nov – 19 Dec	64 Hz	2 min	2 h
Suspended sediment concentration[d]	LISST-100X type B (Sequoia Scientific, Inc.)	NA	11 Dec – 14 Jan	1 Hz	2 min	2 h
Lakebed sediment characteristics	Grab samples (2)	22 July 2008	NA	NA	NA	NA

[a]Field measurements were collected in summer 2008 and winter 2008-2009.
[b]Eight temperature loggers were located at heights of 0.2, 0.5, 1.0, 1.5, 2.0, 2.5, 3.0, and 3.5 m above lakebed
[c]Sampling volume was 0.10 m above lakebed
[d]Sampling volume was 0.20 m above lakebed
NA=not applicable

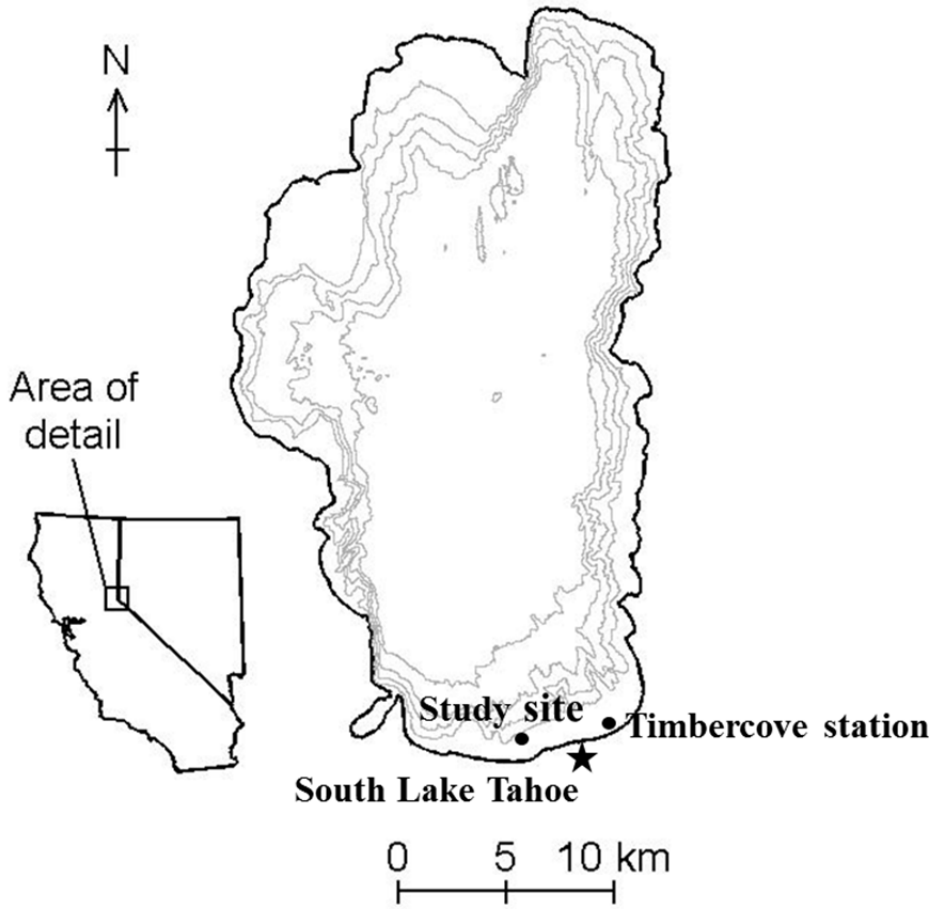

Figure 3-1. Lake Tahoe bathymetry and orientation. Meteorological data were collected at the Timbercove station. Lake measurements were made at the study site. Contours are shown at 100 m intervals. Lake Tahoe is located at approximately 39°N latitude and 120°W longitude.

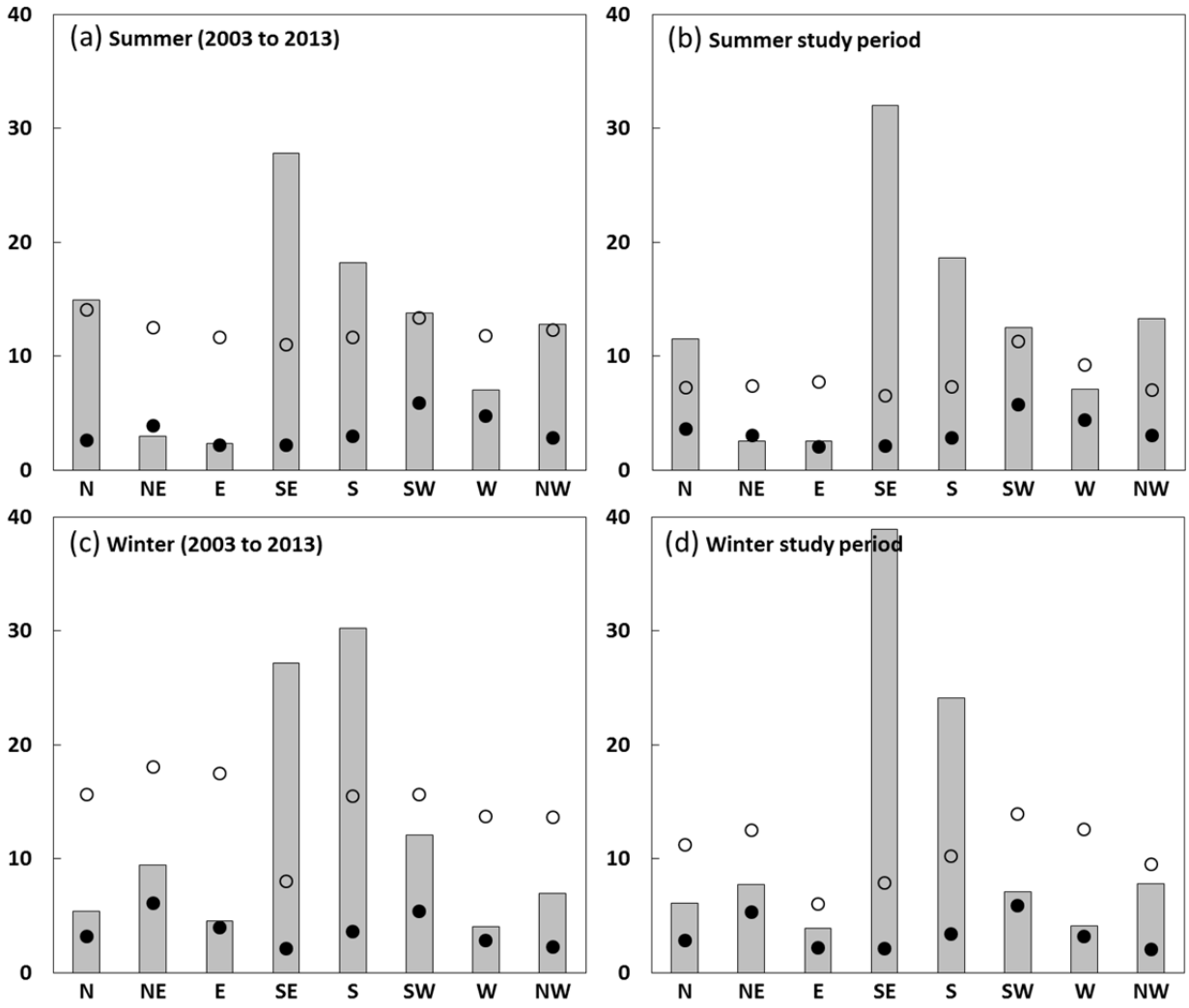

Figure 3-2. Wind statistics separated by wind direction at Timbercove station for (a) summer from 2003 to 2013, (b) summer during the study period, (c) winter from 2003 to 2013, and (d) winter during the study period. Bars represent percent of wind data separated by wind direction. Wind speeds (m s^{-1}) are given as mean (closed circle) and maximum (open circle).

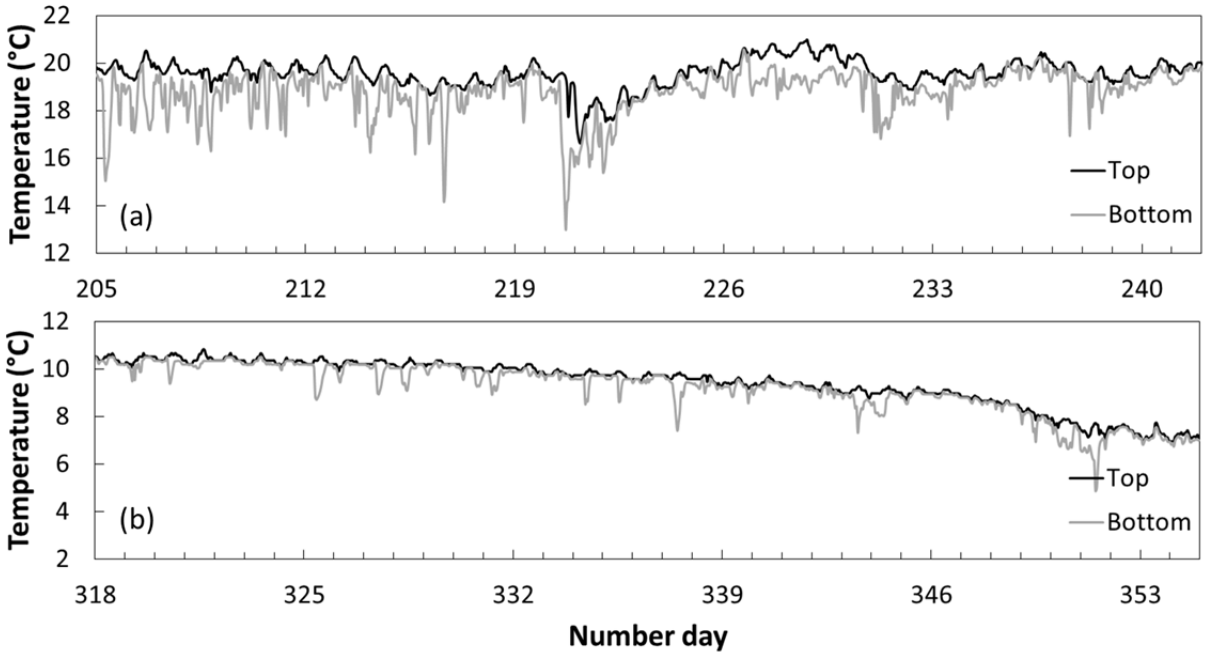

Figure 3-3. Water temperature observed from (a) 23 July to 29 August 2008 and (b) 13 November to 20 December 2008 at the study site for top and bottom thermistors. The temperature at the top thermistor remains nearly equal to or greater than that of the bottom thermistor, implying thermodynamic neutrality or stability.

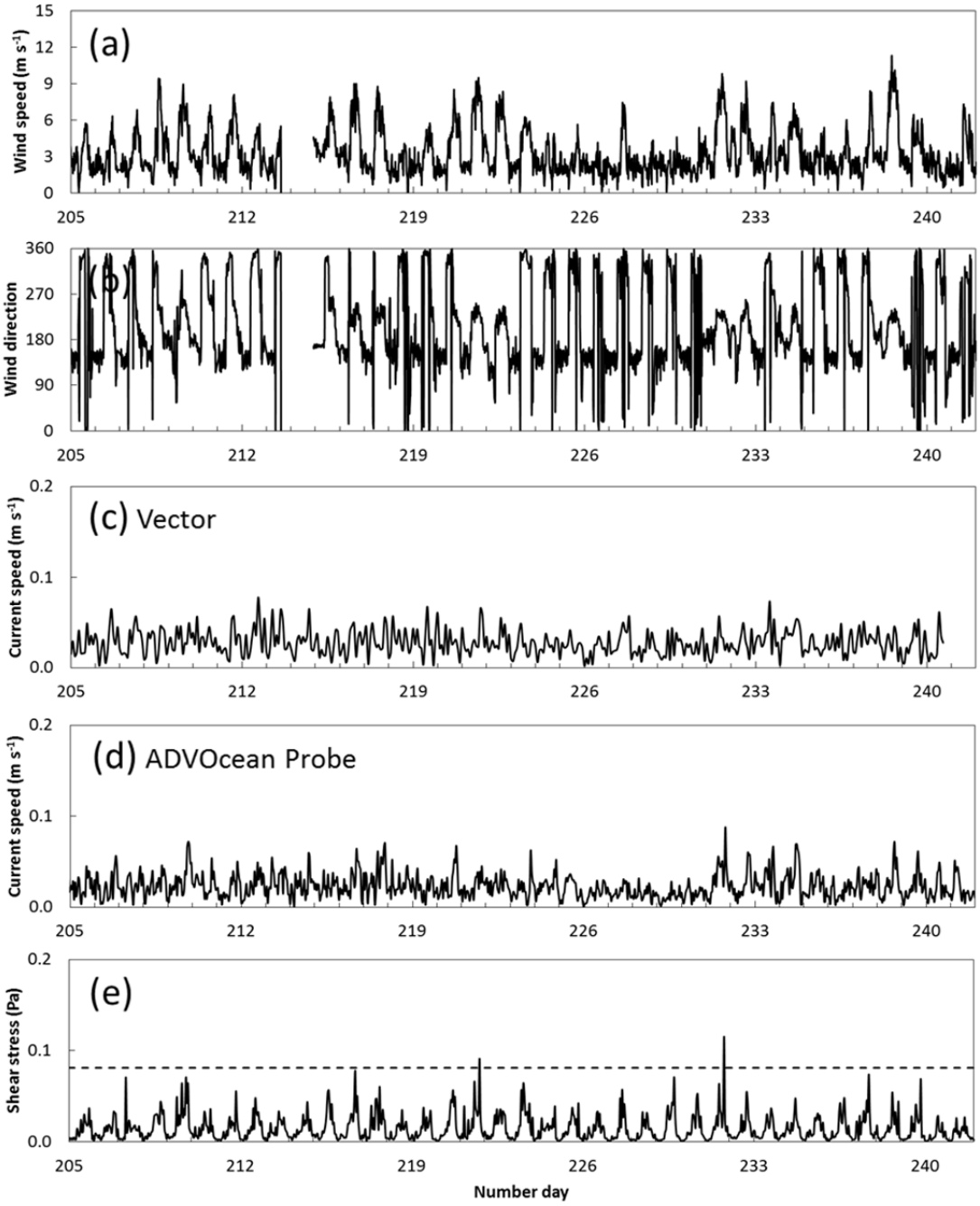

Figure 3-4. Comparison of observed variables from 23 July through 29 August 2008: (a) wind speed and (b) wind direction (degrees clockwise from north) measured at Timbercove station, burst-averaged nearbed current speed in the horizontal plane at (c) 0.20 m (Vector) and (d) 0.10 m (ADVOcean Probe) from the bottom, and (e) total bottom shear stress at a water depth of 5 m computed from data collected by the ADVOcean Probe. The horizontal dashed line at 0.081 Pa indicates the critical shear stress for incipient motion for a representative particle size of 150 μm.

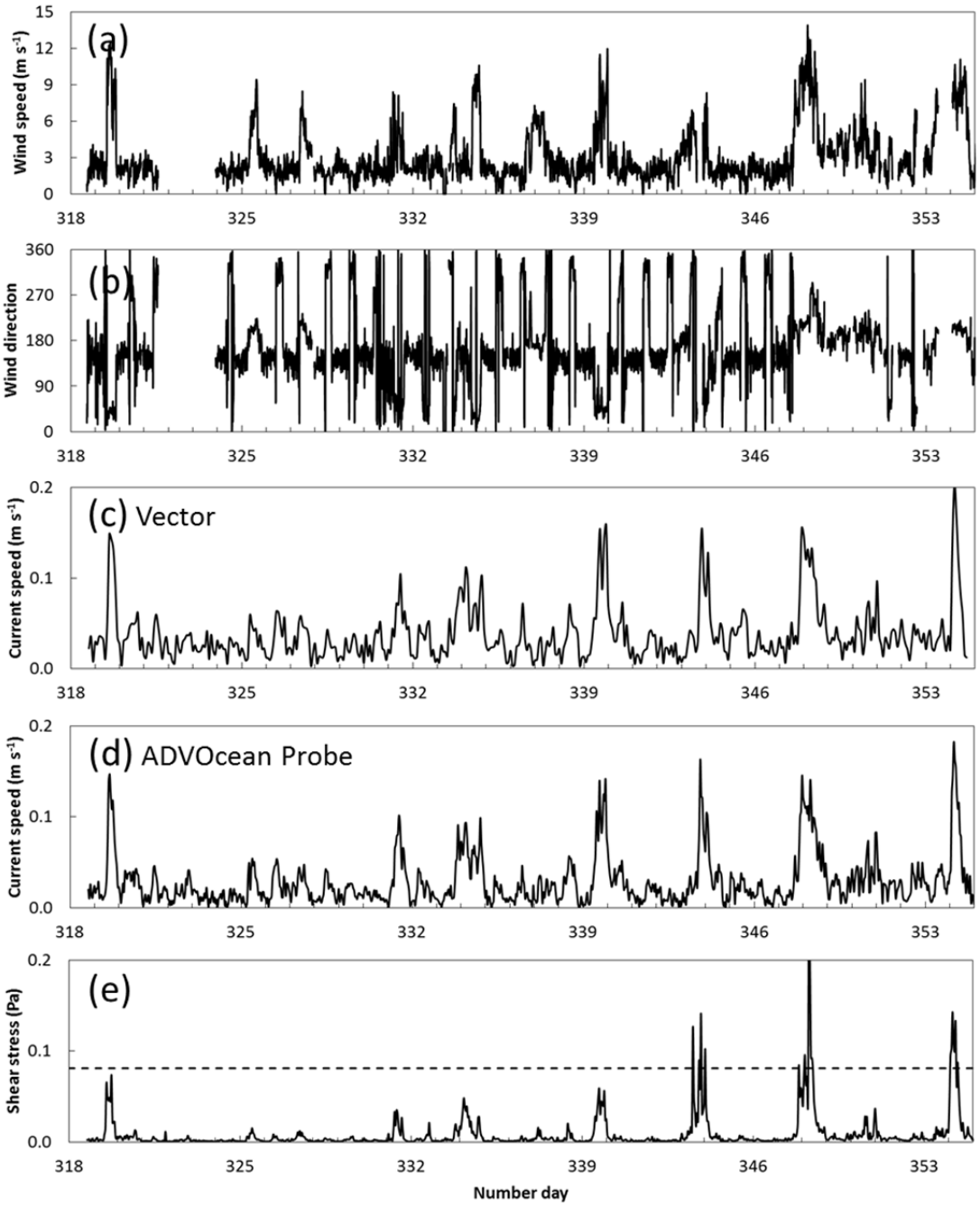

Figure 3-5. Comparison of observed variables from 13 November to 20 December 2008: (a) wind speed and (b) wind direction (degrees clockwise from north) measured at Timbercove station, burst-averaged nearbed current speed in the horizontal plane at (c) 0.20 m (Vector) and (d) 0.10 m (ADVOcean Probe) from the bottom, and (e) total bottom shear stress at a water depth of 5 m computed from data collected by the ADVOcean Probe. The horizontal dashed line at 0.081 Pa indicates the critical shear stress for incipient motion for a representative particle size of 150 μm.

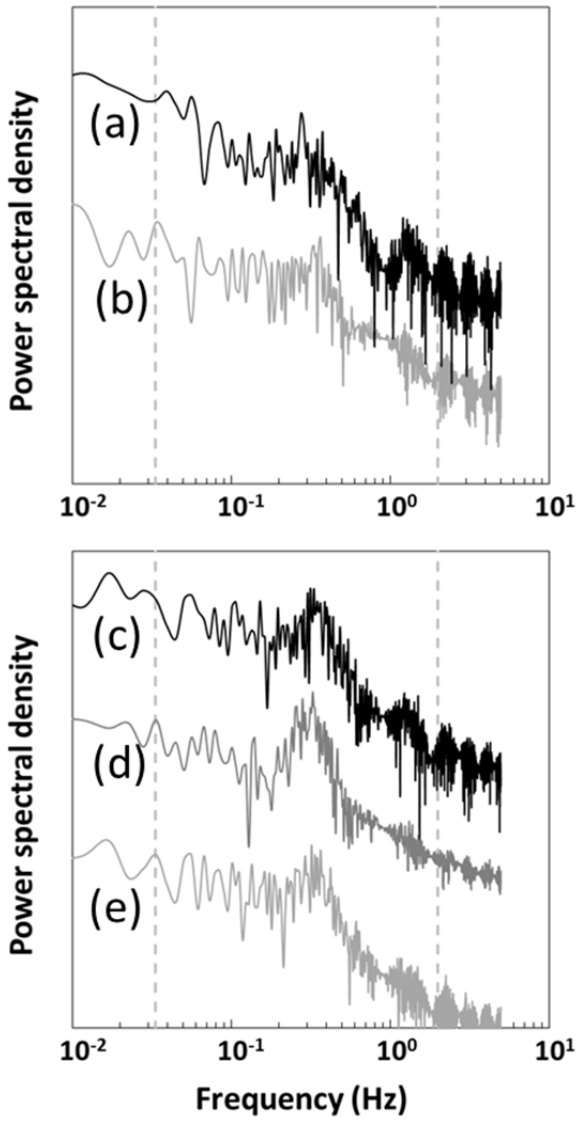

Figure 3-6. Power spectral density for 3-min bursts in 2008 for summer on (a) 8 August beginning at 7 p.m. and (b) 18 August beginning at 5 p.m. and winter on (c) 9 December beginning at 1 a.m., (d) 13 December beginning at 7 a.m., and (e) 19 December beginning at 9 a.m. The vertical dashed lines demarcate the so-called wind-wave band from 0.033 to 2 Hz (corresponding to wave periods between 0.5 and 30 sec). (The spectra have been offset for illustrative purposes.)

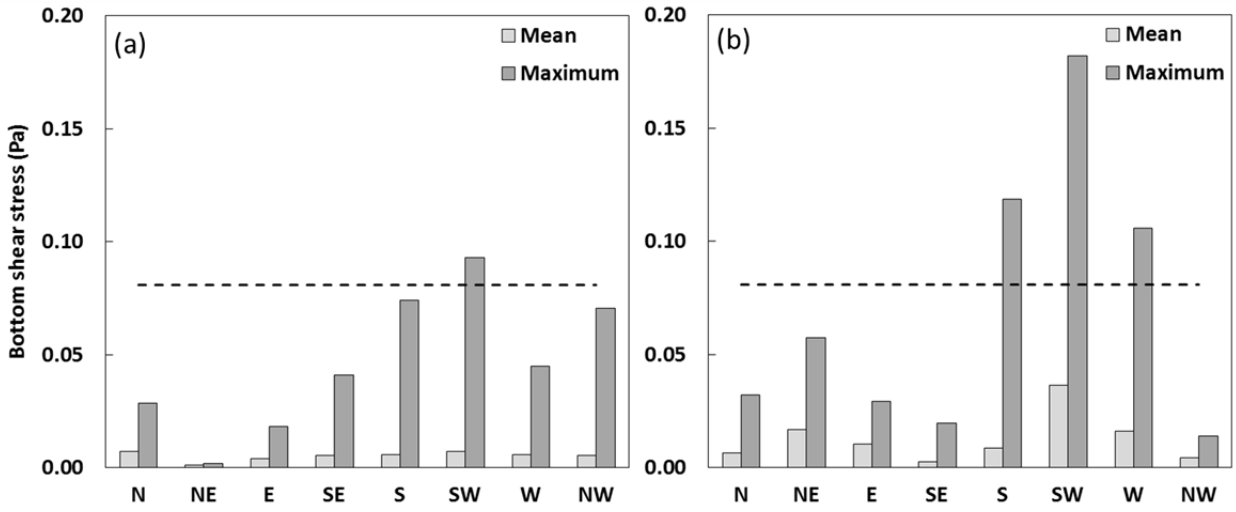

Figure 3-7. Mean and maximum bottom shear stress at a water depth of 5 m separated by wind direction for (a) summer and (b) winter. Bottom shear stress was directly estimated using ADVOcean Probe data. Observations of wind direction were collected at Timbercove station. The horizontal dashed line at 0.081 Pa indicates the critical shear stress for incipient motion for a representative particle size of 150 μm.

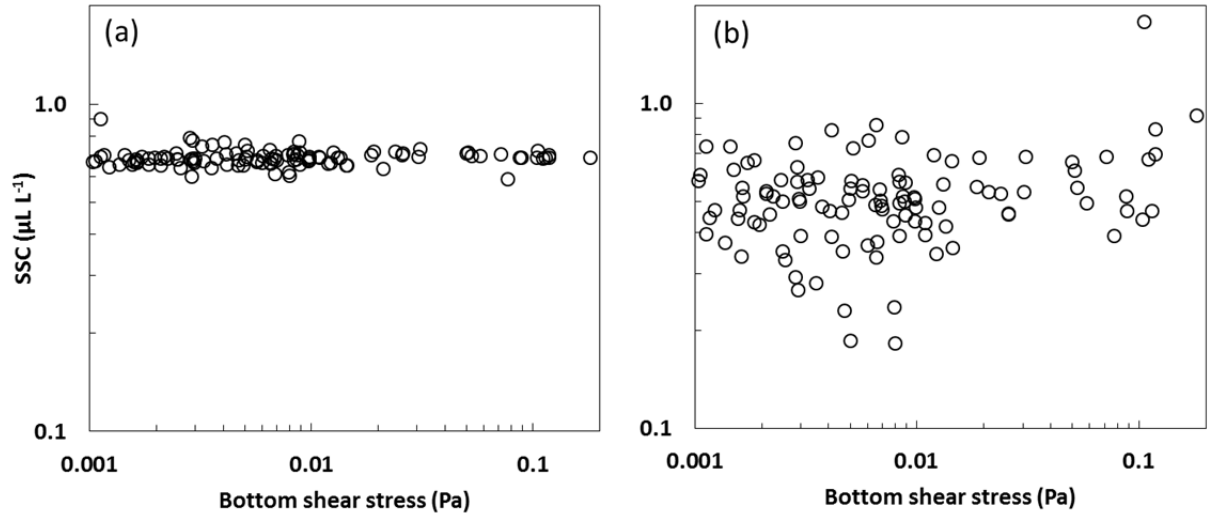

Figure 3-8. Suspended sediment concentration (SSC) versus total bottom shear stress at a water depth of 5 m for particles of median diameter (a) 2.5 to 16 µm and (b) 100 to 250 µm. In situ measurements of SSC were collected with the LISST-100X. Bottom shear stress was directly estimated using ADVOcean Probe data.

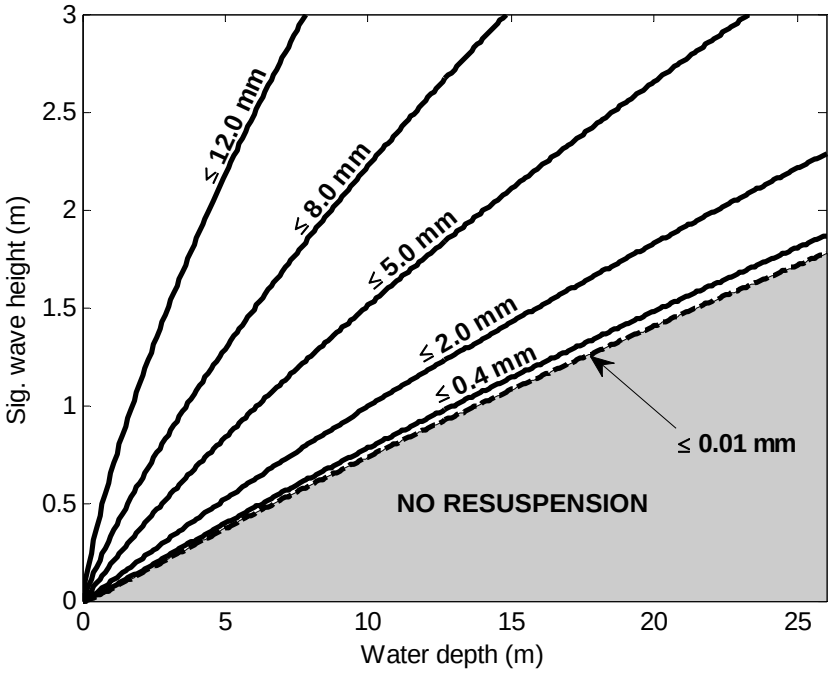

Figure 3-9. Particle resuspension with varying water depths and wave heights. Solid lines show the limit at which different particle diameters are resuspended from the lakebed. Similarly, the broken line shows the case for particles with diameter ≤10 μm. After *Norrman* [1964].

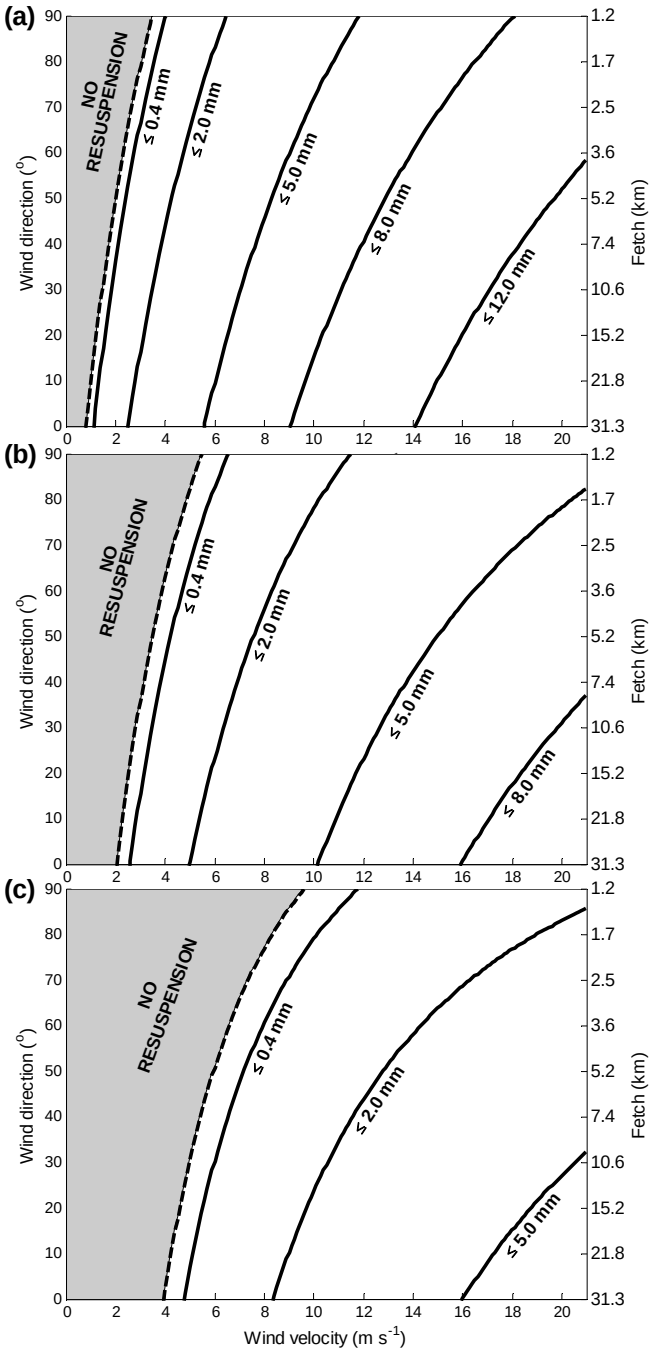

Figure 3-10. Resuspension curves considering different wind speed and direction for water depths of (a) 2.1 m, (b) 4.2 m, and (c) 8.3 m. The corresponding fetch is indicated on the secondary axis. Solid lines show the limit at which different particle diameters are resuspended from the lakebed. Similarly, the broken lines show the limiting case for particles with diameter ≤10 μm.

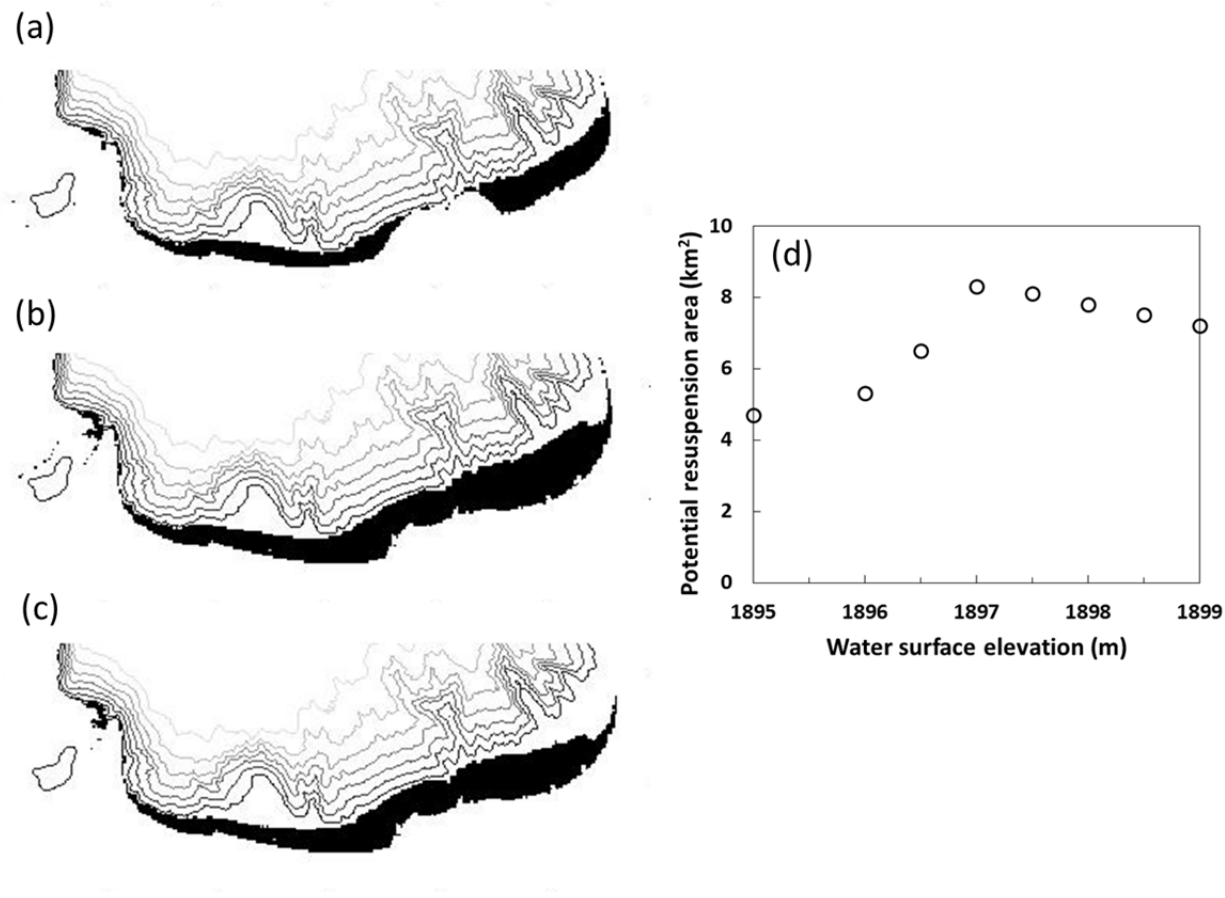

Figure 3-11. The areal extent of wind-driven sediment resuspension (denoted by black) in Lake Tahoe's southern nearshore zone, considering lake water level equal to (a) 2 m below the natural rim (1895 m), (b) the natural rim (1897 m), and (c) the maximum legal limit (1899 m). The area potentially affected by wind-driven sediment resuspension is (a) 4.7 km^2, (b) 8.3 km^2, and (c) 7.2 km^2. (d) Potential resuspension area with changing water surface elevation. Contours are shown at 50 m intervals.

Chapter 4. Inferring nearshore suspended sediment characteristics using acoustic Doppler devices

This chapter is based on work that is in preparation for publication as a technical note in the Journal of Hydraulic Engineering, a journal of the American Society of Civil Engineers. The authors are: Kristin E. Reardon (UC Davis), Fabián A. Bombardelli (UC Davis), and S. Geoffrey Schladow (UC Davis).

4.1 Introduction

Understanding the prevalence and distribution of suspended sediment is critical to assessing and improving water quality in natural systems. In an otherwise deep lake, the shallow, wind-exposed nearshore is of interest because it is susceptible to wind-driven sediment resuspension. Sediment resuspension results in the addition of light-scattering particles to the water column, as well as an increase in the exchange between pore-water and sediment-bound nutrients and contaminants and the overlying water [*Wetzel*, 1983]. Suspended matter, such as fine sediment, phytoplankton, and organic detritus, reduces light transmission through water by increasing the scattering and absorption of light [*Kirk*, 2011]. In this way, the nearshore lakebed becomes a source of fine particles, nutrients, and contaminants that may negatively impact water quality and contribute to reduced transparency [*Kirk*, 2011] and an altered temperature distribution [*Schladow et al.*, 2006; *Swift et al.*, 2006].

Sediment resuspension studies in large lakes that have relied on measurements of hydrodynamic and water quality variables have benefited from the development of in situ instruments that can be autonomously deployed [e.g., *Chung et al.*, 2009; *Hofmann et al.*, 2011]. In these studies, sampling continued during extreme weather events when wind conditions on the

lake would have made boat-based measurements unsafe. Time series were also recorded that would have been too labor-intensive and costly to have been practical without autonomous operation. For this investigation, we consider time series from three different acoustic Doppler devices deployed with the intended purpose of measuring flow and also exploring the backscatter signal amplitude as a proxy for suspended sediment concentration (SSC). Furthermore, we consider direct, concurrent measurements of SSC and particle size distribution (PSD) taken with an in situ optical device

Acoustic Doppler devices are designed to measure three-dimensional flow characteristics using the acoustic Doppler principle. Their operation relies on the presence of particulate matter in the water and measuring the reflection of an acoustic signal. Although the intended purpose of these instruments is to measure water velocity by measuring the velocity of the suspended particulates, they can also provide information about the quantity and type of particulate matter present by measuring the intensity of the backscatter intensity (BSI) or signal amplitude [*Sontek*, 1997; *Nortek*, 2001]. Acoustic Doppler devices are generally robust and well-suited to many lake applications as diverse as the Salton Sea [*Chung et al.*, 2009] and Lake Tahoe.

Although in theory the signal strength of acoustic Doppler devices is a seemingly obvious proxy for SSC, establishing relationships between signal strength and SSC has proven difficult. To date, the literature lacks an accepted standard by which suspended sediment characteristics should be inferred from the signal strength of acoustic Doppler devices. At this time, researchers must consider a priori the water quality conditions and instrument itself for calibration of regression models that are site- and instrument-specific.

Our study uses field measurements with the aim of demonstrating the applicability and reliability of using acoustic Doppler devices to infer suspended sediment characteristics and estimating the vertical profiles of suspended sediment concentration resulting from wind events. In doing so, we explored the merit of using signal strength as a surrogate for SSC in water of high transparency. Specifically, we considered whether these relationships between signal strength and SSC developed under winter conditions could be extended to summer. We also explored whether the Rousean distribution reflects the daily-averaged vertical profile of suspended sediment we inferred in the nearshore.

4.2 Field site and methods

We collected field measurements in summer and winter at the south shore of Lake Tahoe, a subalpine lake located in the Sierra Nevada Mountains on the California-Nevada border (Figure 2-1; Figure 3-1). While Lake Tahoe is oligotrophic as characterized by low nutrient concentrations, high dissolved oxygen concentrations, and transparent waters to great depths, it has experienced a measured reduction in deep water transparency over the last half century [*Goldman*, 1988]. It has also experienced a measureable decline in nearshore water quality [*Taylor et al.*, 2004].

The study site was located about 1000 m offshore in a water depth of about 5 m. Generally, the lakebed sediment at the study site was granular, well-sorted, non-cohesive, and with no apparent bedforms, both in summer and winter. It was composed of sand (>92 percent), silt (7 percent), and clay (<1 percent), and we assumed a representative grain size of 150 μm, corresponding approximately to d_{10} (Figure 2-7). As shown in Chapter 2, for a grain size of 150 μm, the critical shear stress for incipient motion was equal to 0.081 Pa.

Comprehensive field surveys to investigate nearshore sediment dynamics were carried out in summer from 23 July to 3 September 2008 and in winter from 13 November 2008 to 14 January 2009. Measurements included: nearbed velocity using two acoustic Doppler velocimeters (ADVs), a Sontek ADVOcean Probe and a Nortek Vector; and vertical profiles of currents using a Nortek acoustic Doppler current profiler and directional wave gauge (AWAC). In winter, SSC and PSD were measured with a LISST-100X. The instrument locations and sampling strategies for summer and winter were the same. Furthermore, all instruments were self-contained, moored, and autonomously deployed. Chapter 2 contains detailed information about field measurements. Table 4-1 summarizes the pertinent instrument deployment information.

The Laser In Situ Scattering and Transmissometry (LISST) series instruments from Sequoia Scientific, Inc. are optical devices that measure suspended particle concentrations over a range of size classes according to the laser diffraction technique. A laser beam passes through a small sampling volume containing particles in suspension. The light scattered by the particles is measured by photodetectors to give SSC and PSD [*LISST 100-X Particle Size Analyzer User's Manual version 4.65,* 2009].

To quantify SSC from acoustic measurements of signal strength, we assessed the slope and intercept of the calibrated linear regression of the SSC. We explored other regression methods suggested by *Rasmussen et al.* [2009]; however, they proved no better than the simple linear regression. To directly estimate bottom shear stress from ADV-measured velocity data collected from the Sontek ADVOcean Probe we used the method developed in Chapter 2.

4.3 Results and discussion

A comparison of signal strength from the ADVOcean Probe, Vector, and bottom-most bin of the AWAC and total SSC measured with the LISST-100X from 13 November 2008 to 14 January 2009 is presented in Figure 4-1. We observed that the ADVOcean Probe and Vector gave very similar results. Signal strength from the AWAC agreed with that of the ADVOcean Probe and Vector at times when there were very large peaks in signal strength. We assumed that the true measure of SSC was represented by the data collected with the LISST-100X.

To develop a relationship between SSC and signal strength of the ADVOcean Probe, we calibrated a simple linear regression model with slope equal to 0.0631 and intercept of -2.5254 (r^2=0.49; n=120; Figure 4-2). We similarly developed a relationship between SSC and signal strength of the Vector with slope equal to 0.0446 and intercept equal to -0.5739 (r^2=0.55; n=95; Figure 4-3). The LISST-100X provides the suspended sediment particle size distribution in 32 logarithmically-spaced size classes of median diameter from 1.25 to 250 μm. Considering the concentration of each size class and the signal strength of the ADVOcean Probe and Vector, it was possible to improve the linear regression models. The signal strength of the ADVOcean Probe best correlated with the concentration of particle size class of median diameter equal to 85.9 μm (r^2=0.52). The signal strength of the Vector best correlated with the concentration of particle size class of median diameter equal to 61.7 μm (r^2=0.74). This is not ideal, however, as the time series of SSC would reflect only the concentration of particles within the specific size class and not the overall concentration of all particles from 1.25 to 250 μm.

A comparison of bottom shear stress and SSC during the winter study period is shown in Figure 4-4. We observed a regular periodicity of one day for the time series of SSC from 13 November to 9 December 2008 (Figure 4-4b). We speculate that these regular peaks in SSC

could be the result of advection of suspended sediment from daily snow melt. No such pattern was observed for shear stress for the same period (Figure 4-4a). As described in Chapter 2, from 9 December 2008 onward the weather turned very cold with freezing air temperatures night and day and strong and sustained winds in a quasi-constant direction. This change in the weather may have been responsible for an abrupt end to the regular pattern as freezing weather could have ended the snow melt into the lake.

A comparison of bottom shear stress and SSC during the summer study period is shown in Figure 4-5. We observed a regular periodicity of one day for the time series of SSC for the entire period (Figure 4-5b). Similarly, we observed a regular return period of one day for shear stress for the same period (Figure 4-5a). However, these time series did not align. The peaks in shear stress occured in the afternoon or evening of each day; this corresponded to regular peaks in afternoon wind intensity, as discussed in Chapter 2. The peaks in SSC occurred in the middle of the night, nearly always at midnight. The data coming from the Vector were collected independently, yet correlated nearly perfectly (R^2>0.95) with the data coming from the ADVOcean Probe. We suspect that the regular afternoon wind events resulted in sediment resuspension at a shallower water depth, and then we observed the offshore advection of resuspended sediment at a later time.

For both winter and summer, we considered the effect of changing water temperature and thus density on the signal strength of the acoustic Doppler instruments. We reviewed the time series of vertical temperature profiles to see if diurnal patterns of stratification and mixing aligned with the daily fluctuations in signal strength. They did not.

A comparison of profiles of daily-averaged signal strength obtained from the vertical bins of the AWAC and the Rousean vertical distribution of sediment concentration is presented for winter in Figure 4-6 and summer in Figure 4-7. We assume that signal strength reported in each vertical bin is directly comparable. The Rouse equation was developed for open channel flow under equilibrium conditions, indicating a balance between the upward flux of sediment due to turbulence and the effect of gravity which returns sediment to the bed [*Rouse*, 1937; *Julien*, 1995]. Here we found that the shape of the Rousean distribution closely resembles the profiles of signal strength and corresponds to a range of appropriate representative particle sizes.

4.4 Conclusions

We found that there are limitations regarding the use of signal strength of acoustic Doppler devices as a proxy for suspended sediment concentration when deployed in high-transparency water. We assumed that the data collected with the LISST-100X was the true measure of SSC and was therefore used to calibrate the linear regression models. However, *Fugate and Friedrichs* [2001] inferred concentrations of estuarine particle populations in the lower Chesapeake Bay using Sontek ADVs and a LISST-100; compared them to concentrations from pumped water samples collected at regular intervals; and found that the Sontek ADV proved to be the best estimator of concentration. It may prove worthwhile for future research efforts to verify that the data collected from the LISST-100X in fact reflects in situ particle concentrations. We observed that the Rousean distribution reflects the daily-averaged vertical profile of suspended sediment inferred in the nearshore.

Acknowledgements

This research was supported by the University of California, Davis and a grant from the US Department of Agriculture Forest Service Pacific Southwest Research Station using funds provided by the Bureau of Land Management through the sale of public lands as authorized by the Southern Nevada Public Land Management Act. The lead author was supported for two years by the Eugene Cota-Robles Fellowship from the Office of Graduate Studies, University of California, Davis. The AWAC was provided on loan from the California Department of Water Resources. The Vector was provided as a Nortek 2008 Student Equipment Grant Award. The ADVOcean Probe was provided on loan from the US Geological Survey. We also wish to acknowledge key students and staff from the Environmental Dynamics Laboratory and the Tahoe Environmental Research Center, both of the University of California, Davis.

References

Chung, E. G., F. A. Bombardelli, and S. G. Schladow (2009), Sediment resuspension in a shallow lake, *Water Resour. Res.*, *45*, W05422, doi: 10.1029/2007WR006585.

Fugate, D. C., and C. T. Friedrichs (2001), Determining concentration and fall velocity of estuarine particle populations using ADV, OBS, and LISST, *Cont. Shelf Res.,* 22, 1867-1886.

Goldman, C. R. (1988), Primary productivity, nutrients, and transparency during the early onset of eutrophication in ultra-oligotrophic Lake Tahoe, California-Nevada, *Limnol. Oceanogr.*, *33*, 1321-1333.

Hofmann, H., A. Lorke, and F. Peeters (2011), Wind and ship wave-induced resuspension in the littoral zone of a large lake, *Water Resour. Res.*, *47*, W09505, doi: 10.1029/2010WR010012.

LISST 100-X Particle Size Analyzer User's Manual version 4.65 (2009) http://www.sequoiasci.com/product/lisst-100x/

Julien, P.Y. (1995), *Erosion and Sedimentation*, Cambridge University Press, New York, NY.

Kirk, J. T. O. (2011), *Light and Photosynthesis in Aquatic Ecosystems*, 3rd ed., University Press, Cambridge, UK.

Nortek. (2001), Monitoring sediment concentration with acoustic backscattering instruments. Nortek technical note no. 003.

Rasmussen, P.P., Gray, J.R., Glysson, G.D., and Ziegler, A.C., 2009, Guidelines and procedures for computing time-series suspended-sediment concentrations and loads from in-stream turbidity-sensor and streamflow data: U.S. Geological Survey Techniques and Methods, book 3, chap. C4, 52 p.

Rouse, H. (1937), Modern conceptions of the mechanics of fluid turbulence. *Transactions of the American Society of Civil Engineers*, 102, 463-541.

Schladow, S. G., F. J. Rueda, W. E. Fleenor, and E. G. Chung (2006), Predicting the effects of configuration changes on Salton Sea stratification using a three-dimensional hydrodynamic model, Report to CH2M HILL and California Department of Water Resources, TERC Report 06-007.

Sontek. (1997), Sontek Doppler current meters – using signal strength data to monitor suspended sediment concentration. Sontek application note.

Swift, T. J., J. Perez-Losada, S. G. Schladow, J. E. Reuter, A. D. Jassby, and C. R. Goldman (2006), Water clarity modeling in Lake Tahoe: Linking suspended matter characteristics to Secchi depth, *Aquat. Sci.*, *68(1),* 1-15, doi: 10.1007/s00027-005-0798-x.

Taylor, K., R. Susfalk, M. Shanafield, and S. G. Schladow (2004), Near-shore clarity at Lake Tahoe: Status and causes of reduction, Report to Lahontan Water Board (CA), Nevada Division of State Lands, and Tahoe Regional Planning Agency.

Wetzel, R. G. (1983), *Limnology*, 2nd ed., Saunders, Philadelphia, USA.

Table 4-1. In situ measurements

Instrument	Sampling periods[a]		Sampling height or orientation	Sampling strategy		
	Summer	Winter		Sampling rate/interval	Sampling duration	Burst interval
ADVOcean Probe	23 Jul – 29 Aug	13 Nov – 21 Dec	0.10 m above bed	10 Hz	3 min	1 h
Vector	23 Jul – 27 Aug	13 Nov – 19 Dec	0.20 m above bed	64 Hz	2 min	2 h
AWAC	23 Jul – 3 Sep	13 Nov – 14 Jan	Bottom-mounted[b]	10 min	NA	NA
LISST-100X	NA	11 Dec – 14 Jan	0.20 m above bed	1 Hz	2 min	2 h

[a]In situ measurements were taken in summer 2008 and winter 2008-2009.

[b]The AWAC provided profiles in 0.5 m vertical bins; the frame and blanking distance precluded measurements in the first 0.6 m above bed.

NA=not applicable

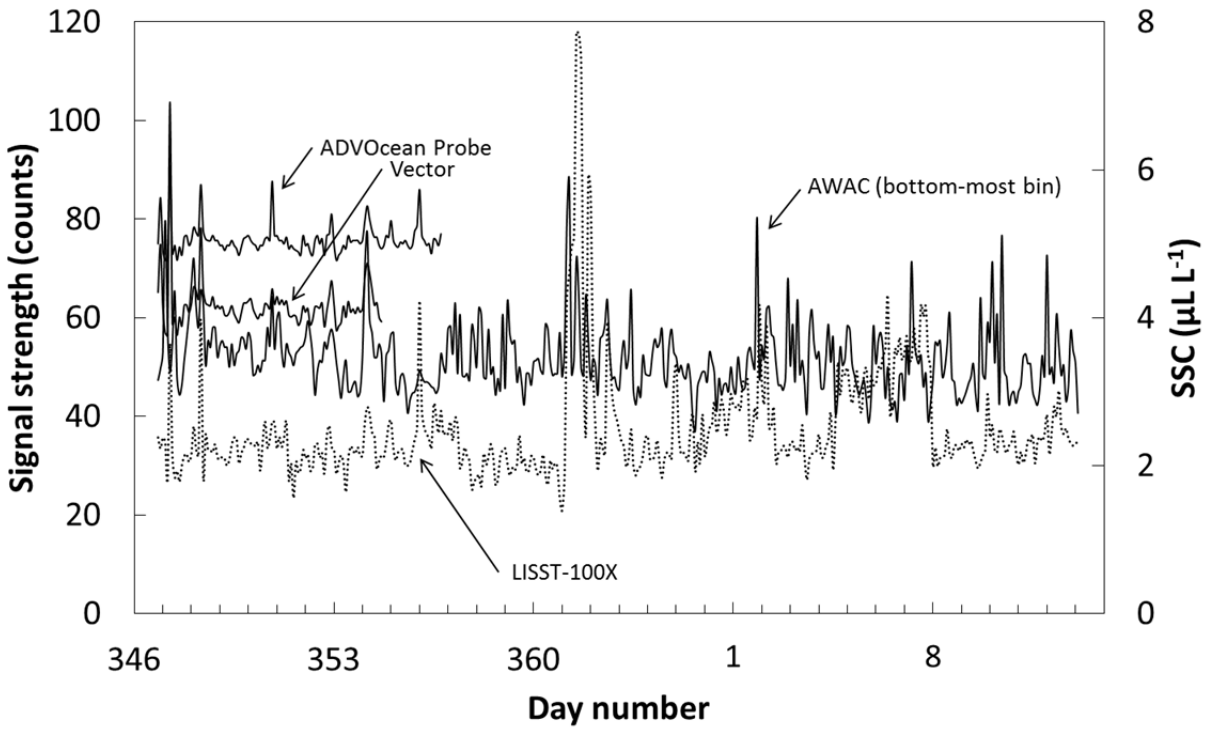

Figure 4-1. Comparison of signal strength from the ADVOcean Probe, Vector, and bottom-most bin of the AWAC and total SSC measured with the LISST-100X from 13 November 2008 to 14 January 2009.

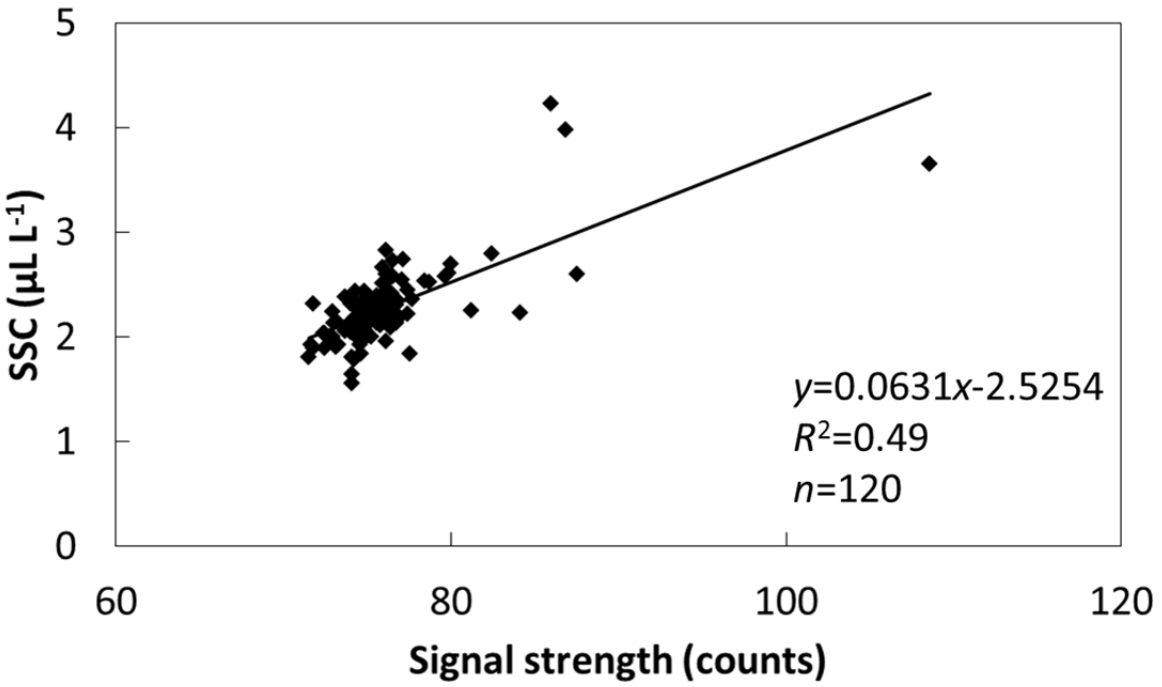

Figure 4-2. Linear regression of suspended sediment concentration (SSC) versus signal strength of the ADVOcean Probe every 2 h.

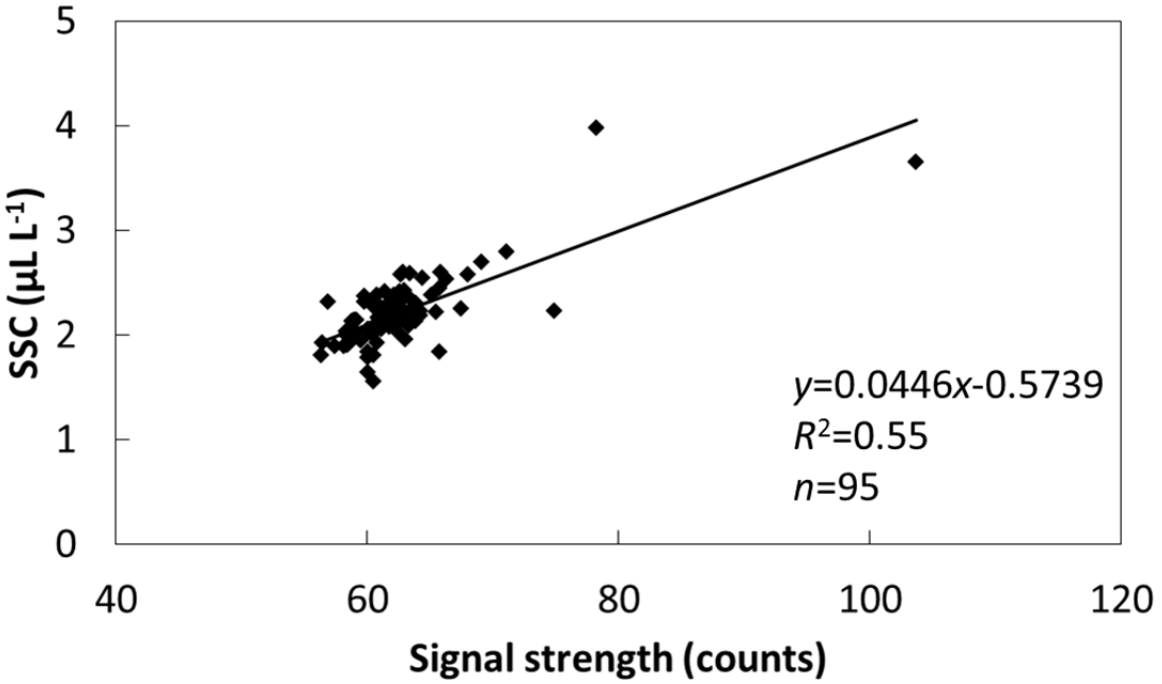

Figure 4-3. Linear regression of suspended sediment concentration (SSC) versus signal strength of the Vector every 2 h.

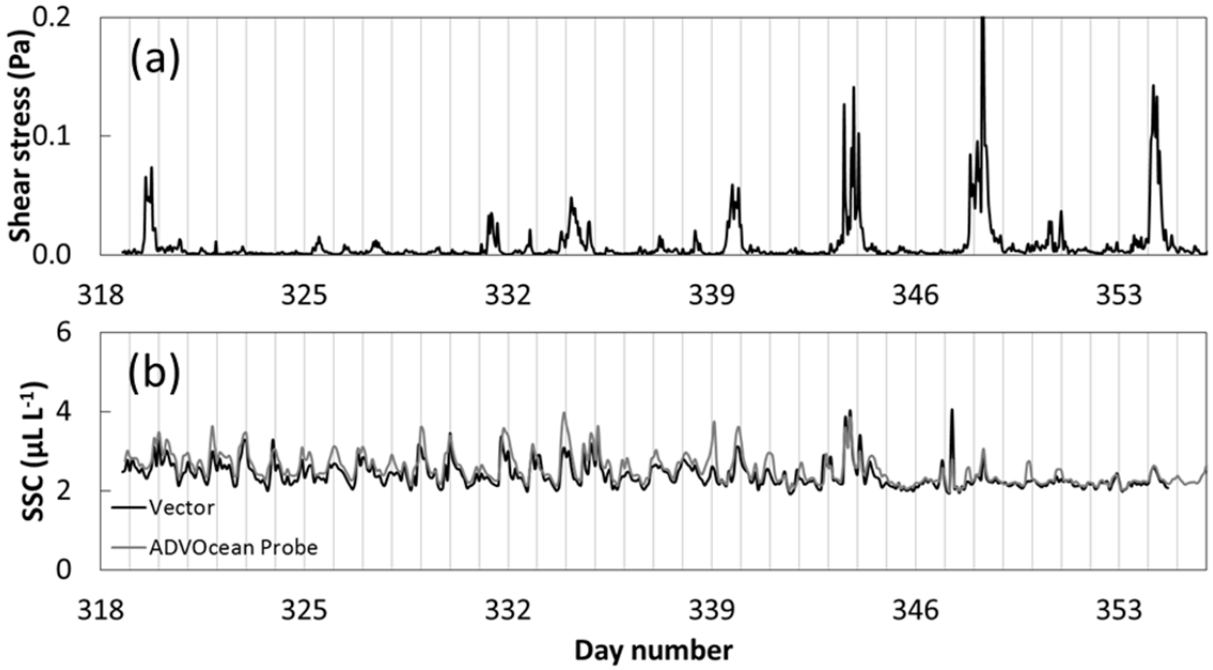

Figure 4-4. Comparison of bottom shear stress and SSC computed from the signal strength of the Vector and ADVOcean Probe for 13 November to 21 December 2008. Gridlines indicate midnight.

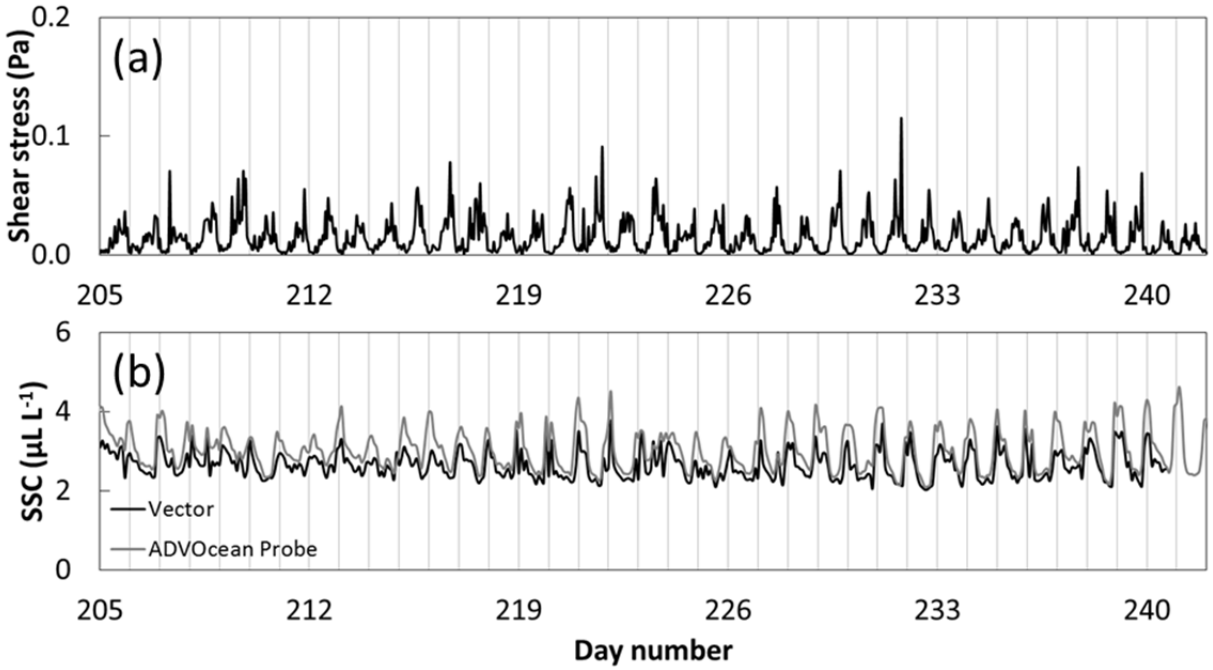

Figure 4-5. Comparison of bottom shear stress and SSC computed from the signal strength of the Vector and ADVOcean Probe for 23 July to 29 August 2008. Gridlines indicate midnight.

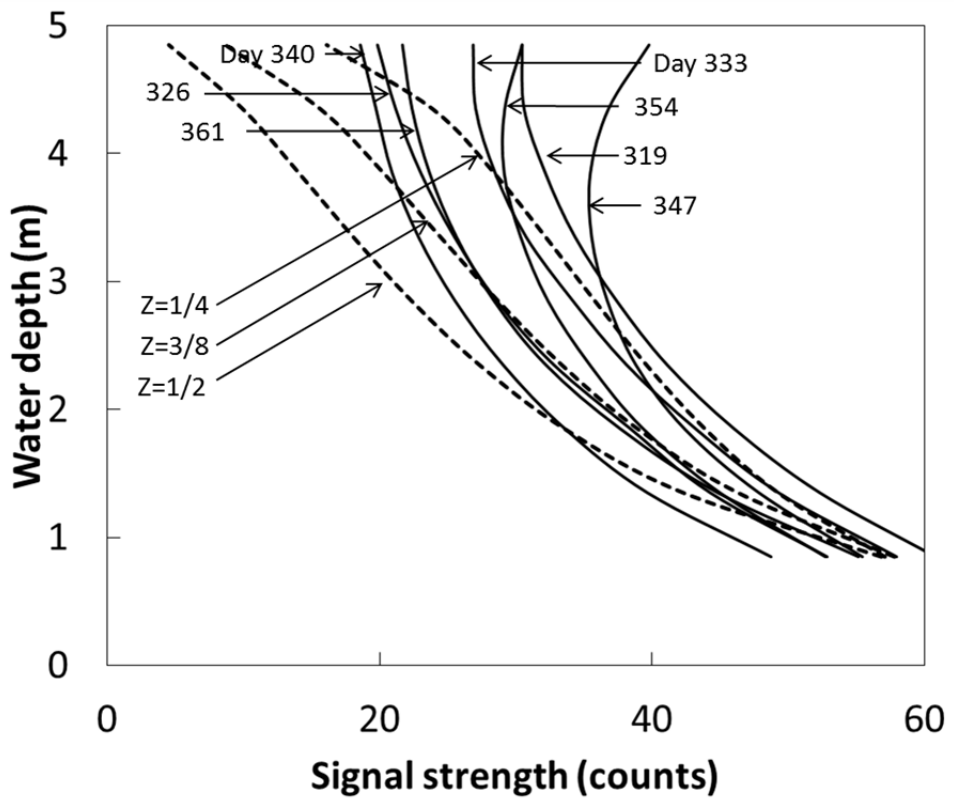

Figure 4-6. Comparison of daily averaged signal strength profiles and the Rousean distribution. Solid black lines are signal strength profiles observed every 7 days for 13 November to 21 December 2008. Dashed black lines show the Rousean distribution for Rouse number, Z, of 0.25, 0.375, and 0.5. Data are from 2008.

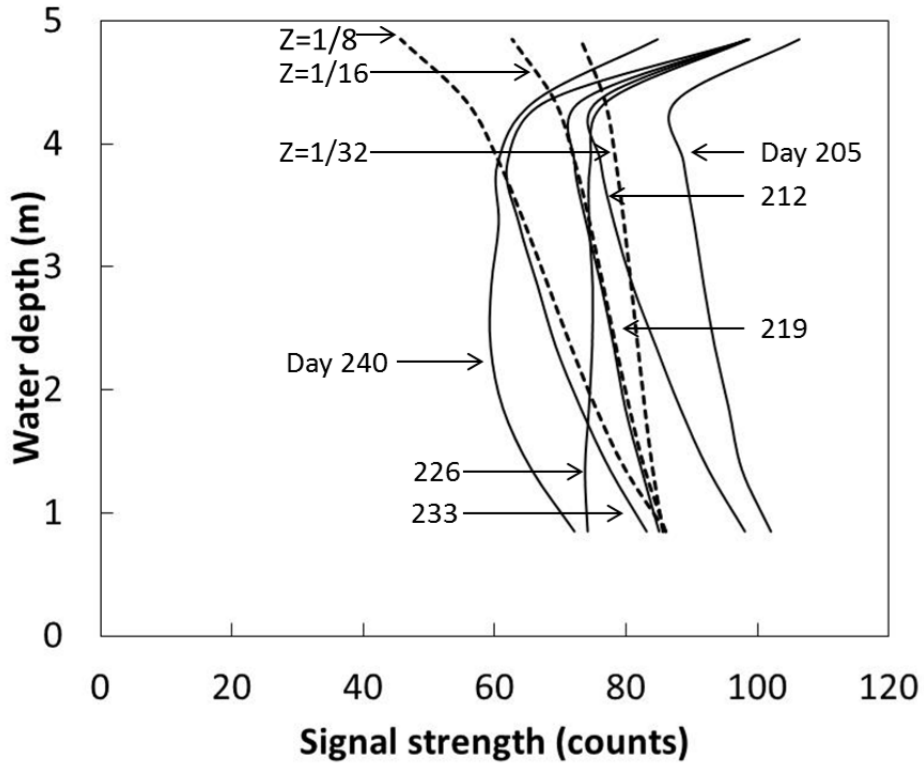

Figure 4-7. Comparison of daily averaged signal strength profiles and the Rousean distribution. Solid black lines are signal strength profiles observed every 7 days for 23 July to 29 August 2008. Dashed black lines show the Rousean distribution for Rouse number, Z, of 0.0313, 0.0625, and 0.125. Data are from 2008. Large values of signal strength near the water surface are attributed to sidelobe interference.

Chapter 5. Summary and conclusions

The research presented in this dissertation was the first study of wind-driven nearshore sediment resuspension and its implications for water clarity at Lake Tahoe. While Lake Tahoe appears startlingly deep and blue, lake transparency has nevertheless been declining since the 1960s. The Lake Tahoe TMDL identifies the external pollutants responsible for the loss of transparency as fine sediment, nitrogen, and phosphorus, but an investigation of the potential for internal sources of fine sediment (e.g., resuspended sediment) had been lacking. Yet at other wind-exposed lakes, sediment resuspension can be a significant source of fine particulates.

We carried out a comprehensive field campaign to observe and quantify wind-driven nearshore sediment resuspension in summer and winter. We identified by experimental observation instances of wind-driven sediment resuspension and used this information to establish a framework for bottom shear stress computations and wind-wave modeling for wind-driven nearshore sediment resuspension. We also explored the nature of the lakebed, wind exposure, wave climate, and hydrodynamic and sediment variables to elucidate nearshore patterns in summer and winter. In summer we observed strong diurnal patterns. In winter we observed low-energy periods punctuated by high-energy events with no regular order.

We developed a novel approach for quantifying the total bottom shear stress in a lacustrine environment according to its components attributed to wind-waves, mean currents, and random motions, validating it with further computations from field data. When the total shear stress exceeded the critical shear stress, the contribution to overall shear stress was about 80 percent from wind-waves and 10 percent each from mean currents and random motions. Therefore, wind-waves resulted in sediment resuspension as corroborated by simultaneous increases in shear stress and total measured sediment concentration. Additionally, by filtering the

high-frequency nearbed velocity signal, we shed light on the nature of the individual flow components. Furthermore, the power spectral density plots provided quantification of the peak wave periods.

We modified the wind-wave model STWAVE by correcting the bottom-friction formulation in order to reflect typical lake conditions with flow regimes that are viscous-dominated. Lake applications of STWAVE had previously been limited to hurricane conditions which result in fully-turbulent flow regimes. We developed what we believe is the first application and validation of a modification of the code STWAVE to simulate wind-wave induced sediment resuspension for a viscous-dominated flow in lakes. The modified STWAVE was used to develop management charts that illustrate relationships between fetch, wind intensity, and wave height and between water depth, wave height, and nearshore bottom dynamics (i.e., the potential for mobilization of different sized particles). For a representative grain size of 150 μm, the wind-driven surface waves influence the sediments to a maximum water depth of about 9 m. Lastly, we evaluated the potential for nearshore sediment resuspension with changing lake levels, considering a range of possible future scenarios.

We validated the 1991 García and Parker formulation for sediment entrainment rates appropriate for a lacustrine environment that was otherwise developed for open channel conditions. We showed good agreement between simulated and measured rates of sediment entrainment into suspension.

We investigated the use of acoustic backscatter from acoustic Doppler devices to infer nearshore suspended sediment characteristics for those times when direct measurements were not available. We explored the nature of the suspended sediment and signal strength of the

autonomously-deployed in situ instruments. We concluded that there is limited applicability of such techniques in a lake of high transparency.

An important consideration is how these research findings can be translated to management strategies. Because the evidence to date does not suggest that wind-driven nearshore sediment resuspension results in an increase in particle loading of the size class that has been identified to most negatively impact water clarity, there are no recommended changes to the Lake Tahoe TMDL at this time. However, long-term monitoring of hydrodynamic and sediment variables is critical. Future changes in the watershed and/or atmospheric sources of pollutants may impact particle loading of fine sediment by wind-driven sediment resuspension. Currently, we attribute very modest increases in suspended sediment concentration resulting from wind-driven sediment resuspension to a relative limitation of fine material in the nearshore. If the prevalence of fine material increased in the future, then there would likely be an associated increase in particle loading of fine material. Additionally, future changes in climate may impact particle loading of fine sediment by wind-driven sediment resuspension. This was investigated here by considering projected changes in lake water level. (We do not consider future scenarios in which the wind intensity changes, because in the Tahoe Basin, wind speeds were projected to decrease very modestly over the next century relative to historical averages.) Yet should these climate projections prove incorrect or incomplete, this research remains useful and can be reviewed and updated considering alternative scenarios. Furthermore, the predictive tools and management charts developed in this work will aid researchers and managers in understanding the effects of changing lake conditions (natural or engineered) on the potential for wind-driven nearshore sediment resuspension.

To identify the potential for internal loading of nutrients by resuspension and hypolimnetic anoxia, additional nearshore studies are necessary. Controlling phosphorus inputs at Lake Tahoe may be the most reasonable means of slowing cultural eutrophication of both the mid-lake and nearshore by further limiting nutrients for primary productivity. However, if at Lake Tahoe internal loading proves to be great enough, then the desired environmental improvements may not be achieved until the accumulated deposit of phosphorus in the lake bed is exhausted. This has not yet been adequately investigated. This study focused on wind-driven resuspension of particulate matter; characterization and quantification of the potential for phosphorus loading was beyond the scope of this work. Further research could result in recommendations to update management strategies aimed at protecting the aesthetic enjoyment of Lake Tahoe's historical deep water and nearshore clarity.

Appendix A. Sampling strategy adequacy

The sampling strategy (3-min bursts at 10 Hz every hour) optimized the balance between the resolution of the flow scales, available battery power, and available memory of the ADVOcean Probe. The instruments were deployed at Lake Tahoe for two months at a time and were not readily accessible by a diver.

In order to show that 3-min bursts adequately represent the flow scales, we present the spectra of two signals. In Figure A-1, we included one 3-min burst measured on 13 December 2008 at 7 a.m. (the burst shown in Figure 2-2); in turn, in Figure A-2, we appended the time series from 13 December 2008 at 7 a.m. with the time series from 8 a.m. and 9 a.m. to mimic a 9-min burst. We see that the spectra have similar form, including a peak at approximately 0.33 Hz, indicating that 3-min bursts were adequate to characterize the waves.

Additionally, we investigated the ratio between the sampling time (T), and the "integral scale" (Tx) because of the so-called "fast-sampling limit" [*Bendat and Piersol*, 2000] and the influence of T/Tx on the variance of the estimator of the mean of the signal. This "fast-sampling limit" corresponds to the case of $\Delta t << Tx$ and $T>>Tx$, where Δt is the sampling time. In our case, Δt=0.1 sec, Tx=3 sec, and T=180 sec, so the conditions above do not hold strictly. Thus, although we believe that the theory (and rules of thumb) is extremely important in these cases, we also consider that it only provides crude guidance in practical cases. We therefore believe that the comparison shown gives compelling evidence that the 3-min bursts successfully capture the wind-wave band.

Reference

Bendat, J. S., and A. G. Piersol (2000), *Random Data: Analysis and Measurement Procedures*, 3rd ed., Wiley.

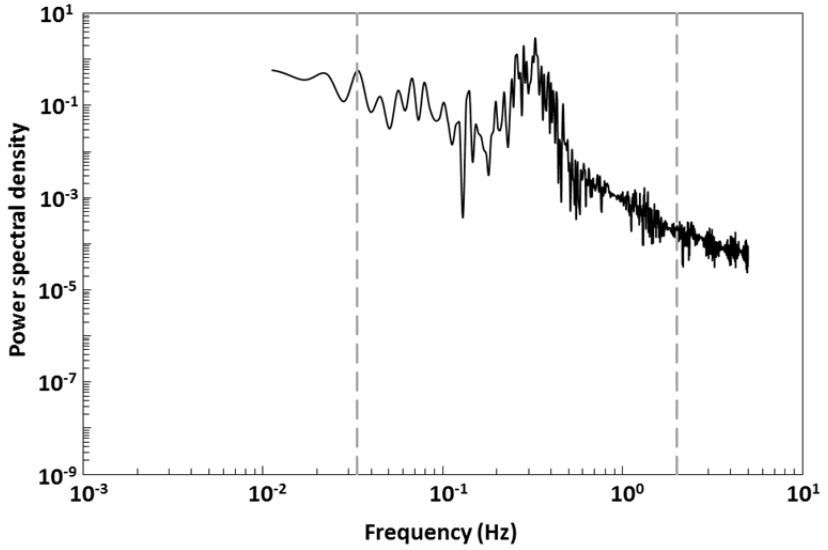

Figure A-1. Power spectral density for a 3-min burst on 13 December 2008 at 7 a.m. (the burst shown in Figure 2-2 of the manuscript). The peak of the power spectral density is at 0.33 Hz (corresponding to a wave period equal to 3.0 sec). The vertical dashed lines demarcate the so-called wind-wave band from 0.033 to 2 Hz (corresponding to wave periods between 0.5 and 30 sec).

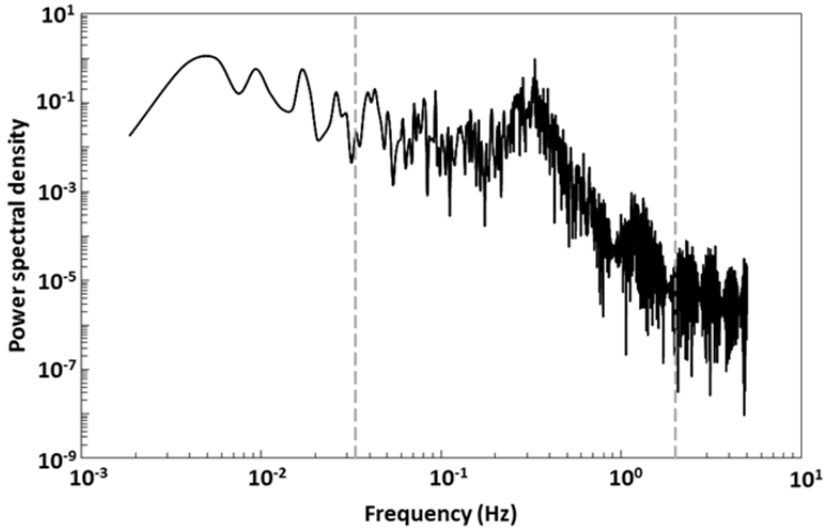

Figure A-2. Power spectral density for three 3-min bursts appended together; these bursts were collected on 13 December 2008 at 7 a.m., 8 a.m., and 9 a.m. (9 min total). The peak of the power spectral density is at 0.33 Hz (corresponding to a wave period equal to 3.0 sec). The vertical dashed lines demarcate the so-called wind-wave band from 0.033 to 2 Hz (corresponding to wave periods between 0.5 and 30 sec).

Appendix B. Sensitivity analysis of the velocity decomposition

We based the decomposition on the general understanding of flows in coastal areas. We carefully considered various aspects of this methodology during the development of the work; furthermore, we have provided checks for the computations to the extent possible. We believe that the methodology offers a plausible solution to a challenging subject in coastal zones in general, and in lakes in particular, initiating a discussion on how to more accurately discriminate among the components of shear stress.

Several factors contribute to our belief that the methodology is sound. First, the decomposition of the velocity signal as the sum of several components of different frequencies is a technique at the heart of methodologies in several branches of science, including turbulence. Second, we found that estimates of shear stress due to waves obtained from the methodology are in agreement with values coming from computations which use estimations of the wave heights (see Table 2-2). In Table 2-2, we adopted values of the wave heights, since we were not able to observe wave heights directly with the AWAC. Third, Figure 2-9 is very compelling. When the wind is intense and the total bottom shear stress is in excess of the critical shear stress, the vast majority of the contribution to the total bottom shear stress (about 80 percent) can be attributed to wind-waves, consistent with findings in the literature [e.g., *Luettich et al.*, 1990]. At these times, there are instances when the random motions contribute to the shear stress as well, but this amounts to 10 percent at most, which is below the uncertainty of any methodology assessing shear stress in natural flows. When the currents are weak and there is very low wind (and the total bottom shear stress is much less than the critical shear stress), then random motions may account for up to half of the bottom shear stress, as expected. However, it is important to remember that in these instances, the total bottom shear stress is nearly zero. Overall, random

motions never contribute meaningfully to the development of bottom shear stress. Thus, the physics-based methodology provides sound results.

We have examined the idea of an adaptive methodology in several ways. First, we performed a sensitivity analysis for different values of the wind-wave band. Second, we compared spectra coming from different bursts. It is worth mentioning at this point that the limits were adopted following standard analyses found in the literature. We originally obtained the band (0.5 to 30 sec) from recommendations by Nortek; these ranges are also consistent with classifications provided by *Horikawa* [1978]. We found that the shear stress attributed to wind waves changes modestly by varying the bands (see Figure B-1), with differences which are within the ranges of errors in field measurements, reinforcing that we have indeed captured the bulk of the influence of wind waves.

References

Horikawa, K. (1978), Present state of coastal sediment studies, *Mitteilungen, Leichtweiss-Inst. f. Wasserbau, Tech. Univ. Braunschweig* 56:77-197.

Luettich, R. A., D. R. F. Harleman, and L. Somlyody (1990), Dynamic behavior of suspended sediment concentrations in a shallow lake perturbed by episodic wind events, *Limnol. Oceanogr.*, *35(5)*, 1050-1067.

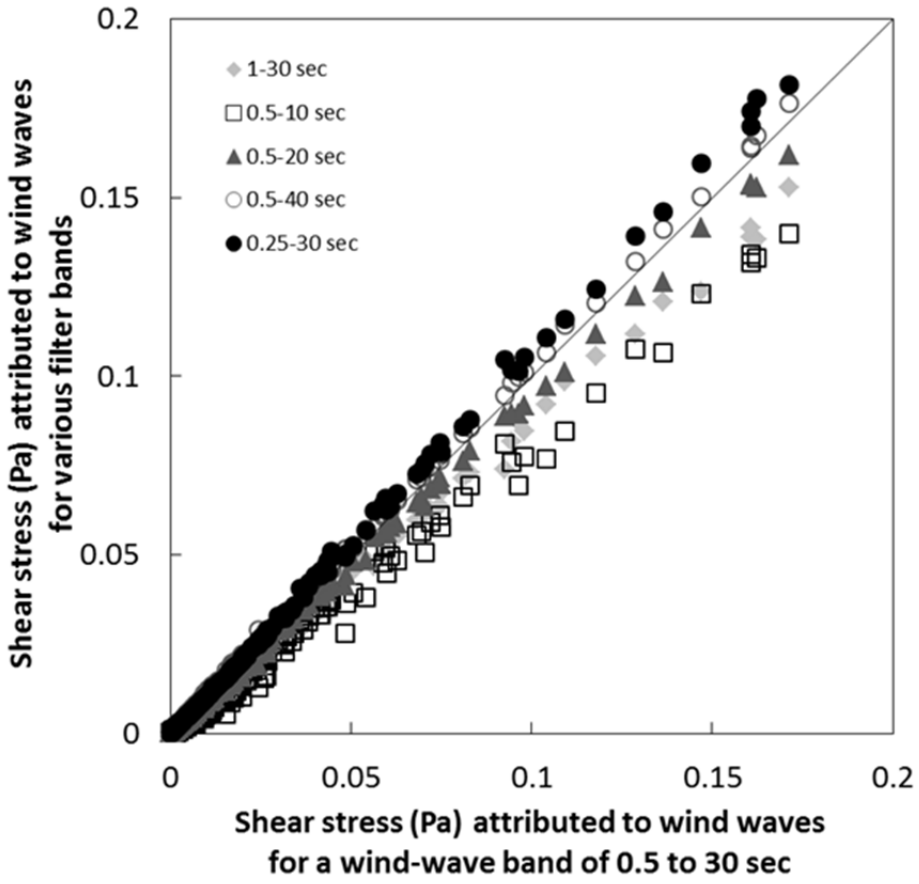

Figure B-1. Comparison of shear stress attributed to wind-waves for the so-called wind-wave band of 0.5 to 30 sec and various band filters (as indicated in the legend).

Appendix C. Background and further comparisons of STWAVE

We have undertaken comparisons regarding the model, as detailed below. We also show below that our modifications to STWAVE resolve what we consider to be a fluid-mechanics inconsistency within the code.

In earlier versions of STWAVE, two elements were missing: 1.) the code could only be used in the so-called "half plane," which precluded the simulation of wave fields in water bodies such as lakes; and 2.) the sink term in the spectral energy density due to bed friction was absent. In the 2001 manual [*Smith et al.*, 2001], the discussion regarding the bottom friction was as follows: "The significance of bottom friction on wave dissipation has been a topic of debate in wave modeling literature. Bottom friction has often been applied as a tuning coefficient to bring model results into alignment with measurements. Although bottom friction is easy to apply in a wave model, determining the proper friction coefficients is difficult."

These two aspects of the code have recently been modified [see *Massey et al.*, 2011]. To address the first issue, a "full plane" model was developed. This modification made the model especially suitable for lakes. To address the second issue, the 2011 version of STWAVE uses Manning's equation to account for bed friction.

According to the 2011 manual [*Massey et al.,* 2011], a Manning's *n* value between 0.01 and 0.05 should be used. Units of Manning's *n* should be $m^{1/6}$. A value of Manning's *n* of 0.01 pertains to glass, an unrealistic condition for lakes. Although the USACE acknowledges that *n* is a "calibration parameter" [*Massey et al.*, 2011], we strongly believe that it should not be used as a "garbage dump" [*Yen*, 2001, personal communication]. Numerous early runs with STWAVE

were developed considering no bottom friction and, more recently, with Manning's *n* equal to zero (which corresponds to no bottom friction).

We believe that the formulation of the shear stress embedded in STWAVE using Manning's equation involves conceptual shortcomings for the simulation of wave fields in lakes, where the flow condition is often far from being fully rough – and therefore outside the range of applicability of Manning's equation [see *Gioia and Bombardelli*, 2002]. In lakes, orbital velocities close to the bed are usually so small that the corresponding wave Reynolds numbers are also very small. This is fundamentally different from the case of open-channel flow. Furthermore, STWAVE was validated under mostly energetic, fully-rough conditions, very different from those occurring in most lakes. STWAVE has been validated against observations with wave heights much larger than the usual conditions experienced in lakes (e.g., at Willapa Bay, WA; Grays Harbor, WA; and Ponce de Leon Inlet, FL). We believe that the code needed to be modified to account for this deficiency, which led to the development of our approach.

We have compared the model results of STWAVE with a fixed Manning's *n* value of zero (no friction) and the modified STWAVE (formulated for viscous-dominated flow) for wave height, wave period, and root-mean-square of the nearbed velocity (u_{rms}). Our comparisons indicate that our modification resulted in very modest differences when considering northerly winds of 3 m s^{-1} (Figure C-1a) and 12 m s^{-1} (Figure C-1b), and slightly greater differences at 21 m s^{-1} (Figure C-1c) for the south shore of Lake Tahoe. Note that winds of 21 m s^{-1} are much greater than what we would reasonably expect at Lake Tahoe considering the wind record at Timbercove for the years from 2003 to 2013. The highest wind speed observed during our study period was approximately 15 m s^{-1} (Figure 3-2).

Additionally, we have compared the model results of STWAVE with a fixed Manning's *n* value of 0.02 (as it would have been run for fully-turbulent conditions) and the modified STWAVE (formulated for viscous-dominated flow) for wave height, wave period, and root-mean-square of the nearbed velocity (u_{rms}). Our comparisons indicate that our modification resulted in appreciable differences when considering northerly winds of 3 m s^{-1} (Figure C-2a), 12 m s^{-1} (Figure C-2b), and 21 m s^{-1} (Figure C-2c) for the south shore of Lake Tahoe. It should be noted that $n = 0.02$ is an arbitrary value selected for illustrative purposes.

In summary, we have developed a methodology that accounts for the viscous-dominated conditions typical in many lakes (i.e., having little bottom friction and low Reynolds numbers), which is based on the underlying physics, rather than an arbitrary assumption of Manning's *n*.

References

Gioia, G., and F.A. Bombardelli (2002), Scaling and similarity in rough channel flows, *Phys. Rev. Letters*, *88(1)*, 014501.

Massey, T. C., M. E. Anderson, J. M. Smith, J. Gomez, and R. Jones (2011), STWAVE: Steady-state spectral wave model user's manual for STWAVE, Version 6.0, ERDC/CHL SR-11-1. Vicksburg, MS, U.S. Army Engineer Research and Development Center, Vicksburg, MS.

Smith, J. M., A. R. Sherlock, and D. T. Resio (2001), STWAVE: Steady-state spectral wave model user's manual for STWAVE, Version 3.0, ERDC/CHL SR-01-1. Vicksburg, MS, U.S. Army Engineer Research and Development Center, Vicksburg, MS.

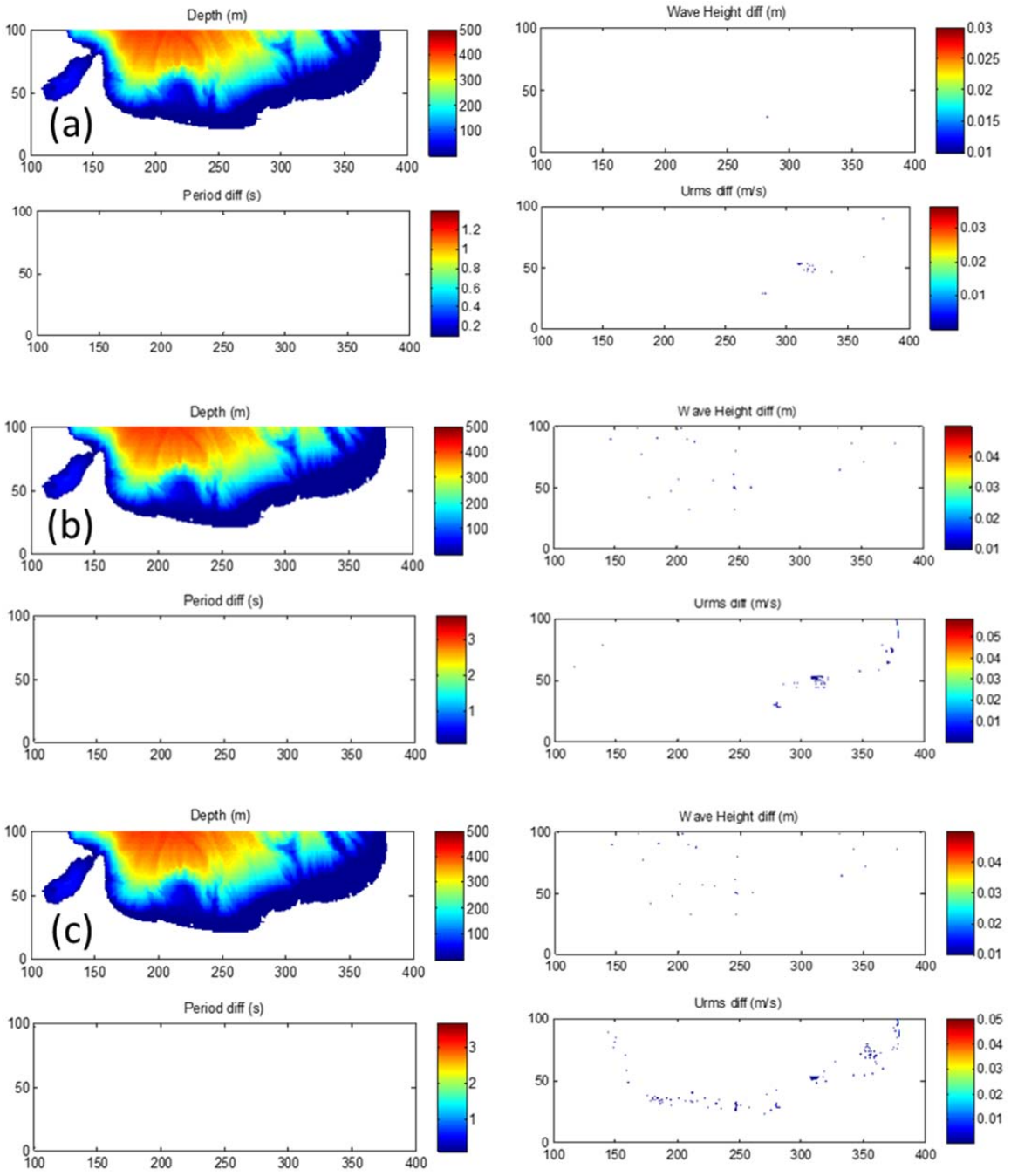

Figure C-1. Difference of results for wave height, period, and root-mean-square of the nearbed velocity (u_{rms}) resulting from a northerly wind of (a) 3 m s^{-1}, (b) 12 m s^{-1}, and (c) 21 m s^{-1} obtained with the original and modified STWAVE models. The water depth based on the bathymetry of Lake Tahoe is shown for reference. Original STWAVE model results obtained using n=0.

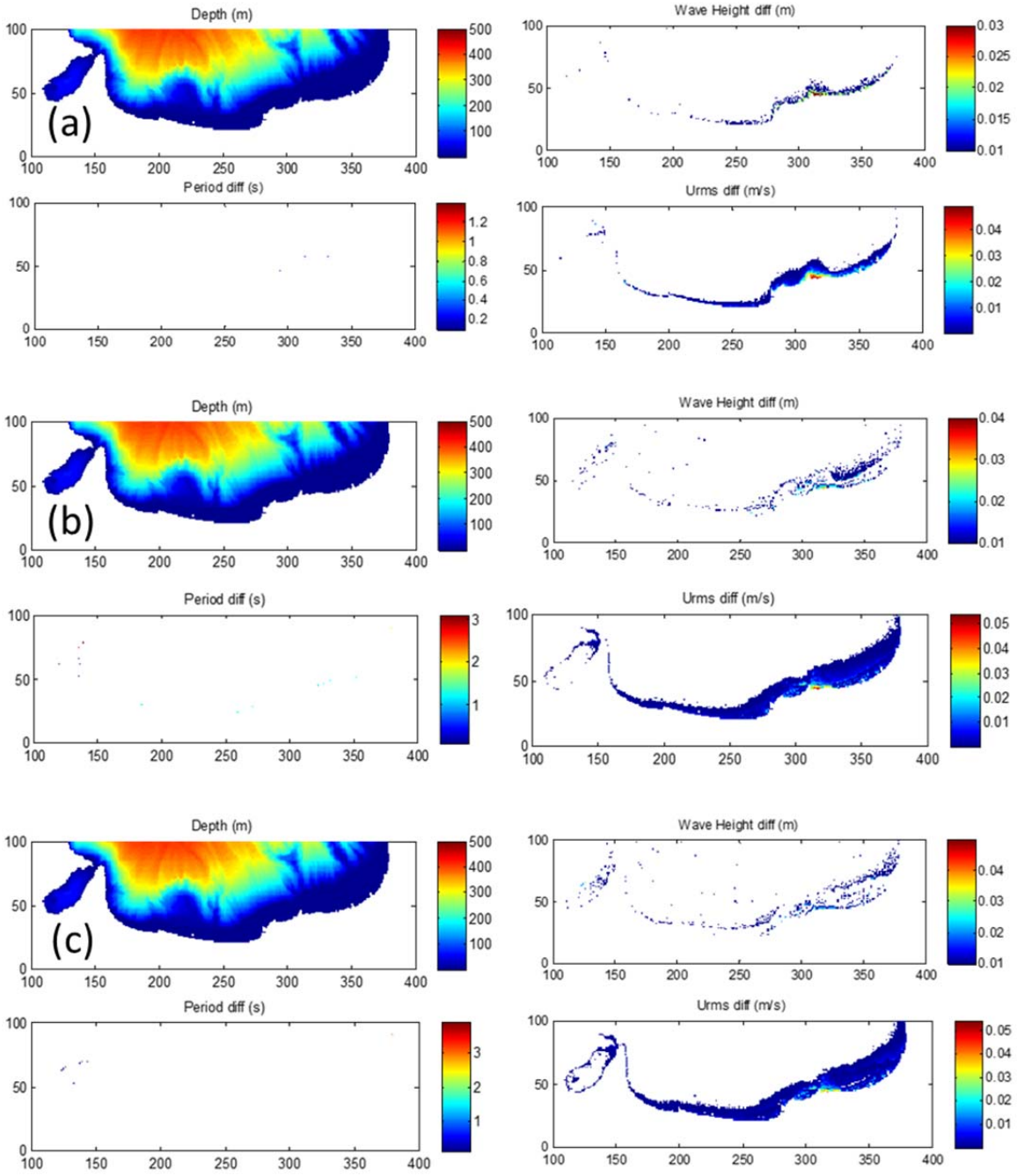

Figure C-2. Difference of results for wave height, period, and root-mean-square of the nearbed velocity (u_{rms}) resulting from a northerly wind of (a) 3 m s^{-1}, (b) 12 m s^{-1}, and (c) 21 m s^{-1}, obtained with the original and modified STWAVE models. The water depth based on the bathymetry of Lake Tahoe is shown for reference. Original STWAVE model results obtained using n=0.02.

Appendix D. Mid-lake stratification during the winter study period

From a subset of field measurements that included vertical temperature profiles collected at mid-lake to a depth of 440 m (referred to as the Glenbrook Thermistor Chain in Figure D-1) from 14 March 2008 to 4 May 2010 (unpublished data), we see that internal waves in Lake Tahoe occur at depths of about 50 to 75 m during the study period (see Figure D-1). Additionally, the nearshore water temperatures were colder than any temperature recorded at the mid-lake thermistor chain. We speculate that the appearance of cold water at the study site was due to density currents. The important point for this work is that at the study site, the water column remained unstratified.

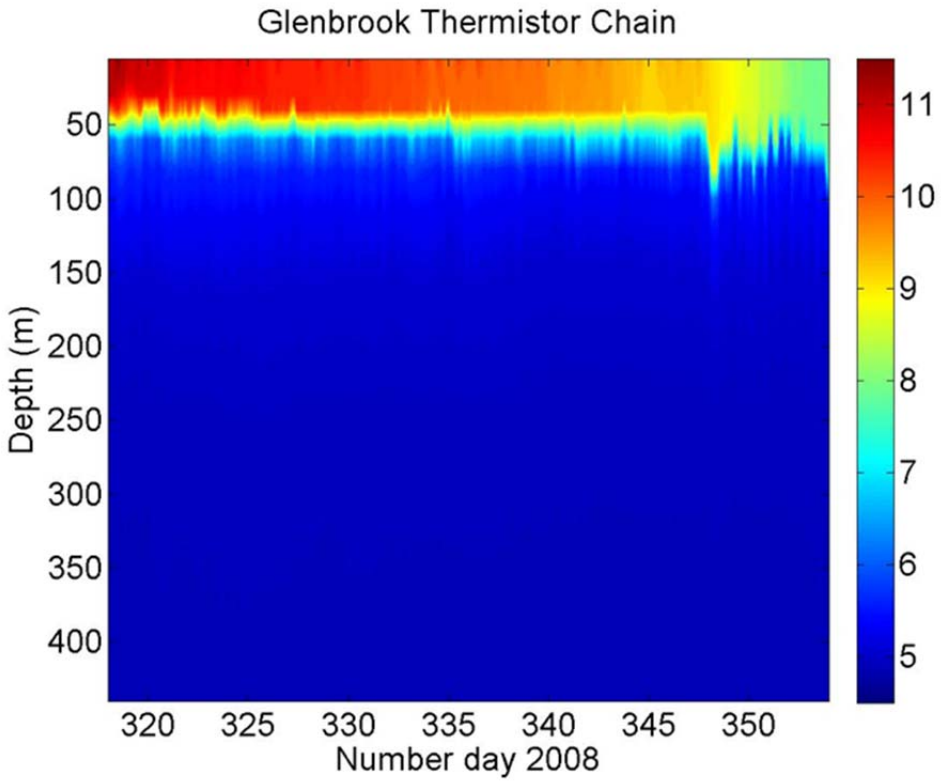

Figure D-1. Mid-lake temperature profiles to a depth of 440 m at Lake Tahoe. Temperature is in degrees Celsius.